Powerline Communication and Demand Side Management for Microgrids

Derek Neal

Balliol College

University of Oxford

A thesis submitted for the degree of

Doctor of Philosophy

Michaelmas 2023

Statement of Originality

I declare that this thesis is entirely my own work, and except where referencing other work, describes my own research. No artificial intelligence tools were used in this study or the writing of this text. The corresponding author is an active duty officer in the United States Air Force and his studies are funded by the Air Force Institute of Technology. The views expressed in this article are those of the author and do not necessarily reflect the official policy or position of the United States Air Force, the Department of Defense or the U.S. Government.

Abstract

Motivation: The greatest challenge for microgrid deployment is making energy affordable, especially in remote low-income communities. This thesis answers the following research question:

> *Can digital communication reduce the price of electricity for an islanded low voltage microgrid and if so, can broadband powerline communications meet microgrid control requirements?*

Approach: This study conducts a cost-benefit analysis of the addition of a field area network to a microgrid. Broadband powerline communication is selected as a candidate technology and tested on various microgrid networks to determine its suitability.
Results: The main contributions of this study are:

> *A demand-side management strategy and unsubsidised cost reflective tariff structure for rural microgrids in the developing world.*
>
> *A cost-benefit analysis that shows the addition of a low bit rate, medium latency communication system (*1 kbps *per customer,* 100 ms*) may reduce the levelized cost of energy by 32%.*
>
> *A performance evaluation of broadband HomePlug powerline communications for microgrids which shows the Homeplug AV2 has a range of* 600 m *and functions well on complex radial distribution networks.*

Conclusion: Investment in a minimally capable communication system has significant economic benefit to both customer and utility by enabling smart grid services such as automatic meter reading and demand side management. Since communication technologies share similar bit rate and latency capabilities and are similarly priced, the technology choice is driven more by microgrid geography, complexity, availability and reliability. Powerline communications require no additional cable, but boast reliability similar to dedicated cable solutions. The HomePlug AV meets bit rate and latency requirements, is affordable, reliable, simple and widely available around the world. This study concludes it is a solid candidate for low voltage islanded microgrids.

The material presented in this thesis has been published or submitted for publication in an abbreviated format in the following publications:

D. Neal et al, "Demand side energy management and customer behavioral response in a rural islanded microgrid," in IEEE PES/IAS PowerAfrica, 2020.

D. Neal, D. Rogers and M. McCulloch, "A Techno-Economic Analysis of Communication in Islanded Microgrids," unpublished. Submitted Oct 2023 to Elsevier Renewable and Sustainable Energy Reviews.

D. Neal, D. Rogers and M. McCulloch, "Broadband Powerline Communication for Low-Voltage Microgrids," unpublished. Submitted Oct 2023 to IEEE Transactions on Power Delivery.

Contents

List of Figures

List of Tables

List of Abbreviations

ABL . . . . . adaptive bit loading

AFE . . . . . analog-front-end

AMI . . . . . advanced metering infrastructure

AMR . . . . . automatic meter reading

AV . . . . . HomePlug AV

BB . . . . . broadband

BEP . . . . . break-even-point

bps . . . . . bits per second

CAPEX . . . . capital expenses

CML . . . . . customer minutes lost

CPR . . . . . common pool resource

CRT . . . . . cost-reflective tariff

DER . . . . . distributed energy resource

DR . . . . . demand response

DSM . . . . . demand-side management

DSO . . . . . distribution system operators

DUT . . . . . device under test

EE . . . . . energy efficiency

EMI . . . . . electromagnetic interference

EMS . . . . . energy management system

EV . . . . . electric vehicle

FAN . . . . . field area network

FEC . . . . . forward error correction

FFT . . . . . fast Fourier transform

FSK . . . . . frequency shift keying

GP . . . . . HomePlug Green PHY

HAN . . . . . home area network

IEA . . . . . International Energy Agency

IHD . . . . . in-home display

IP . . . . . internet protocol

IPP . . . . . independent power producer

IRR . . . . . internal revenue return

KPLC . . . . . Kenya Power and Light Company

LCOE . . . . . levelised cost of energy

LPF . . . . . low-pass filter

LV . . . . . Low voltage

MAS . . . . . multi-agent system

NB . . . . . narrow band

NGO . . . . . non-governmental organization

NTL . . . . . non-technical losses

OES . . . . . Open Energy System

OFDM . . . . orthogonal frequency division multiplexing

OPEX . . . . . operational expenses

PAYG . . . . . pay-as-you-go

PLC . . . . . powerline communication

PSK . . . . . phase shift keying

PV . . . . . photovoltaic

QAM . . . . . quadrature amplitude modulation

QCA . . . . . Qualcomm Atheros

RTP . . . . . real time pricing

RELCON . . . Robust Extra Low COst Nanogrids (title of an EPSRC research project)

ROBO . . . . . Robust OFDM

SCADA . . . . supervisory control and data acquisition

SE4ALL . . . . Sustainable Energy for All

SG . . . . . smart grid

SHS . . . . . solar home system

SOC . . . . . state-of-charge

SNR . . . . . signal-to-noise ratio

SR . . . . . spinning reserve

SSA . . . . . sub-Saharan Africa

SWA . . . . . steel wire armoured

TCP . . . . . transmission control protocol

TLM . . . . . transmission line mode

TOU . . . . . time-of-use

TSO . . . . . transmission system operators

UDP . . . . . user datagram protocol

UNB . . . . . ultra-narrow band

UEC . . . . . user-enable communication

UPV . . . . . user perceived value

USD . . . . . United States Dollar

VNA . . . . . vector network analyser

VRLA . . . . . valve regulated lead acid

WAN . . . . . wide area network

WTP . . . . . willingness-to-pay

List of Symbols

A CAPEX independent of the number of customers ($)

B CAPEX for each added customer ($/customer)

C annual OPEX independent of the number of customers ($/year)

D annual OPEX for each added customer ($/year-customer

E energy served (kWh/year-customer)

I current (A)

L lifetime (years)

N number of...

S scattering parameter

T eigenvector

V voltage (V)

Z admittance (S)

Z impedance (Ω)

a cross sectional area (m^2)

c per-unit capacitance (Ω/m)

d conductor distance from cable centre (m)

f frequency (Hz)

g per-unit conductance (F/m)

l per-unit inductance (H/m)

p communication service bit rate level

r per-unit resistance (S/m)

r_s shield radius (m)

r_w conductor radius (m)

s distance between conductors (m)

$\tan\delta$ loss tangent

v_p phase velocity (m/s)

w_s shield width (m)

x powerline length (m)

z position of wave signal on powerline

α attenuation constant (nepers/m)

$\hat{\alpha}$ discount factor for CAPEX independent of the number of customers

β phase constant (radians/m)

$\hat{\beta}$ discount factor for CAPEX for each added customer

Γ reflection coefficient

Γ_p propagation constant matrix (m^{-1})

$\hat{\gamma}$ discount factor for annual OPEX independent of the number of customers

$\hat{\delta}$ discount factor for annual OPEX for each added customer

δ_{skin} skin depth (m)

ε_0 permittivity (H/m)

η technical losses as a fraction of supplied energy

θ angle between conductors (rad)

Λ eigenvalue matrix

λ propagation constant (m^{-1})

μ permeability

ρ resistivity of annealed copper

σ conductivity (S/m)

ω frequency (rad/s)

1 Introduction

Global energy demand continues to rise with modernization, especially in developing nations. Despite progress in the past decade, 1.3 billion people remain in poverty and 940 million still live without electricity, relying primarily on carbon-based fuel sources for heating and lighting [1], [2]. Procurement of these fuels for rural residents is time intensive, leads to ecosystem loss and causes systematic health problems. Lack of access to clean and sustainable energy remains an impediment for rural communities in the developing world. The definition of electrification per the International Energy Agency (IEA) is binary and conveys minimum access to basic services such as lighting, phone charging and television or radio. However, even those that are considered "electrified" may not enjoy continuous service and often lack sufficient levels of power for productive uses [3]. The degree of development is proportional to the quantity and quality of energy access.

1.1 Defining electricity access

The non-profit organization Sustainable Energy for All (SE4ALL) characterizes access to electricity with a multi-tier spectrum where Tier 0 illustrates no electricity, to a modern service, round-the-clock availability at Tier 5 as detailed in Table 1.1 [3].

Table 1.1: Electricity Access Service-Value Tiers

Tier	Min capacity rating	Min daily service (hours)	Min night service (hours)	Service description
1	3 W	4	1	one light, phone charger,
2	50 W	4	2	... additional light, TV, fan,
3	200 W	8	3	... small fridge, computer, slow cooker,
4	800 W	16	4	... kitchen appliances, small machines,
5	1.2 kW	23	4	... large machines, electric cooking,
6	10 kW	24	12	... EV, electric heating

The customer-oriented tiers in Table 1.1 define the necessary energy supply required to deliver certain services. Conventionally, higher tiers of access are achieved through *macrogrid* systems: large, centralized generation power stations that distribute electricity to customers via extensive and expensive transmission line networks. However, modern energy access does not have to come from such macrogrids and, in many situations (*e.g.*, rural communities in the developing world), such an approach can be unjustifiably expensive and logistically challenging due to long or rugged transmission routes. Alternatively, generation and distribution can be decentralized and localized through *microgrids*.

The African continent is the most solar-rich on earth and photovoltaic (PV) generation will play a major role in meeting rising demand that is projected to quadruple in the sub-Saharan Africa (SSA) region by 2040 [4]. Around 15 million Africans are now electrified via 1500 operational microgrids (with 4000 more in planning), the majority of which are powered by PV due to an 80% drop in solar module prices in the past decade [5], [6]. Millions more (*e.g.*, 47 million Kenyans) have limited energy access through prolific Tier 1 and 2 solar home systems (SHS) [5]. These alternate decentralized solutions provide the most cost-effective method to extend reliable electrical services to the remaining unelectrified rural and peri-urban Africans by 2030 [4]. The IEA suggests a massive deployment of microgrids and SHS to 370 million Africans [4]. Furthermore, investment in the African power sector would need to double even to minimally achieve the SE4ALL electrification

goal [4]. Therefore, the ultimate challenge lies in finding innovative methods to finance expensive infrastructure in regions of extreme poverty.

1.2 Defining Microgrid

A microgrid is a self-contained power system distributing electricity to a community of loads from one or more local distributed energy resource (DER) [7]. DERs include non-dispatchable generation (*e.g.*, PV, wind), dispatchable generation (*e.g.*, diesel generator), and storage assets. This thesis focuses on islanded microgrids, *i.e.*, microgrids with no grid-tie connection to a macrogrid. Islanded microgrids must source all their energy internally and so the quantity and mix of the generation must be chosen carefully to provide the desired power availability at acceptable cost. In many cases, the generation is not dispatchable and dispatchable generation is either not available, or expensive per unit of electricity produced. An islanded microgrid must manage supply and demand, firstly to avoid the collapse of the network because of over-loading, and secondly to maximise the use of non-dispatchable generation by encouraging load to correspond with generation output.

Despite the attractiveness of microgrids as a means to address the electrification challenge, the reality remains that microgrids are expensive. Energy system development requires large upfront capital investment with financial break-even lifetimes of 10-30 years [8]. This investment can be covered by public funds or financing, and unless covered by philanthropy, costs and profit margin overhead are ultimately amortised to the customer. To maximize the reach of electricity service, cost per unit of energy must be below willingness-to-pay (WTP) thresholds and sustainably affordable for low income customers. In remote rural communities that live below poverty lines, this can be extremely difficult. Technological advances and mass manufacturing continue to lower energy system hardware costs. Further cost reductions are available by:

1. Increasing the capacity factor of hardware, by
   (a) shifting demand in time to better match availability of generation,
   (b) improving the accuracy of plant sizing.

2. Reducing the peak-to-average demand ratio.
3. Reducing maintenance costs.

Microgrid communication can enable these cost reductions by facilitating improved metering and control. While communication is not essential for microgrid operation, it tends to enhance performance because it can be used to notify loads about the instantaneous availability of generation. The literature is replete with analysis of microgrid communication technologies and techniques, still there is yet a cost-benefit analysis to evaluate whether adding a communication system to a microgrid is justified, *i.e.*, a communication system can provide an internal rate of return (IRR). The decision depends on many factors, and in some situations the additional complexity of a communication system is not economical, necessary or desirable.

1.3 Defining Demand-Side Management

Traditionally, power generation is designed to meet demand. However, demand-side management (DSM) aims to reverse this perspective by manipulating the load in order to curtail the need for increased generation capacity. The backbone of DSM is remote load monitoring or advanced metering infrastructure (AMI). AMI is the physical equipment necessary to perform automatic meter reading (AMR). The smart meter is the fundamental building block of AMI. An electricity meter becomes a smart meter with the addition of digital communication. Smart meters facilitate four DSM categories [9]:

1. spinning reserve (SR)
2. physical demand response (DR)
3. market demand response
4. energy efficiency (EE).

These techniques define interactions between the *utility* (microgrid manager/electricity provider) and the customer. Appropriate implementation can reduce system capital and operational costs and hence, the amortised levelized cost of energy (LCOE, United States dollar (USD) per unit of energy, \$/kWh). DSM is accomplished using coordinated actions between the primary, secondary, and tertiary levels of

microgrid control which range from short term to long term energy management [10]. The degree to which a meter is "smart" can vary depending on its technological capability and the goals of the microgrid DSM strategy. SR are instantaneous control reactions to maintain microgrid stability triggered by voltage or frequency deviations. Physical DR are utility interventions to prevent energy shortages. Market DR are tariffing methods to incentivise certain consumption patterns. Using EE strategies, the utility educates the customer of consumption habits and microgrid status to spur efficient consumption decisions.

1.4 Defining Communication

Communication here means the transfer of data from one microgrid component to another or to the utility either manually, by the customer, or automatically by wired, or wireless mediums. Although many of the concepts presented hereafter may apply to grid-tied microgrids, this thesis concentrates on low voltage (LV) microgrids limited to approximately 1 km geographic radius. Such microgrids will tend to use a single common distribution voltage and, if communication is implemented, a single common Field Area Network (FAN) as illustrated in Fig. 1.1. The FAN communicates between DERs, electricity meters, and the energy management system (EMS) and requires a long-range (> 10 km) wide area network (WAN) backhaul to connect the microgrid to the utility's supervisory control and data acquisition (SCADA) system [11].

A FAN is a link between the microgrid EMS and the smart meter. The example FAN in Fig.1.1 is organized in a bus network topology implying the use of powerline communications (PLC). There are various FAN topologies and technology options. The two basic mediums for FAN communication are wired and wireless. Without a backhaul, the utility would have to extract FAN information by sending utility personnel to the site, and particularly for small, remote, autonomous microgrids, removing the need for permanent or regular on-site personnel and associated expenses is desirable.

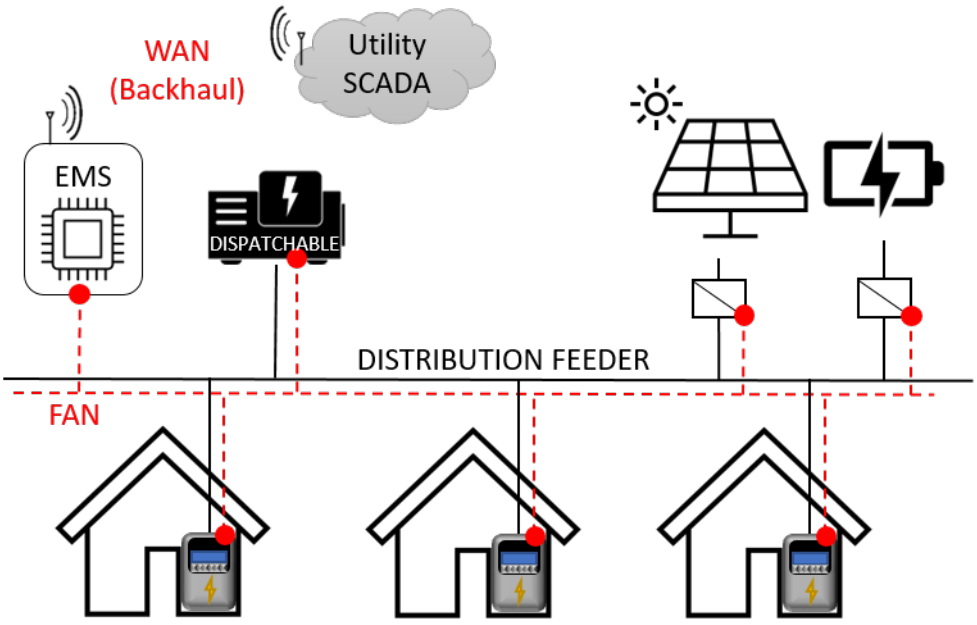

Figure 1.1: Example of microgrid with FAN. The FAN communicates between DERs, smart meters, and EMS to transfer data between microgrid components. Communication between the microgrid and the utility SCADA (or macrogrid) occurs through a WAN (or backhaul link). The example FAN is configured in a bus network topology following the power lines which implies the use of PLC on a radial power distribution feeder. The presence of an EMS implies centralized control.

1.5 Powerline Communication

The popularity of PLC has historically varied; however, it continually induces appeal due to the ubiquitous pre-existence of vast networks of powerline cables that electrify the modern world. PLC promises digital communication over a 'free medium', similar to wireless technologies, whilst offering reliability like other wired communication technologies. Three frequency ranges are commonly used for PLC: ultra-narrow band (UNB: $< 3\,\text{kHz}$), narrowband (NB: $3 - 500\,\text{kHz}$), and broadband (BB: $> 1\,\text{MHz}$) [12]. Following the HomePlug Alliance initial standards release in 2001, there has been steady interest in PLC modelling and implementation in a variety of applications. Much of the first wave of interest concerned BB internet access whereas more recent research mainly concentrates on *smart grid* applications, meaning the connectivity of power systems for distribution automation, AMI, DSM, distributed power electronics control, energy management, and data harvesting [12],

(a) (b)

Figure 1.2: HomePlug PLC devices. a) dLAN GreenPHY module [14] b) TP Link AV500 [15]

[13]. This study compares the HomePlug Green PHY (GP) and HomePlug AV (AV), two BB off-the-shelf products in Fig. 1.2, as quick solutions for microgrid developers.

BB PLC technologies (*e.g.*, HomePlug, G.hn) rose with the societal dependence on internet in the mid-2000s and was heavily explored as an access solution to compete with other 'last mile' wired technologies (*e.g.*, DSL, coax, fibre). WiFi dominates the home and business internet market, primarily because PLC must contend with a much noisier channel that cannot deliver comparable and stable bit rates in buildings with dynamic loads such as power electronically controlled motors. However the AV has had great success as an indoor internet extender in situations where other technologies fail to satisfy network requirements (*e.g.*, difficult to reach rooms within a building). Consequently, devices implementing the AV technology can be found all over the world at affordable prices. Recently, PLC solutions have reemerged as a potential solution for the smart grid. Most smart grid applications only require NB capabilities with bit rates less than 1 kbps and latencies less than 100 ms [16]. Although BB PLC solutions far exceed the bit rate and latency requirements for microgrid control, it is chosen as a viable candidate because of its plug-and-play simplicity and ubiquitous availability. Additionally, as the number of sensors, sample frequencies, and controllable devices increase, BB bit rates may become necessary. Furthermore, many smart grid structures aspire

to integrate all devices into cloud-based, internet-accessible control centres. BB communication solutions customarily utilize IP-based protocols making them a good candidate to be integrated in cloud infrastructure [17].

Powerlines are designed for the transmission of power rather than information and therefore offer a problematic environment for digital communications. Cables intended for communication are geometrically designed to have standardized characteristic impedances (*e.g.*, $50\,\Omega$ or $75\,\Omega$). In addition to the standard challenges inherent to any communication medium (*e.g.*, attenuation, dispersion, distortion), powerline cables can have non-homogeneous dielectrics and non-standard characteristic impedances that cause frequency dependent reflections. Powerline networks are difficult to model due to their often complex branching structures and because generators and loads may dynamically/unpredictably connect and disconnect, changing the electrical behaviour of the network over time. Generators, power converters, and dynamic loads inject broad- and narrow-band noise into the powerline. Ambient noise from nearby radio-electric systems can cause further electromagnetic interference (EMI). Therefore, powerlines are highly variable communication channels, and so channel models must depend on transmission band, cable type, network configuration, and load characterization.

Most PLC research focuses on modelling the harsh powerline communication medium to best predict performance. Methods fall into two main categories: top-down models based on measurements of the channel, and bottom-up models based on analytical characterisation of the channel using the transmission line model (TLM) [18]. The powerline channel can be modelled as a TLM element in a two-port network and measured using scattering parameters (s-parameters) with a vector network analyser (VNA). Two-port elements cascaded together form complex networks. Network models can predict PLC performance on a given microgrid architecture.

1.6 The microgrid laboratory testbed

This thesis was supported by the Robust Extra Low COst Nanogrids (RELCON), a collaborative research project aimed to electrify a rural community in Kenya [19].

Motivated by the United Nation's Sustainable Energy for All (SE4ALL) initiative and the electrification policy priorities of African governments, the goal of the RELCON project was to develop and deploy off-grid Tier 3 microgrids at the cost of current Tier 2 systems with the option to connect to a wider grid. There exists a stark correlation between access to electricity and human welfare indicators [20]. The RELCON team consisted of researchers at the Universities of Oxford and Cardiff, social scientists at the Cooperative University of Kenya (CUK), and advisors at the Kenyan Power and Light Company (KPLC) and energy company Tropical Power. The RELCON system was designed as an entry-level power system for an unelectrified rural community. Deployment of a ten-home trial system was scheduled for early 2020 to an unelectrified village southeast of Nairobi, Kenya but was delayed multiple times and eventually cancelled due to COVID. Still, the microgrid serves as the laboratory test-bed to develop the contributions found in this study. A full system description will follow in Section 3.4.

1.7 Contributions

This study answers the following questions that face microgrid developers:

1. How does integrating a communication system in the microgrid design reduce both capital and operating costs?
2. What are the costs and benefits of adding a digital communication system to the microgrid?
3. What are the minimum capabilities that a microgrid communication system must have (bit rate (bps) and latency (ms)) to meet various service requirements?
4. And lastly, is powerline communication (PLC) a competitive technology compared to dedicated wires or wireless to meet the communication requirement?

The first contribution of this work is a DSM strategy for an unsubsidised islanded LV microgrid for an unelectrified remote rural village. The approach is threefold. First, customers pay a fixed monthly fee for a maximum power rating subscription. This effectively operates as a form of physical DR curtailment where customers'

peak power is capped. But the subscription principally serves as a method of facilitating low-income access by offering a range of power ratings for various income levels whilst simultaneously providing flexibility for future energy growth. Second, market DR is accomplished with a two-period time-of-use (TOU) tariff. During the period of high DER production, energy is free. Energy during the low production period is charged at a high rate to incentivise energy consumption during high production periods and reduce storage usage. Third, EE initiatives are accomplished through an in-home display (IHD) to educate customers about the microgrid status and their consumption, including potential SR and physical DR forecasts. This empowers new electricity users to learn the true cost of energy, understand the limitations of the microgrid, and to make consumption decisions that will maximize their access. These DSM measures increase system longevity, reduce system cost, and ultimately reduce the LCOE for the customer [19].

The second contribution of this thesis is a cost-benefit analysis of adding a FAN digital communication system to a microgrid, the potential service value added to the grid from that addition, and the limit of services available without it. Just as energy access can be quantified in tiers as in Table 1.1, this thesis quantifies the following in the context of a LV islanded microgrid:

1. services available to a microgrid customer through the addition of a particular communication bit rate,
2. technology requirements for a given bit rate,
3. cost of a microgrid FAN, and
4. benefits (if any) achieved at each bit rate level.

The investigation concludes that upon investment in a minimally capable communication system (< 100 ms latency, > 1 kbps), multiple high impact services become possible, such as AMR and DSM, reducing the LCOE by 32%. FAN hardware costs for this capability depend on technology, but range between \$0-\$33 per customer. When this cost is amortised over the microgrid lifetime, the additional cost becomes almost irrelevant. As the capability of the communication system increases above 10 kbps there occurs a point of diminishing returns where the capability of the

communication system does not yield further reductions in LCOE due to increased hardware and data costs. Since the various technologies available to meet this minimum capability are similar in cost and capability, the selection becomes more nuanced, based on other factors such as microgrid geography and hardware and software complexity, availability and reliability [16].

The last contribution of this thesis is to model and empirically evaluate the viability of two commercially available BB PLC technologies for digital communications in a LV microgrid. The HomePlug GP and AV2 are compared to evaluate their capability and affordability as a communication solution for microgrid developers [21]. This study synthesizes the PLC modelling literature to suggest a bottom-up analytical distributed element TLM as a tool for microgrid developers to quickly determine if a particular powerline configuration will be conducive to BB PLC functionality. The model is based on the two-wire TLM building block, but also incorporates proximity effects from multiconductor theory and frequency dependencies of dielectric insulation materials to better predict attenuation at high frequency. The model is validated with s-parameter measurements of the RELCON testbed. The study reveals that despite the GP's intention to be a tailored solution for smart grid applications, it cannot compete with the performance, availability, and affordability of the AV2 technology. The GP functions well on dedicated star feeders up to 450 m in length and on radial feeders with long branches. However, functionality is unreliable with short branches. Attenuation due to the powerline channel must be less than -60 dB at 30 MHz and any notches in the full path frequency spectrum must not extend below -70 dB in depth. The AV2 can connect reliably up to 600 m and functions well on most conceivable network architectures. Attenuation due to the powerline channel must be less than -122 dB at 68 MHz and mean signal-to-noise ratios must exceed 1.0 [22].

1.8 Outline

The thesis is organized into the following chapters: first, Chapter 2 contains a literature review of the major topics under investigation (electrification, microgrids,

DSM, microgrid communication, and PLC).

Chapter 3 introduces the three levels of microgrid control and expounds on how the levels are used to implement the four DSM strategies. The various communication methods for AMR and market DR tariff structures are systematically developed and their communication requirements defined. The RELCON electrification project is described. A DSM strategy for an unsubsidised remote rural LV islanded microgrid is proposed.

Chapter 4 provides a techno-economic analysis of microgrid communication to determine if adding a digital communication system to a microgrid is worth the cost and complexity. It incorporates the communication requirements derived from Chapter 3 and conducts a thorough comparison of various wired and wireless technologies that meet those requirements. It culminates with a case study to illustrate the cost-savings achievable through microgrid communication based on the real-world RELCON project.

Chapter 5 overviews transmission line theory and s-parameters. These are used to build a bottom-up analytical powerline model from the cross sectional geometry of the cable. The model incorporates proximity effects learned from multiconductor transmission line theory and frequency dependent dielectric material behaviour to accurately predict signal attenuation at high frequency. The model is validated with s-parameter measurements taken with a 2-port VNA on the RELCON laboratory testbed.

Chapter 6 contains the experimental results of BB HomePlug GP and AV2 performance tests on various network structures. The modified two-wire TLM from Chapter 5 is validated by VNA s-parameter measurements and used to predict PLC performance on various networks. It is proposed as a quick and simple tool for microgrid developers to determine the functionality of BB PLC on a given network topology. Suitability of BB PLC for microgrid communication is stated.

Lastly, Chapter 7 offers concluding remarks and opportunities for further research.

2
Literature Review

The United Nations (UN) Human Development Index (HDI) considers life expectancy, education, and gross national income to assign a percentage score communicating the general quality of life to a nation [1]. There exists a stark correlation between access to electricity and these development indicators [20]. The IEA definition of electrification falls somewhere between Tier 1 and 2 as defined in Table 1.1. Tier 1 and 2 systems still have capacity to extend work hours, provide educational opportunity, enable welfare activities and foster participation in modern commerce through information and communication technology (ICT). However, more substantial advancement occurs at Tier 3 and beyond with machine loads, refrigeration and heating to spur income generation through industry, food production and conservation, and climate control [3]. Higher tiers can also support community infrastructure like street lighting, sanitation systems, health facilities, public spaces, schools and marketplaces [3]. Up to three billion people lack *modern* energy services ($\geq$ Tier 4) that enable socioeconomic transformation [3]. Tier 3 generally coincides with an HDI of 0.6 which exceeds the current Kenyan average of 0.58 [1], [20].

Energy deficiencies are most apparent in rural SSA where governments, non-governmental organizations (NGO) and entrepreneurs alike struggle to provide sustainable electricity to 55% of its citizens, many of whom are scattered in sparsely

populated corners of the continent [4]. There also remain an estimated 95 million sub-Saharan Africans living "under the grid" who are unable to access grid electricity service due to high connection fees [23]. Electricity theft is common in such areas, aggravating power quality issues, increasing risk of electrocution and mounting financial stress on utility companies [3]. National grids cover primarily urban areas and deliver low quality power, prone to frequent outages. Universal access to modern energy by 2030 is one of the UN initiatives to continue lifting families from debilitating poverty. It is estimated to cost a lofty $890 billion (ten times the GDP of Kenya) and will require a multifaceted approach capitalizing on multiple energy and funding resources [3]. Much of this investment will need to occur in Africa and will inevitably include fossil fuels, centralized generation and traditional national power grids. Yet rapid progress must also include decentralized approaches and renewable resources such as solar, wind, hydro, and biomass. For example, Kenya has electrified one million people per year since 2013 through aggressive governmental initiatives, favourable import structures, flexible energy policy and nationwide support of mobile money banking. Such an environment has enabled private and governmental energy entities to collaborate and experiment with various business models, generation sources and grid structures [4].

Aggressive electrification goals require the inclusion of decentralized solutions like off-grid microgrids. Solar and battery prices continue to fall and supply structures are now well established. Automated tariff collection through mobile money combined with smart metering to remotely monitor consumption can lower operating costs. Since SSA has abundant solar irradiance, PV microgrids have become the default choice for energy generation. Microgrid development has advanced beyond research projects and NGO initiatives leaving a list of lessons learned. Now private investors seek to capitalize on a $400 billion potential market to meet the large demand for energy among Africa's unelectrified citizens [6].

2.1 Microgrid Development Obstacles

Obstacles that continue to impede microgrid development can be bundled into four categories:

1. Government regulation
2. Financial stability
3. System longevity
4. Dependency on centralized generation

2.1.1 Government Regulation

Developers overwhelmingly agree that government policy has the greatest influence on progress. Governments are not able to meet electrification goals through public programs and funds alone. This is partially because of a lack of financial capacity, but also due to a lack of political will and continuity [8]. Rapid electrification requires not only centralized top-down expansion of the grid, but also the full participation of decentralized approaches from the private sector which, in SSA, is significantly impeded by government restrictions [24]. For example, less than 20% of SSA nations permit private participation in grid distribution and transmission [4]. Over 40% do not allow private companies to generate power [4]. Another hurdle is procurement of permissions for independent power producers (IPP) to sell electricity. In more lenient Kenya, a license to sell electricity is not required for systems smaller than 3MW; however, they still require a permit from the regulatory authority. Such bureaucratic processes can be time consuming and have even completely stalled projects into failure. Governments should strive to approach decentralized electrification efforts with a "light-handed regulatory system" [24]. PowerHive was the first IPP to be granted permission to sell electricity in Kenya in 2015 [6]

In addition to government permissions, restrictions on energy pricing can stifle IPP survival. Many African countries have fixed national electricity tariffs and mandate that microgrid implementers, including private projects, charge the national tariff at great revenue loss [24]. This lack of freedom to set customized tariffs based on market driven cost analysis, called cost-reflective tariffs (CRT), introduces

devaluation of energy and uncertainty for investors who depend on revenue returns to mitigate lending risks [8]. Kenya's standard national tariff is around 20 cents per kWh. However, rural communities have shown WTP as high as \$4/kWh [6], [25]. For developers to recover expenditures, let alone make an attractive IRR, they must be permitted to set CRTs or have unfettered access to subsidies enjoyed by public utilities [8]. In fact, [26] states that national tariffs are:

> the biggest barrier to more rapid power development in sub-Saharan Africa [because] while often perceived as equitable to customers, national tariffs are in practice often the most restrictive for micro-grid developers as it forces them to compete with rates far below what they would otherwise charge to recoup expenses.

The analysis continues to highlight that national tariffs induce a

> market-distorting effect whereby customers—particularly those in remote regions—do not understand the utility's true cost to provide their individual service, which can set unrealistic expectations about how much they should pay for power and exacerbate tariff-setting challenges in remote areas [26].

It should also be noted that RELCON (a 15 kW system) started seeking a permit to sell electricity for research purposes from the Kenya Energy Regulatory Commission in 2018 and was not granted a permit before the project was delayed due to COVID in 2020. Regulatory delays contributed to the full cancellation of the endeavor in 2021.

2.1.2 Financial Sustainability

National grid tariffs enjoy heavy subsidies from public funds, deflating the true value of energy and making it difficult for IPPs to set CRTs for decentralized systems. The Last Mile Connectivity Program (LMCP) in Kenya has a \$700 million budget to decrease connection fees for potential grid customers from \$343 to \$147 in an effort to electrify the under-grid populace [27]. Such subsidies are not readily available for the private sector. There is also an absence of transition procedures for microgrid operators when the national grid absorbs the system. These ambiguous transitions can lead to significant revenue losses for IPPs and even deter investors

from providing financial support [6]. Policies should define the relationship of IPP with the national utility and tariff procedures when the grid arrives to microgrid communities to provide protections to both the existing customers and the IPP [24].

Like all power systems, microgrids require immense upfront capital to initiate the project and then they rely on consistent revenue over several years to eventually reach a break-even-point (BEP) and profitable IRR. Financing opportunities vary from traditional bank loans, donations from NGOs, investments from development financing institutions (DFI), or even public funds from government initiatives. Lenders have traditionally minimized risk through large government sponsored grid infrastructure projects. However, since many of these public efforts have not yielded substantial results and are often stalled due to political discontinuities, emphasis is shifting towards smaller decentralized projects [8]. Policy must support partnerships between developers and investors to build the foundation of successful microgrid installations and mitigate financial risks [8].

Kenya's approach was to create the Rural Electrification Authority to spearhead 120 microgrids, built by IPPs and managed by the public utility Kenya Power and Light Company (KPLC). Although this model may encourage cooperation between the public and private sectors, it also contributes to the public monopoly on energy [27]. Unfettered access to develop and collect tariffs for IPPs can accelerate electrification efforts and could leapfrog Africa beyond the previous century's western model of monopolized national grids. Kenya does not tax solar import products and has welcomed a flood of entrepreneurs to establish robust SHS and mobile money markets which have paved the way for microgrid planning [6]. PowerGen, jump-started with USAID money in 2011, operates 15 microgrids in three SSA countries together with Steamaco (who provides smart meter services) funded by DFIs Vulcan Impact Investing and Ashden [27].

Once empowered into the market, IPPs must establish solid business models to find a balance between WTP, low customer income, national tariff levels and system recovery costs. The largest impediment for impoverished communities to grid or off-grid connection is large upfront fees. Steamaco charges, on average,

a reasonable $11 in comparison to the $147 required to connect to the national grid [27]. Like other microgrid developers, they instead distribute connection costs into energy tariffs which must be set carefully to account for variable and seasonal oscillations of customer income. One noted best practice is concrete tariff collection schemes with clear penalties for non-payment [28].

One collaboration between researchers in Nepal and Norway, funded by donation, designed an AC micro grid connecting two villages to a hybrid generation system of solar, wind and hydro with batteries. The study reported low collection rates because villagers were paying in cash to fellow community members and there was no clear penalty for non-payment. The tariffs were set to only compensate local technicians for maintenance services and were not designed to recover system costs since the project was made possible through donation. A growing number of villagers now have access to the expanding national grid which offers even lower energy rates further threatening the sustainability of the project. No provisions were made to connect the microgrid to the national grid. Survival of the system falls to the community itself [29]. Community owned systems are often unsustainable because the participants do not agree to high enough tariffs to establish a commercially viable model. When large maintenance costs arise, the community cannot afford them and the system goes into disrepair wasting the donor's investment. They also often lack the training and capacity to seek proper regulatory frameworks for survival [24].

Traditionally electricity has been a post usage billing service which can lead to non-payment and utility losses. Smart meters coupled with mobile money applications easily address this [24]. Customers prepay for service much like a cell phone network provider sells minutes or data bundles. Once the energy balance is exhausted, the smart meter remotely terminates service until another payment is made [30]. Some providers charge fixed monthly rates while others utilize pay-as-you-go (PAYG) schemes where customers purchase energy when needed with their mobile money application.

Off-grid power systems are an example of a common pool resource (CPR), *i.e.*, a centralized capacity with limitations. Users must be prioritized to maximize

the reach of the system and spur the desired community outcomes. Customers can be divided into one of three categories [31]:

1. anchor loads that occupy the highest priority supporting public services or industrial productive use processes,
2. businesses operating for commercial profit, and
3. residents that consume primarily in the evening hours.

Diversity of these three categories will flatten demand profiles balancing day time commerce with night residential. Battery costs remain the largest financial influence for battery storage based microgrid developers highlighting the importance of power flow and DSM to minimize battery cycling, prevent deep discharge, increase longevity and reduce replacements [6].

2.1.3 System Longevity

System longevity includes three major factors [8]:

1. tariff structures that sustain the system,
2. reliable power to support productive use, and
3. maintenance resources.

Tariff structures

First, the success of an isolated rural electrical system heavily depends on tailored tariffs and community integration structures that enable economic growth and guarantee the survival of the system beyond installation and investment funds expiration. Projects usually begin with great enthusiasm, but often stagnate, and even fall into disrepair because measures are not taken to sustain it. The tariff structure must guarantee the developer's financial survival, as discussed previously, and cover all operational and maintenance costs such as technical support for troubleshooting, repair, and component replacement (*e.g.*, battery replacement).

Productive use

Second, long term survival can only be achieved if the microgrid design electrifies the productive activities that drive local industry [32]. Developers should collaborate with the local community to understand the user perceived value (UPV) of the electricity. In other words, community input should drive the design process to electrify the productive use activities critical to the economic growth of that specific village [32]. Although resident-only electrification projects (or SHSs) offer life changing value, they often fail to lift impoverished communities into prosperity [32]. Such transformations only occur when key activities like agricultural irrigation, commercial milling, sanitation systems, health services and education centres are electrified to amplify their productivity, reduce labour-to-yield ratios, reduce disease and suffering and spur innovation [32]. Rural community microgrids often fail due to consumption stagnation since users do not have electrical appliances, or they lack the training to realize its potential.

SHS companies send highly trained retail specialists to unelectrified communities to educate potential customers on displaced cost benefits of electrical energy. Electricity can displace kerosene, battery, and phone charging kiosk expenses and can save time by eliminating the need for trips to the market or fuel gathering excursions. SHS retailers also finance appliance costs into the price of the SHS and demonstrate to the customer how those appliances will improve their livelihood [33]. Significant social development often lags microgrid electrification by around five years while users slowly adapt to new behaviours and acquire the appropriate appliances that lead to lifestyle changes. Developers can accelerate this timeline by offering a customer appliance acquisition plan [34]. Otherwise, low revenue in the early years could cause business failure.

Another approach is to package electricity access with services such as internet access, refrigeration, or water pumping and sanitation. Such services spur more usage and lead more quickly to economic development, especially if the service targets local industry [6]. However, these advancements can digress if the microgrid does not provide reliable power. Power interruptions, brown outs and unexpected

shortages discourage user dependency on electricity leading to a reversion to previous behaviours. Community members lose trust in the electrical system or its provider and can be sceptical of future energy projects [32].

Maintenance

Third, there are two layers of maintenance. First, each microgrid system user must have immediate access to technical support. This can be provided in one of two ways. The developer can hire and train a local member of the community to respond to technical questions, malfunction troubleshooting and minor repairs. Otherwise, the developer must provide a direct link to such a technician that can access the system within a reasonable period of time. For example, the microgrid developers could contract technical support from the nearest grid utility. Technical issues should be resolved promptly to maintain community trust in the system and to prevent digression of positive habitual behaviour shifts. The second layer of maintenance is managerial governance. This typically takes the form of a community representative or council that liaise with the microgrid developer to manage regulatory compliance, tariff structures, maintenance issues and potentially the integration of the microgrid into the national grid system [31]. Case studies show villages require either a trusted and active relationship with their utility provider or training that leads to a complete transference of operation and maintenance to the village [8].

2.1.4 Dependency on Centralized Generation

The previous obstacles are all socio-economic factors whereas this last obstacle is a technical design obstacle. Traditional microgrid design mimics the macrogrid with a centralized generation hub and distribution lines to loads. Microgrids generally rely on a single source of generation often with some source of storage or auxiliary generation. Centralized generation and storage make up the bulk of the system cost analysis. Referencing the AC microgrid built in Nepal mentioned in Section 2.1.2, the introduction of electricity brought many social benefits to the communities, but there was a surplus of energy during the day and shortages at night. This exposes

the uncertainty of load behaviour and the subsequent difficulty of the sizing exercise. In the high demand hours after sunset, the villages are dependent on the hydro capacity and one centralized battery storage bank [29]. Over-sizing the generation or increasing the battery storage could fix the evening deficiencies, but it would increase cost and lead to even higher surpluses during the day.

Each microgrid system location is unique with variations in geography, climate, load type and size, customer spacing, income and cultures. Therefore, proper sizing of PV and storage requirements based on an unknown load profile present significant design challenge. Size specifications drive the capital installation cost of the power system that are passed on to the user through tariffs. However, little energy data exists from rural communities to inform this decision or to predict how demand will grow over time [35]. This data void often leads to ill-sized microgrid designs that inflate prices due to over-sizing or suffer from unexpected blackouts and customer frustration caused by under-sizing [29].

There are a variety of available tools to assist in system sizing such as HOMER, RETScreen, and LoadProGen. The creators of LoadProGen use a bottom-up approach to build appliance profiles based on survey data and then aggregate them using a Matlab based stochastic algorithm to account for uncertainty. The load profile creating model is compared to actual metered data in Cameroon [35]. HOMER on the other hand, is an off-grid system sizing optimizer originally developed at the National Renewable Energy Lab (NREL). It makes assumptions about a hypothetical load shape and scales it as necessary or accepts tabular input load data. Incorporating weather databases, market prices and a variety of user input preferences, it performs a cost benefit analysis to recommend an optimal generation and storage combination [36]. Developed by CANMET Energy Diversification Laboratory, RETScreen is a systems level analyser that assesses carbon footprint, budget, and performance over time and includes some default load profiles for various building structures such as a residential home. Although both HOMER and RETScreen can be useful to plan or validate system sizing calculations,

neither can be considered a detailed rural load profiling tool, but rather are helpful tools after assumptions about the load are already established [6].

One way to mitigate dependency of centralized generation and storage is to distribute them throughout the network. DERs could be completely decentralized, and would be described as interconnected nano-grids (*e.g.*, a community of interconnected SHS). In fact, this is similar to the distinctions between microgrid control architectures discussed later in 2.4. [37] proposes the interconnection of individual SHSs to form a community microgrid that taps into unused storage and generation potential to enable larger Tier 3 loads. This study is especially helpful because it contains actual SHS load data from Bboxx (SHS company operating in SSA) that verify Tier 2 consumer behaviour used to inform load profiles in this study. From 64 SHSs the average consumption was 55 Wh/day with peak power of 10W around 2000 hrs [37].

A similar idea was simulated and tested by A. Werth et al. who connect various SHSs to form an "Open Energy System" (OES) on a central DC bus, each acting as a node in a multi-agent network to trade energy. One OES can connect to others to form larger networks, each OES acting like a Virtual Power Plant, to form a bottom-up distributed grid. Trading negotiations within an OES are based on battery state-of-charge (SOC) threshold comparisons. During energy exchanges, one node is selected as the master agent, acting as the voltage-controlled reference, while the other nodes act as current controlled sources or sinks. Communication between nodes is accomplished using internet protocol over Ethernet. Computer simulation shows successful trading can lead to 95% utilization of solar resources versus 84% without it [38]. One OES was implemented in a residential village in Okinawa in 2014 and monitored for a year. Public grid connection existed to each home as an auxiliary power source when the OES supply was exhausted. The maximum achieved independence from the grid was 55% and the team observed that although communal energy exchange increased OES capacity, it also added significant losses through increased DC-DC conversions and transmissions during trading [39]. Most importantly, the study highlights an important benefit to distributed storage in

a microgrid. These fast responding energy buffers decrease dependency on the centralized power source and provide each node a degree of energy independence to absorb transients caused by differences between source and load power [38]. Such distribution also increases DSM opportunities.

Interconnected SHSs in [40] form a community microgrid where each customer is allotted an energy daily allowance (EDA). Excess energy is designated a CPR and used to power community loads (*e.g.*, street lighting, tools, public washing machine or refrigerator). Each SHS is controlled by a PAYG smart meter. The EDA establishes a load limitation thus eliminating demand uncertainty whilst providing a clear expectation to the customer who must budget that allowance accordingly. It also eliminates the problem of certain customers unfairly consuming a centralized storage capacity.

2.2 Microgrid Cost

Despite the need and demand for decentralized microgrid electrification solutions in the developing world, there are few cases of successful commercial endeavors and very little data to inform such projects. In Kenya, there are examples of IPPs that have deployed unsubsidised microgrids [24]. These examples shed light on the expected load profiles, customer WTP, BEP, and LCOE. The aforementioned PowerHive builds hundreds of microgrids with smart meter technology to remotely monitor consumption and tariff electricity via mobile money applications [41]. Similarly, Vulcan Inc. invested in 10 solar microgrids in rural Kenya starting in 2014 [25]. The goal of the initiative is to prove the financial viability of unsubsidised remote microgrids to provide electricity to low-income Africans. Each grid consists of a 1.5-8.6 kW solar array with battery storage deployed by PowerGen to serve 12-60 customers. Electricity is metered and monitored remotely with SteamCo smart meters and tariffs are collected via mobile money. In 2017, Vulcan estimated 34.3 years average BEP based on payback rates. The report suggests several strategies to reduce the BEP and increase the IRR:

1. Reduce capital costs,

2. spur energy demand growth, and
3. provide startup subsidies to customers to serve as loans for low-income participation.

These findings are consistent with the obstacles discussed in 2.1. One of the objectives of this study is to demonstrate that the addition of a digital communication system can reduce capital costs and aid in spurring energy demand growth. The results of these IPPs demonstrate that deploying sophisticated power systems to remote communities is extremely difficult.

2.2.1 Willingness-to-pay

Rural customers in SSA have been found to be willing to pay up to $4/kWh [6], [30]. Survey data of in [42] show customers paying between 2-24% of their income for off-grid PV system electricity which equates to approximately $8/month. The WTP for grid connected customers was very similar. They also found PV customers preferred isolated PV systems over the grid due to their superior reliability when compared to the fickle grid electricity. They suggest not exceeding 10% of income which is also echoed in [3] who suggest anything above 20% would require subsidies. Later in the report "affordable" electricity is defined as 5% of income. As a specific example, [43] reports the average wage of rural Kenya at $124/month. Most of these do not have electricity, but those that do pay around $6/month ($\sim$%5 of income) as compared to the average $9/month for urban grid users. Wages in the RELCON target community in southeast Kenya is much lower at $65/month [19]. Non-electrified rural homes spend on average $22.50/month on energy (18% of income) including $9/month for cell phone charging and disposable or rechargeable batteries and another $13.5/month on kerosene or other combustibles for heat and cooking [43]. Electricity can potentially displace these expenses. Customers are willing to pay beyond the affordable threshold of 5%, but may still lack sufficient income to pay the market value of an energy system. This is evidenced by Vulcan's experience, struggling to achieve reasonable BEP lifetimes caused by unpaid bills [25]. SHS companies also experience high levels of payment delinquency. Survey

data from [44] reveal that despite effective marketing techniques and high demand for off-grid renewable energy systems, only 20% of surveyed SHS customers in [44] made payments on-time and 30% eventually defaulted. They found that WTP for solar kits was 30-41% below market value.

2.2.2 Solar Home Systems

SHS companies typically charge customers using a lease-to-own program over 1-5 years. Most SHS systems can only provide Tier 1 or 2 electricity (see 1.1) but their success offers a glimpse into the energy market, WTP, and energy system business models. Mobisol (now ENGIE) and M-KOPA sold thousands of SHS in the past decade in Africa. SHS companies are essentially micro-loan services. A typical SHS from M-KOPA costs $200, far too expensive for most rural Africans. Therefore, customers pay a $35 down payment and then make daily payments of $0.45 for a year [45]. The kit includes a solar panel, battery, LED bulbs, flashlight, radio, and phone charging adapters. The inclusion of appliances is the core ingredient for the success of the SHS boom since it attempts to remedy the difficult problem of low consumption discussed in 2.1.3.

After subtracting the cost of the appliances (∼$45) and using the Bboxx estimate of 55 Wh/day from [37], this equates to approximately $8/kWh. Although this is much higher than the WTP thresholds discussed previously, SHS companies have found success in a particular demographic of higher income rural and peri-urban families [44]. Although the LCOE of SHS is extremely high, over time, the customer will own the solar kit and no longer make payments, reaping the benefits of displaced costs for upwards of 20 years. If the cost of the lease is spread across the entire life of the SHS, the LCOE plummets to approximately $0.65/kWh (assuming lithium-ion battery replacement every 3 years). Marketing strategies focus on long term displaced cost, but low income customers still lack the short term capital to afford the down payment and the daily payments (which accumulate to $13.50/month). Ideally, the SHS initiates a domino effect of increased energy demand and economic activity to further reduce the LCOE which is why SHS is often considered an

entry level energy system [46]–[48]. This introduces the challenge of load profile estimation to properly size a remote energy system.

2.2.3 Load Profile

There are a myriad of software tools to size microgrids as discussed in 2.1.4. Various rural load profile curves are provided from the literature review in [49]. The focus of the review is to establish curve shapes by looking at rural samples from around the world to fill the gap of data in rural Africa. They provide a function for rural African residential electricity consumption:

$$P_{\text{load}} = e^{\sin(0.3409 - \sin(0.68039t) - 0.16801t)} [\text{W}] \tag{2.1}$$

where t is the time of day [49]. The shape can then be scaled to fit local amplitudes. The review also includes an estimate of 150 kWh/year (484 Wh/day) for a rural African customer not using electricity for cooking (*i.e.*, Tier 3) [49]. If Eq. (2.1) is scaled by 0.0235, it provides a load profile to reflect this type of customer in Fig. 2.1.

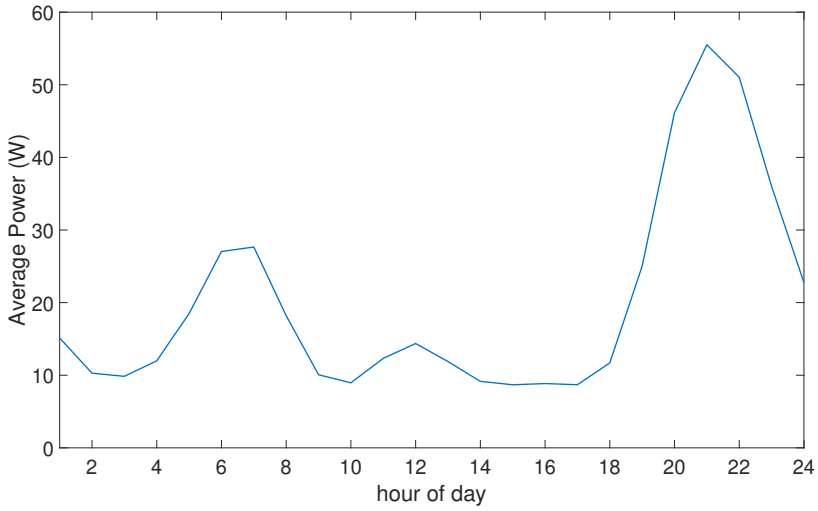

Figure 2.1: Rural Africa Tier-3 residential household load profile adapted from (2.1) [49].

A Tier 3 load is defined in [3] as consuming a minimum of 365kWh/year which equates to 1 kWh/day. However, the companies installing Tier 3+ microgrids in rural communities are not seeing these numbers, at least, not initially. PowerHive customers consume just under 300 Wh/day [41]. Similarly, SteamCo customers consume

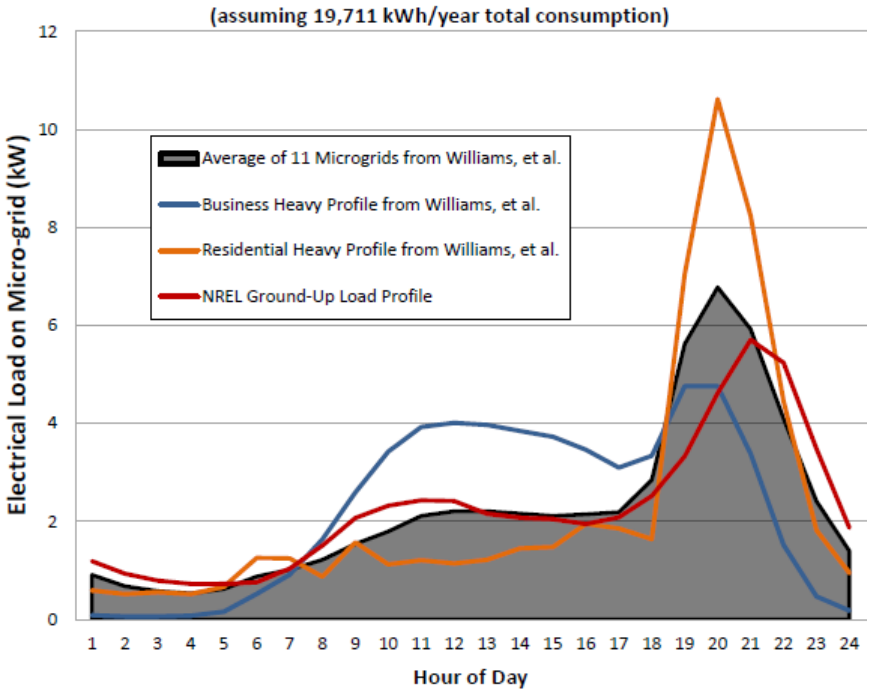

Figure 2.2: Average microgrid load profile reproduced from literature review in [26].

less than 250 Wh/day [25]. Survey data from five rural Nepali microgrids (including two PV-based systems) show a wide range of consumption (80-400 kWh/year) [50]. Data shows increased consumption as energy prices decrease. Smart meters with remote monitoring, remote isolation and peak limiting were utilized in both PV microgrids, but little data was collected as to their effect. Survey questions indicated that customers with a smart meter were more aware of their consumption and its effect on the grid than the traditional metered customers. KPLC public microgrid customers use between 50-100 kWh/year [27]. Using data from 11 PowerGen Tier-4 microgrids in Kenya and Tanzania, [51] creates a generic rural load profile for HOMER sizing software. Consumption ranges vastly between 0.6-40 kWh/day. They also show that some PowerGen customers' consumption actually decreases over time. Another helpful model of Tier 3 consumption in [52] predicts daily consumption of 187 Wh without base loads (*i.e.*, loads that consume continuously like a fridge) and 1178 Wh with base loads. These models were generated using Tier 2 consumption data from a community with access to a solar hub charging kiosk in rural Kenya. The literature review of rural load profile creation in [26]

concluded that residential users consume 136 kWh/year (373 Wh/day). Commercial users were closer to the Tier 3 definition at 1214-1961 kWh/year depending on the size of the enterprise. Included in the review is an averaged graphical depiction of the load profile expectation of a microgrid in Fig. 2.2.

2.2.4 System losses

In addition to the customer load are technical and non-technical losses (NTL) itemized in [53] as:

1. Technical
   (a) System Losses
   (b) Transmission and Distribution (T&D) losses
   (c) Customer minutes lost (CML)
2. Non-technical
   (a) Theft
   (b) Unpaid bills

In SSA, up to 50% of generated electricity is lost [54]. This is echoed in [55] with some examples. In India 35% of generation was lost in 2005 with 10-15% due to technical factors with the remaining 20-25% due to NTL. Bangladesh offers another perspective reporting 35% losses, 21% from technical factors and 14% to NTL, Africa's utilities losing 20% total (half of which are from T&D [56]), or Indonesia reporting 7-12% losses from theft alone [53]. Another study estimates the fraction of losses attributed to NTL in Africa at 11% and offer ways to detect and classify NTL in microgrids [57]. One of the African countries surveyed in [56] (Cameroon) reported losses of 45%. Detailed information is given on Jamaica with recent losses at 26%, 17% of which are NTL. Many more examples are given in [58] including 31% total losses in Liberia, 15% NTL in Colombia, 5% loss due to theft Brazil, and 18% loss from theft in Jamaica. Customer minutes lost is the duration of electricity service interruptions per year that a customer experiences. From the utility's perspective, these are periods of lost revenue and they decrease IRR. National grid customers in Kenya experience 216.3 hours (9 days) of lost electricity

per customer per year according to [59]. One advertised benefit of microgrids is a drastic reduction in CML. Microgrid CML is estimated by [60] as 16.2 hours per year per customer. When designing a microgrid, system sizing must account for losses or the system could be inordinately undersized and the tariff will be too low to recover capital costs. DSM can reduce losses through AMR, prepayment tariffs, and control mechanisms to detect anomalies and either isolate or correct them [54].

2.2.5 Levelized Cost of Energy

KPLC operates and subsidises 19 microgrids that average $1000 per connection with average tariffs of $0.56/kWh compared to $0.12/kWh for a macrogrid customer using less than 1500 kWh/year [27]. As of 2017 there were 21 IPP microgrids in Kenya with CRTs averaging $0.80/kWh. The IPP SteamCo in Kenya provides a 24-hour service Tier 4 capable grid charging customers an average monthly payment of $6.75 which equates to an average LCOE of $2.54/kWh [25]. PowerHive monthly payments average $4.25/month and average consumption of 7.5 kWh/month resulting in an LCOE of $0.57/kWh [41]. Microgrid capital costs in Kenya average $1430 per customer [30]. This is on par with the $1400 required for a national grid connection in Zambia [26]. Cost analysis in [6] recommends at least $1.70/kWh for 24-hour service Tier 4+ grids in order to achieve 20% IRR based on experiences like those of PowerHive and SteamCo in Kenya. The main reason for inflated LCOEs arises from the customers' under-consumption notwithstanding the capacity of the system. In theory, LCOE would drop over time as customers increase consumption [46]–[48].

Simulations always tend to underestimate LCOE mainly because they do not account for all the installation, logistics, and labor costs. But they are still worth exploring. Models in [26] estimate microgrid LCOE between $0.70/kWh to $1.70/kWh for Tier 4 microgrids. The simulation in [61], published in 2018, estimates decentralized Tier 5 90% reliable microgrid LCOE for SSA between $0.40-0.60/kWh. They show that this price increases by 10-15 cents to achieve 99% reliability. It is important to emphasize that these prices depend on Tier 5 consumption. Additionally, they postulate that the price of energy will drastically

fall by over 50% in the next few years due to advancements in PV and battery technologies and manufacturing. Their price estimates for solar ($0.60/W) and batteries ($100/kWh) have largely come to pass and are the estimates used in this study. Tariffs for the Nepali grids surveyed in [50] range wildly between $0.04-$0.98/kWh. This range encompasses both public and private projects and several community owned grids. Those owned by the community have very low tariffs, just enough to cover the cost of maintenance. Capital costs for these projects were likely covered by philanthropy. The simulation in [62] estimates LCOE at $0.35/kWh for a Tier-2 DC microgrid (similar in design to RELCON) with distributed battery storage at each smart meter with power electronic power management control systems. An example PV-battery microgrid model was verified by a government funded field experiment in India. The system provides 6 hours/day of electricity capped at 100W per customer resulting in an LCOE of $0.63/kWh [63]. They conclude that a 24-hour service is cost prohibitive. Peak power and time limits are a very aggressive form of DSM in order to make energy affordable. As mentioned earlier, Tier 2 SHS cost approximately $0.65/kWh when the cost is spread across 20 years. Based on this review, a Tier 3 microgrid should expect a LCOE between $0.60-$1.00/kWh.

2.3 Demand Side Management

As shown in Fig. 2.3, the DSM strategies listed in Section 1.3 are used to shape demand to better match generation [9]. EE actions seek ways to lower demand,

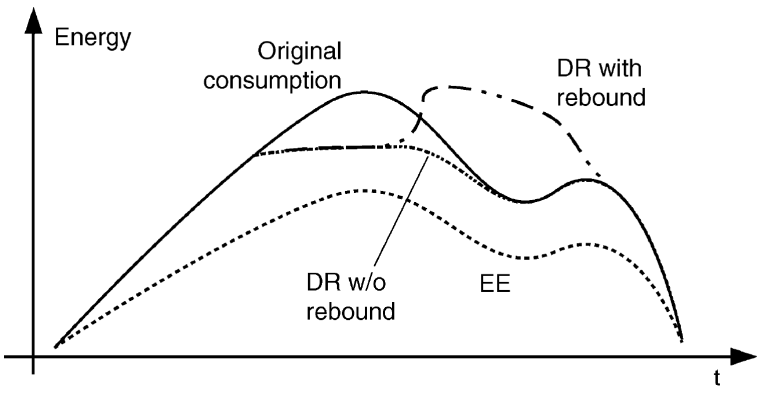

Figure 2.3: Impact of DSM on shape of daily load profile curve reproduced from [9]

typically accomplished through education or incentive programs. Utility inspections of load facilities or remote power monitors can identify outdated, malfunctioning or inefficient equipment or settings. Advanced smart meters, training, and monetary incentives amplify customer awareness of power usage leading to more efficient behaviours to decrease peak magnitudes and flatten the load demand curves [64]. These methods are not especially important in a rural microgrid context since demand is already so low. However, as discussed earlier, microgrid developers can provide appliance acquisition programs where customers can buy or lease efficient appliances. Furthermore, microgrid developers can offer education on DER limitations to encourage power usage during periods of production, and then offer monetary incentives to solidify such efforts [50]. Energy consumption education can include basic understanding of the electrical system and reminders to monitor energy meters, turn off appliances after use and energy budgeting [65].

Market DR aims to manipulate demand through tariffs and incentives. Usage during high demand is monetarily penalized while peak production periods offer discounts. Tariff structures typically include charges for one or more of the following [24]:

1. Connection fee
2. Flat rate
3. Energy tariff
4. Peak power tariff

In order to reduce monthly charges and quickly absorb some of the cost of expensive power systems, utility companies sometimes charge new customers a connection fee [45]. As discussed earlier, connection fees impede many lower income customers the opportunity of electrification [28]. There are some programs to lower entry costs through subsidies, otherwise the utility can amortise the fee [27]. Flat rates are fixed charges per pay period (*e.g.*, month, week or day). Depending on the electrification contract, rates may vary between pay periods, but they do not vary within a pay period. In reality, they are usually energy or peak power tariffs

(described shortly) averaged and hidden in a flat rate. The main advantage of a flat rate is its simplicity; however, it can lack flexibility to enable DSM.

The most common tariff is an energy tariff, or a charge per unit of energy consumed measured in $/kWh. Energy tariffs can be fixed or vary with time-of-use (TOU) [24]. Complexity can even extend to real time pricing (RTP) where customers are charged according to live changes in the energy market. Such complexity requires sophisticated smart meters and is only widely used with large industrial users under detailed contract with their utility [9]. For a microgrid in a rural community, RTP may not be necessary or even feasible. Rural microgrid energy tariffs are also difficult to set since low income rural customers use such low levels of energy, inflating the value of energy. Energy tariffs are normally post-paid, but PAYG systems are becoming more common, especially in the rural African context where mobile money applications combined with smart meters enable prepayment for energy.

The last market DR technique charges users for maximum power consumption or $/W. The tariff increases as a user's peak power demand rises into higher power levels designed to discourage large consumption peaks [24]. Such tariffs are also often post-paid, but can also take the form of a flat rate which caps users to a certain power level via a triggered auto-disconnect. Utilities can combine market DR techniques [9].

When market DR insufficiently balances generation and consumption, or the utility wants greater influence, they apply physical DR measures to curtail the load [9]. Some curtailments are forecast based on trends or triggers allowing for customer coordination. Emergency curtailments are needed if unexpected load spikes, generation failure, or distribution faults cause grid instability. Predetermined loads, which are often agreed upon via contract, can be shed to prevent brown or black out. Smart meters and smart appliances have expanded physical DR options allowing for utilities to create virtual storage through targeted load shedding. Dynamic load shedding can shift peak demand to a different time of the day but rarely can eliminate the peak completely as seen in Fig. 2.3 [9].

This leads into the idea of spinning reserve. It usually refers to inertial storage in rotating AC generation systems, but can also encompass any type of network

energy storage that can absorb load transients or supplement generation when demand exceeds production. As discussed in Section 2.1.4, distributed storage assets can rapidly respond to load transients [38]. Controllable loads can be shed or added to support voltage or frequency fluctuations [9]. PV microgrids do not have rotating inertia but rather derive spinning reserves from storage or backup generation. Different time scales require different reactions. For example, certain inductive loads may demand high inrush currents when first plugged in. A diesel start-up would be too slow to react to such a request, but it could be activated for longer-term shortages or scheduled as grid support for a forecast shortage [66]. A running gen-set can also act as rapid spinning reserve in emergencies. In microgrids with high levels of power electronics (*e.g.*, parallel inverters), rapid response from DC-DC link capacitors can be used to prevent voltage sag or system collapse[66].

2.3.1 Case Studies

The techno-economic analysis in [67] models a small rural microgrid and then simulates the cost reductions possible through hierarchical control of loads. Certain loads are deemed critical and awarded near 100% power delivery reliability. Other loads are classified as non-critical with reduced reliability. They project a 26% reduction in capital costs using this form of DSM. Another detail to note is the per-home cost estimate of $108.41 leading to an LCOE of $0.38/kWh. This estimate is lower compared to other studies primarily due to the lack of accounting for real-world installation and labour costs. For example, the estimates for cable and power converters are an order of magnitude lower than current market averages. However, their estimates of PV and battery costs are well formulated at $0.78/W and $0.10/Wh respectively.

DSM is often associated with the concept of the *smart grid*. The US Department of Energy defines the smart grid as “an intelligent electricity grid, one that uses digital communications technology, information systems, and automation to detect and react to local changes in usage, improve system operating efficiency, and, in turn, reduce operating costs while maintaining high system reliability” [68]. Smart

meters located at each load are the backbone of the smart grid. The promise of the smart grid from [69] is a 20% reduction in peak load demand. Additionally, it claims that pilot projects have reaped 7% EE consumption reductions due to IHD and up to 13-15% reductions when combined with pre-pay schemes [70]. These are averages of 21 projects which lasted several years to only a few months. It is unclear whether reductions can be sustained. This is echoed in [71] during various case studies all over the world that found a 5-15% consumption reduction due to IHDs displaying current and past usage. Researchers in [72]–[74] caution that these reductions are not consistent, customer interactions with IHDs are not fully understood, and the benefits of IHDs are exaggerated. Their case studies show very negligible changes in consumption. This ambiguity may explain why IHD technology, implementation, and acceptance has stagnated. A thorough meta review of IHDs in [75] lists lessons learned. Most helpful to a rural microgrid designer is that the IHD should be customized to the audience and communicate consumption using well understood and simple motivators (*e.g.*, instead of numerical displays of kWh, using traffic-light color indicators of energy translated into a monetary balance). Based on this mixed review, microgrid developers can expect only modest changes in customer behavior due to energy feedback through the IHD. However, DSM strategies hold promise of significant cost savings which are partially enabled by the IHD. In other words, the IHD in of itself is not a game changer, but it can be an integral tool to implement market DR measures.

The extensive review of DSM literature in [64] lists implementations of DSM in software and hardware, mainly in modern macrogrids. Expanding on the list of tariff structures listed above, the review details the various DR classifications:

1. Physical DR
    (a) Curtail: utility turns off or reduces load in accordance with contractual agreement,
    (b) Industrial response: largest consumers interrupt non-critical processes,

(c) Commercial: taking advantage of thermal inertia of buildings; adjusting HVAC variable frequency drives; smart buildings that react to RTP; scheduling demand to optimize consumption,

(d) Residential response: home energy management systems control appliances to schedule consumption or provide frequency grid support, and

(e) electric vehicle to grid: charge cycles regulated to either take or give depending on grid needs.

2. Market DR

(a) incentive: utility pays or discounts user for load reduction,

(b) bidding: customer sells energy from local generation or through load reduction,

(c) time-of-use (TOU): tariff step changes to reflect supply cost of electricity,

(d) critical peak tariff: temporary price increase during critical periods, and

(e) real time pricing (RTP): live or day ahead tariff structures

This list is echoed in [76] with estimates of DR benefits that suggest DR measures can reduce peak to average (*i.e.*, flattening the load curve) consumption by 10-30% demonstrated by case studies using varying complexities of TOU and RTP algorithms. As explained by [9], peak reductions typically cause rebounds as illustrated in Fig. 2.3. Therefore, peak reductions can be seen more accurately as demand shifting. The algorithm in [77] shows demand shifting in an autonomous microgrid can reduce total load by 1-2%. Simulations in [78] yield similar results where capital costs of a grid-tied DC microgrid are reduced between 2-8% by shifting demand 10-30%. Lastly, an optimisation exercise in [79] applies demand shifting combined with an multi-agent system (MAS) control algorithm to minimize customer cost in grid-tied microgrids. Demand shifting reduced costs by 15% in a residential microgrid and then reduced costs an additional 4% (19% total savings) when incorporating MAS control. The authors compare their results with other algorithms in [80] that achieved 5-15% energy bill savings for customers. Using similar demand shifting techniques combined with other DSM measures,

[81] boasts a 22% reduction in the customer's energy bill using a game theory control algorithm in a grid-tied 100-home smart grid simulation. Another demand shifting simulation in [82], [83] estimates a 12-15% decrease in capital costs in an rural African grid-tied microgrid.

DSM can specifically address NTL. Various studies show the reduction of NTL through the installation of prepaid meters. NTL were almost eliminated for one Rwandan utility between 1998 and 2008 with the installation of prepayment meters [84]. Another Rwandan study found a 70% decrease in NTL with prepaid meters [85]. The same study NTLs dropped by 13.2% for a Ghanan utility with prepaid meters in 2019 [86]. AMR can also potentially reduce NTL by 20% [85]. Remote meter reading can also reduce CML [87].

The comprehensive UK study in [88] provides a cost benefit analysis of a smart meter upgrade program for a macrogrid utility. It begins with a cost breakdown including estimates for the hardware: $44 per smart meter, $52 for a prepaid meter, and $9 for a traditional analogue meter. Prepaid meters are estimated to cost between $35-$50 in [89]. The communication hardware (GSM-based) are $34 per meter and the IHD costs on average $18 [88]. Smart meters are estimated to consume 2.6W more than an analogue meter. Biannual readings of analogue meters cost approximately $4.40/year. The study calculated that low risk smart meters must be physically checked every five years costing $0.47/year and high risk meters are checked every two years bringing the cost up to $0.64/year [88]. The smart meter is projected to reduce demand by 3%, theft by 10%, and CML between 5-35%. The meter will enable between 1-60% demand shift over 15 years [88].

2.4 Communication

Communication requirements for microgrid control are organized into the three hierarchical layers: primary, secondary, tertiary [90]. Primary control occurs at each converter to maintain local voltage and frequency [91]. Secondary controllers restore global set points after a disturbance which can be done either through communication signals from a central controller, peer-to-peer exchanges distributed

throughout the network, or via *communication-less* decentralized decisions [92]. Each of these secondary methods have advantages and disadvantages. Tests are performed in [90] to compare grid stability with and without secondary control. The distinction between grid-forming and grid-following controllers is the focus of [93] which highlights the stability challenges associated with communication-less methods, especially during step load changes or islanding events. Simple microgrids with unidirectional power flow can operate without communication relying on only local primary controllers. However, power sharing and complex network configurations require secondary control and, most often, need communication to facilitate it.

The review in [94] provides a list of various types of microgrids and methods of controlling them. It highlights the need for communication for secondary control except in decentralized well-defined grids. Methods of communication-less secondary control are compared in [95]. They recall the disadvantages of adding a communication system: added complexity, latency and data loss, which can all cause control issues. The communication-less droop control method proposed in [96] actually does use a form of power electronic powerline communication by injecting a small AC signal into the converters that shares a global set point to the grid. A truly communication-less method for an AC grid is given in [97] but is limited to a network with a common shared bus. An example of a distributed secondary control MAS using a uni-directional controller area network (CAN) bus is explored in [98]. Another distributed method described in [99] measures the effect of latency and data packet loss on grid stability. Researchers in [100] advocate for the addition of communication to avoid circulating currents, slow dynamic response, and instability issues inherent to communication-less droop methods. Despite the added complexity, they argue that communication unlocks the full potential of microgrid performance.

Tertiary control handles both short and long term power balance and energy management decisions for the microgrid [101]. This higher layer of control can be used to assist secondary controllers to optimise power sharing as in [102]. Tertiary control manages grid-tied power flow and islanding decisions [103] and are responsible for power quality through appropriate compensation [104]. Therefore, tertiary

control is often referred to as an EMS. They are generally not required for basic microgrid functionality and vary in complexity depending on the needs and budget of a particular microgrid. EMS tasks are listed in [105] and include harvesting data to make optimisation decisions through forecasting, scheduling, and interactions with the customer. DSM strategies discussed in the previous section are tertiary functions [64]. Therefore, the tertiary control is used to implement the smart grid concept by coordinating reactions to real-time energy prices, weather forecasts, and sensor data to manage the grid down to the load specific level [106].

2.4.1 Requirements

Communications latency and data rate [107] are key considerations for microgrids. Reliability is often mentioned, but communication transmissions must be near 100% reliable for serious consideration in an energy system design, eliminating this as a delineating factor [13]. Latency requirements for hierarchical control decrease moving up from primary to the tertiary control level as shown in Fig. 2.4 reproduced from [108] and are also listed in [92] and echoed in [109].

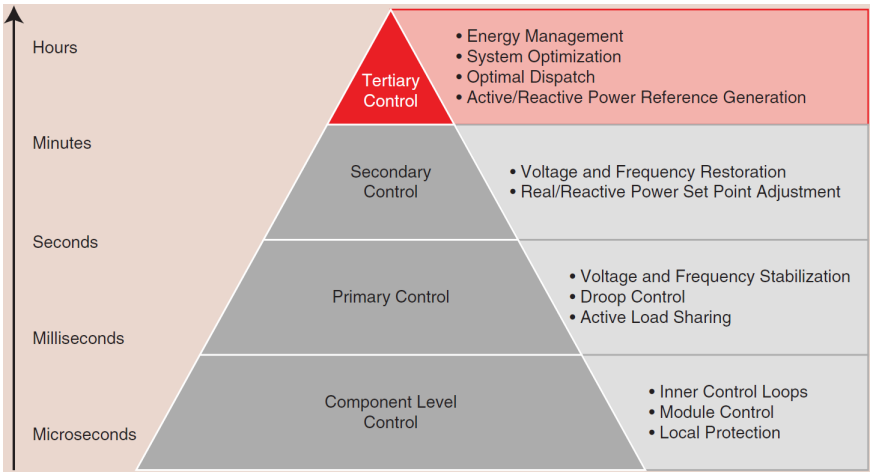

Figure 2.4: Time response for hierarchical microgrid control reproduced from [108]

Protection requires sub 10 ms latency and should not rely on communication. Secondary control requires sub 100 ms latency. Both [92] and [109] list requirements for tertiary functions such as monitoring and DSM which need latencies between 1 second to several minutes and bit rates from 10 kbps to

100 kbps. More guidance on tertiary requirements are found in [107] and [13] with similar numbers. It is important to note that these are specifications for grid-tied microgrids or even smart macrogrids. Sources of delay originate from signal propagation, message traffic queuing, data processing, and serialization [11]. Delays are exacerbated by large transmission distances, network complexity, intersections and re-transmission requests [64].

2.4.2 Technologies

There are two primary mediums for digital communications: wired and wireless. Within wired technologies are dedicated cables and PLC. Wireless technologies vary from short to long range and can be either wholly-owned by the microgrid utility (*e.g.*, LoRa, Zigbee) or provided by a third party (*e.g.*, GSM, 4G). These technologies are compared in [110], [111]. Generally, dedicated cable technologies (*e.g.*, fibre, coaxial, twisted pair) have high bit rates above 100 Mbps. NB PLC achieves less than 500 kbps and BB reaches above 1 Mbps. Generally, wireless technologies perform at less than 1 Mbps with a few exceptions (*e.g.*, WiFi). Cellular capability depends on technology generation. The most likely in a remote area of SSA is GSM with rates less than 100 kbps. Similar rates are echoed in [12], [112]. Latency for various technologies is calculated with a model in Table II of [113] based on the physical limitations of the mediums. This table provides a good first order estimation of latency and shows that wired technologies inherently are faster with latency less than 1 ms. PLC and wireless depend heavily on protocol but typically have latency greater than 1 ms but less than 1 s. WiFi can have latencies below 1 ms, while other short range wireless technologies have values between 1-20 ms. Latency decreases with each generation of cellular technology: GSM between 4-16 ms and 4G less than 0.1 ms. Advantages and disadvantages of each technology are inventoried in [92]. Most notably, wired technologies tend to be more reliable but more physically complex, whereas wireless methods are easily scalable but susceptible to interference.

2.4.3 Field Area Network

Similar to microgrid control, communication networks are organized in hierarchical layers [114]. Within a home or business, interconnected DERs and loads share a home area network (HAN). A collection of HANs and DERs in a community form a field area network (FAN) (also often called neighborhood area network (NAN)) which overlays the microgrid power network. Connected FANs constitute nodes in a wide area network (WAN) through which a utility interacts with several microgrids or distribution networks. Technological requirements increase moving up the hierarchy as shown in Fig. 2.5 reproduced from [100]. Detailed descriptions of each layer are in [13]. The smart grid concept extends through all 3 layers [17]. In remote islanded microgrids, the network of most interest is the FAN which facilitates all three levels of microgrid control. Fibre optics and cellular technology are commonly used for WAN communications, and wireless radio solutions and PLC for FAN.

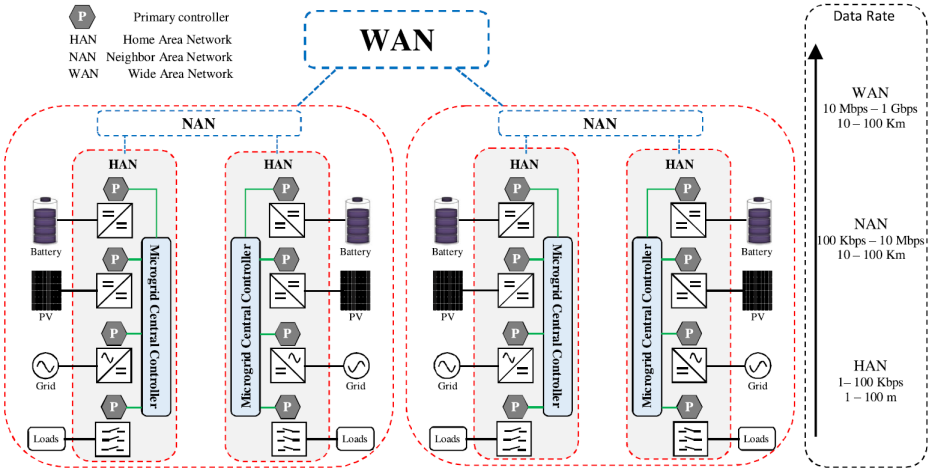

Figure 2.5: Communication requirements for hierarchical microgrid control reproduced from [100]. The FAN is labeled neighborhood area network (NAN) in this diagram.

DSM requires a robust communication network to enable utilities to interact with loads. Recent advancements in AMI along with the development of smart meters have given rise to growing DSM opportunities [64]. These technologies have enabled transmission system operators (TSO) and distribution system operators (DSO) to implement DSM contracts with large industrial users who offer reliable and rapid DR options for grid stability. Widespread use in the residential sector

has yet to become a reality mostly due to the inflexibility of such users combined with limitations in communication network capabilities. High fidelity load control requires bidirectional communication between the utility controller and the load [11].

2.5 Power Line Communications

PLC can be used for all three layers of the hierarchical network structure pictured in Fig. 2.5. By using existing power cables as the communication medium, PLC eliminates the need for additional communication cables and avoids the myriad of challenges that come from radio wave communication (environmental dependence) [115]. However, power cables are designed to transmit power, not communicate information and therefore they are subject to various sources of electromagnetic interference (EMI) and noise (radio-electric and non-intentional emissions (NIE)) [12]. PLC was extensively used to form WANs by power utilities on AC grids for long haul protection signalling prior to the adoption of fibre optics. Contemporary uses of PLC vary widely, such as the formation of internet HANs [116]. It is also being adapted by utilities to form FANs that monitor smart meters and potentially smart devices (*e.g.*, electric vehicles (EV)) opening up a new frontier of AMI and smart grid for more prevalent and complex DSM implementation. Generally, PLC is "technically inferior" to other mentioned methods, purely because it cannot achieve equivalent data rates in comparable frequency bands as other methods [117]. Despite its disadvantages, Narrowband PLC (NB-PLC) dominates macrogrid smart metering because it operates on pre-existing and pre-financed infrastructure while providing sufficient data rates ($< 1\,\text{Mbps}$) and distances (1-2 km) to achieve monitoring objectives [116]. The utility owns and controls the communication medium, transmitting on dedicated and licensed frequency bands according to established standards, and they can reliably reach meters that are hidden deep inside of buildings or far into rural areas without cellular coverage [117]. The choice of communication medium depends on the application, budget, and system constraints [64]. PLC is an attractive option in a rural microgrid context where low cost and system autonomy are paramount.

Research reveals three main categorizations of PLC based on data transmission rates:

1. Ultra Narrowband PLC (UNB-PLC)
2. Narrowband PLC (NB-PLC)
3. Broadband PLC (BB-PLC)

These transmission rates generally align with the hierarchical network layers because as bit rate increases, range decreases. Using single carrier frequency modulation techniques such as spread frequency shift keying (S-FSK) below 3 kHz and data rates less than 1 kbps, UNB-PLC can be used for long haul communications to read remote meters and is currently used for basic DR in North America [12]. Two common NB-PLC popular standards for smart grids are PRIME and G3 which operate in the CENELEC and FCC bands (35-487 kHz) and modulate data using multi-carrier techniques like orthogonal frequency division multiplexing (OFDM) achieving data rates up to 1 Mbps. Broadband PLC (1-250 MHz) is widely used for internet HAN and has the inherent disadvantage of low transmission distance (< 300 m) [118]. However, it offers data rates comparable to wireless solutions (> 1 Mbps) [119].

2.5.1 Homeplug

Various affordable commercial routers are available such as HomePlug standard compliant plug-and-play products [12]. Although other standards exist, they are all very similar in nature and the following discussion will focus on HomePlug AV that is designed primarily for high bandwidth (200 Mbps) applications like internet over power line including voice and video data.

It is organized in network layers, as shown in Fig. 2.6, starting with a physical layer that modulates digital data using binary phase shift keying (BPSK: 1 bit per subcarrier) up to quadrature amplitude modulation (QAM: 1024 bits per subcarrier) based on the strength of each subcarrier channel (called adaptive bit loading (ABL)) [120]. The modem then distributes data on multiple orthogonal subcarriers (each subcarrier peak intersects adjacent subcarrier zero crossing) in the frequency domain to form OFDM time domain symbols with added forward error correction (FEC)

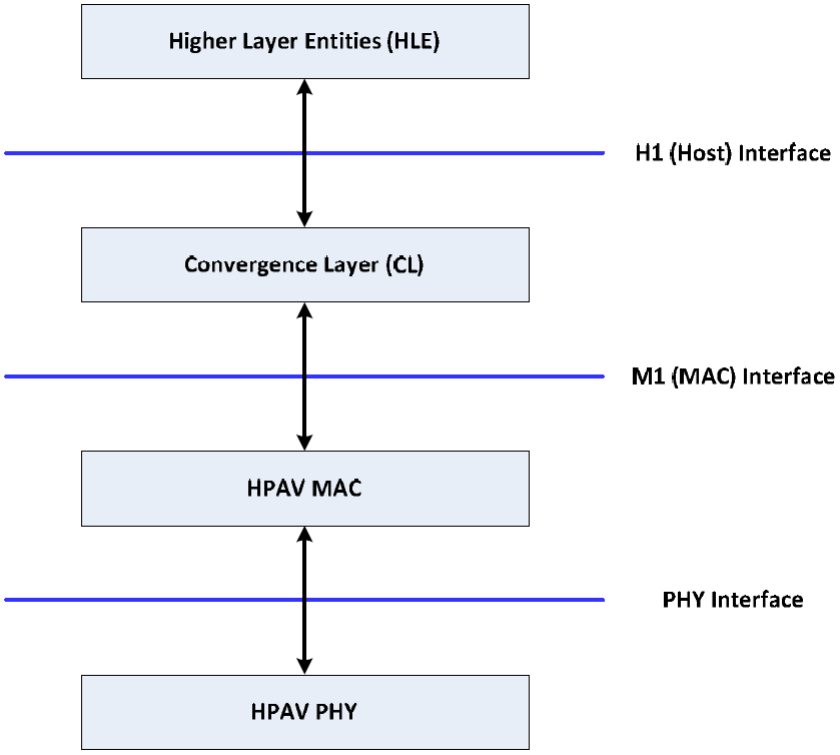

Figure 2.6: Open Systems Interconnection (OSI) block diagram of HomePlug AV protocol standard reproduced from [120]

codes. The MAC layer organizes and prioritizes the data for transmission via Carrier Sense Multiple Access (CSMA) and directs Automatic Repeat Requests (ARQ) to ensure error free data reception (called Robust OFDM (ROBO)). Lastly, the convergence level classifies data with sourcing and destination information [119]. The latest HomePlug technology is the HomePlug GP which reduces MAC layer complexity, lowers the FEC rate and eliminates ABL by limiting modulation to Quadrature Phase Shift Keying (QPSK: 2 bits per subcarrier) on all subcarriers while maintaining ROBO repeat coding. These simplifications decrease cost, power consumption, and implementation size to tailor for lower data rate (< 10 Mbps) smart grid applications [118]. The second generation HomePlug AV2 incorporated many of the GP's standby power modes achieving similar efficiencies and increased the usable band up to 86 MHz to boost bit rates beyond 1 Gbps [15].

2.5.2 Powerline Modeling

Apart from communication protocol focused investigations, PLC implementation research efforts are numerous and mostly focus on channel characterization and modelling [121]. Methods fall into two main categories: top-down models based on measurements of the channel, and bottom-up models based on analytical characterisation of the channel using transmission line theory [18]. Top-down models consider the communication network as a black box characterized as a transfer function derived from probability density statistical analysis of propagation measurements in and out of the box [122], [123]. Such transfer functions contain two primary terms: attenuation and delay [124], [125]. Ultimately, the top-down method requires physical access to the channel for measurements.

Conversely, bottom-up models are built by defining each element of the network by its physical geometry and cascading those elements together with multi-port mathematical matrices (*e.g.*, s-parameters, ABCD) [126]. Deterministic methods derive network port coefficients dependent on frequency, cable length and even time. Parametric models characterize the line as lumped impedances that vary with frequency. Lumped impedances can be cascaded to add accuracy. Propagation models sum attenuation coefficients that affect the channel gain due to multi-path reflections [127]. Method combinations can generate random channel predictions [128], [129]. Time variance due to dynamic loads and noise can be added to either model [130].

PLC must overcome three main obstacles: impedance mismatch, frequency selective attenuation, and noise. All these obstacles can either be permanent phenomena due to the grid structure or vary in time due to dynamic loads, charging cycles, EMI, and transients (*e.g.*, contactor operation, lightning). Noise sources can be native to the network (*e.g.*, power converters, loads) or interference from external equipment (*e.g.*, EMI) [131]. AV and GP use differential coupling which reduces these effects [132]. Performance depends on feeder length and grid topology (*e.g.*, star, radial). BB PLC systems are naturally limited to link lengths of a few hundred meters due to the high frequency attenuation of power cables. Some

carriers may be attenuated further if the feeder length equals a multiple of the carrier's quarter wavelength. Branches on radial feeders cause multipath reflections that can also create deep attenuation notches in the frequency response depending on its length and termination [133].

2.5.3 Case studies

There are some examples of PLC-based microgrid field experiments in the literature. The Lianxiangyuan pilot project features BB-PLC service delivery (on-demand video, IP phone, internet) to several homes [134]. The services are funnelled through the distribution feeder to individual home smart meters, then fanned out to individual appliances where an IHD informs users of power consumption. The project's most ambitious goal is to provide the utility the ability to control individual appliances. The project determined that the community PLC link was not robust enough to sufficiently support all the homes, which motivated a conversion to a fibre link from the distribution feeder to each smart meter in a follow-on project [134].

Another study in [135] demonstrated energy management of a two node PV/battery using PLC G3 protocol to control battery charging states and one LED light achieving data rates of 34 kbps and 3 ms latency. In another two-node experiment from [136] both the HomePlug AV and GP communicated basic ping messages from an inverter to a rectifier along 500 m of 4-core DC power cable. Both inductive and capacitive signal-to-cable coupling were attempted from line-to-neutral (LN) as well as neutral-to-neutral (NN) in a bipolar configuration. The NN results were obviously superior since the two conductors essentially form a dedicated communication channel. The LN results are therefore of more interest and yielded data rates of 3.5 Mbps and latencies around 6 ms. The effect of power converter noise and cable termination impedances are investigated. They propose dedicated cores on star feeders to achieve up to 500 m transmission.

Cascaded s-parameters are used to simulate branched medium voltage radial feeders in [137] and they compare cumulative capacity (in Mbps) of underground cables to overhead lines. The researchers conclude that overhead lines tend to be

more conducive to PLC due to their separation, but buried cables allow higher injection power and help suppress noise, which can equalize performance. They also observe that short branches impair the channel response more than long branches due to quarter wave resonance. Researchers in [138] build complex PLC networks using NS-3, a software tool primarily used by wireless IP-based network simulation. Similarly, in [139], networks are made using EMTP-ATP, a power grid transient simulator. While both offer a GUI and employ the same fundamental TLM, the software isn't readily available and models are not validated by experimental data.

Additional considerations for PLC are the effects of cable burying, bundling, shielding, stubs, loading and input/output impedances of power electronic converters. A buried cable of three bundled cores, PVC insulation and steel armour shielding is considered in [140]. They use parametric methods to determine the effect of grounding schemes on a NB-PLC ($< 500\,\text{kHz}$) signal injected between one core and the shielding by building an admittance matrix for a medium voltage cable with one branch. The frequency responses show notching due to the branch and attenuation of higher frequency signals that worsened with low impedance grounding of the shield. This is to be expected if the signal is essentially shorted to ground.

PLC research also includes improving speeds and reliability of in-home PLC broadband access like the EU Open PLC European research alliance (OPERA) completed in 2008 to advance data rates and commercial product availability for prevalent broadband access in European cities [121]. Commercial broadband PLC products now abound using various standards, mostly intended for plug-and-play application with building AC power receptacles to establish broadband connectivity, typically internet over Ethernet [121].

2.6 Conclusion

The literature establishes the need for decentralized power systems to meet energy demands of the developing world. Microgrids are identified as a potential solution to electrify remote communities. However, system costs have prevented the microgrid from large commercial success in low-income communities. Research

efforts seek methods of reducing both capital and operational costs through smart grid technology like AMR and DSM. Much of the literature assumes the smart grid concept can reduce the cost of a power system. There are also various studies that define smart grid technological requirements. However, the literature lacks a thorough analysis to quantify the costs and benefits of smart grid technologies and whether they can reduce energy cost sufficiently to address sustainability energy goals. This thesis fills that gap with a comprehensive techno-economic investigation of microgrid communication to explicitly define the possible cost reductions through smart grid technologies.

PLC has been utilized in multiple applications in the literature, but has yet to be applied widely to islanded LV microgrid control. This thesis synthesizes the extensive powerline channel modeling research to propose a simple two-wire model that can predict PLC performance on microgrid networks. Since PLC uses pre-existing power cables, it has the potential to reduce the cost and complexity of a communication system. Two PLC technologies are selected as representative samples to evaluate suitability for microgrid control.

3
Demand-Side Management

The primary findings of this chapter have been published in the following publication: D. Neal et al, "Demand side energy management and customer behavioral response in a rural islanded microgrid," in IEEE PES/IAS PowerAfrica, 2020.

Chapter 3 introduces the three levels of microgrid control and expounds on how the levels are used to implement the four DSM strategies. The various communication methods for AMR and market DR tariff structures are systematically developed and their communication requirements defined. The RELCON electrification project is described. A DSM strategy for an unsubsidised remote rural LV islanded microgrid is proposed.

3.1 Microgrid Control

The communication requirements for microgrid control are organized into the three layers of communication: primary, secondary, tertiary [90]. These requirements depend on design specifications. For example, a Tier 2 (see Fig. 1.1) SHS may be designed with minimal complexity to provide low-cost electricity access for a few hours a day. In contrast, a remote Tier 5 electric vehicle charging station mandates high reliability 24 hours a day for a high-power variable load. The SHS presents a simple example where only protection and primary control layers are necessary,

Table 3.1: Per-node communication requirements for LV islanded microgrid control

Control Level	Subcategory	Latency*	Bit Rate*	Service Description
Protection	Decentralized			safety, damage prevention [92]
Primary	Decentralized			voltage, current, frequency regulation [92]
Secondary	Decentralized			voltage & frequency
	Distributed	100 ms	100 bps	restoration, power sharing,
	Centralized	100 ms	100 bps	fault isolation [92], [109]
Tertiary	Monitoring	1 min	1 kbps	AMR, load profile data, control efficiency, design optimization [12], [13], [92], [110]
	Scheduling	1 min	1 kbps	power flow optimization [12], [13], [109]
	Demand Response	1 s	1 kbps	demand reduction, peak shifting & shaving [12], [109]
Additional Services	Firmware Update	1 s	$>$ 10 kbps	remote improvements and upgrades [110]
	Tele-communications	$<$ 100 ms	$>$ 1 Mbps	bundled internet, telephone [110]

*Requirements are per node. Node is assumed to have a local clock

Legend
Communication-less
FAN/direct-WAN

whereas the charging station may need all three layers. Simple protection systems and primary control algorithms do not require any communication and rely on local measurements of frequency, voltage and current [94]. There are many microgrid designs that only require local primary controllers to meet design specifications [29]. The numbers in Table 3.1 emphasize minimum per-node values required in a low-voltage islanded microgrid.

Low voltage power distribution feeder topologies are shown in Fig. 3.1 [141], [142]. The simplest is a star topology, best suited to either single-DER microgrids or collocated DERs that can share a common bus from which individual feeders extend to loads. Although individual feeders may require more total power cable length, the cables can be lower capacity, and each load can be individually controlled from a centralized point of common coupling. Radial feeders consist of a main distribution line with dispersed branches extending from it. Each branch termination is separated

from other terminations by cable impedances thus eliminating a true shared bus. It is often the lowest-cost topology since it requires less cable and associated infrastructure (*e.g.*, trenching or overhead utility poles). The ring topology is actually just a radial feeder that loops back to itself offering redundancy at the expense of simplicity and similarly lacks a true common bus.

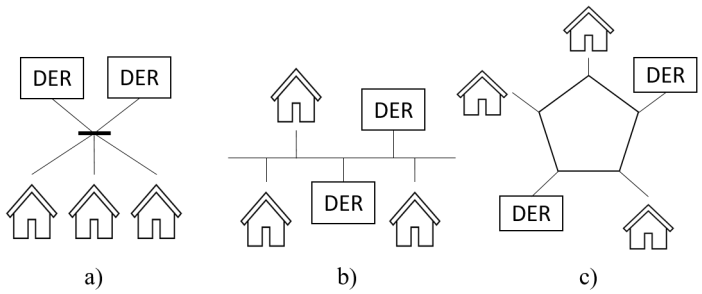

Figure 3.1: Power distribution topologies: a) star, b) radial, c) ring

Microgrid control methods will differ based on topology. Grids with a shared bus voltage often do not need communication in order to maintain operating set points. However, as grid complexity increases, the need for communication also increases as inter-nodal impedances reduce the commonality of shared references.

3.1.1 Primary control and protection

Primary controllers typically operate independent of and without communication from other microgrid elements. DERs and loads connect to the feeder either directly or through power electronic converters (*e.g.*, inverters). Converters step voltages up or down and convert between AC and DC as necessary. Primary controllers adjust voltage, current, and frequency outputs in response to local droop control feedback loops to share active and reactive power demand, mimicking synchronous generator-based macrogrid behaviour [90], [94]. DER converters are programmed to either be grid-forming devices to set the microgrid bus references, or to act as grid-followers [93]. Storage assets often serve as the grid-forming converter in an islanded microgrid until they reach SOC extremes, at which point another converter must assume the responsibility [95]. Since an islanded microgrid cannot rely on a utility grid-tie, in times of shortage or surplus it must be programmed

to autonomously react. The absence of an infinite bus from a stiff macrogrid grid-tie means the microgrid must establish and maintain stable native voltage and frequency references. As distances between DERs and feeder complexity increase, the impedances between them create challenges, necessitating secondary control to managing voltage and frequency stability [143]. Depending on the configuration of the microgrid and the reliability of the grid-forming sources, added communication hardware may not be necessary [95]. In some cases, a communication-less microgrid is sufficient to meet the power system objectives.

Each individual microgrid component must also have local protection mechanisms to protect network infrastructure, power converters, DERs and loads from faults [93]. This primary level protection could include fuses, relays, blocking diodes, filters, and software thresholds within control loops. Protection hardware must react in less than one second and generally does not solely rely on communication links [92].

3.1.2 Secondary control

Secondary control typically requires communication between DERs to provide global references for voltage and frequency restoration following load or supply changes [144]. Secondary control categories may be centralized, distributed, or decentralized [90]. Centralized secondary control relies on bidirectional data links between each DER and an EMS where the reference signals are calculated and then transmitted to each converter [145]. Distributed control methods utilize consensus communication between neighbours. Communication-less decentralized secondary control uses advanced droop control algorithms tailored to specific microgrid configurations, DER combinations, and linear loads [99]. Therefore, decentralized solutions either need detailed knowledge of connection impedances [98] or operate on a star feeder networks where each converter is connected to a well-defined common bus [95]. Radial feeders are more difficult to control due to the transmission line impedances between DERs [97]. Decentralized control may rely on large droop deviations to trigger desired adjustments which can lead to

power quality problems [146]. Another challenge of decentralized secondary control arises from clock drift between isolated controllers [92].

Communication for centralized and distributed secondary control has medium latency and bit rate requirements ($\sim$ 100 ms, $\sim$ 100 bps) since DERs exchange small amounts of data approximately every second [147]. The same communication system can also be used to enhance protection schemes to better isolate faults and avoid full grid failures [92].

3.1.3 Tertiary control

The highest layer of control is tertiary control. It deals with battery management, monitoring, scheduling, and DR [92], and always requires a communication system. In grid-tied microgrids, tertiary control determines when to island and manages the import and export of power from/to the macrogrid. In an islanded grid, tertiary control uses data collection to optimize intra-grid power flow [144]. A backhaul connection to the utility permits remote management. Services provided at the tertiary level are not time-critical and thus generally do not require high bit rates or low-latency.

The following tertiary control functions are of general interest to microgrid operators: [110]

1. *Battery management*: Due to the intermittency of renewable DERs, batteries are often a critical component of a microgrid design. Batteries are expensive and have relatively short lifespans, (3-5 years) [148] compared to other microgrid components (20 years) [30]. Although primary and secondary controllers are directly responsible for charge and discharge schedules, a tertiary controller operates on battery health data (temperature trends, discharge rates) to adjust charge schedules to lengthen battery lifetime [149]. Tertiary controllers also determine when batteries should be allowed to exceed nominal tolerances (*e.g.*, to maintain supply to critical loads during generation shortages).

2. *Scheduling*: Live and forecast inputs from weather, generation status, storage status, and fuel prices can trigger tertiary controllers to adjust DERs and load scheduling. Set points can be adjusted to optimize DER efficiency in response to weather or demand peaks. Power quality compensation measures are controlled at this level (*e.g.*, dynamic filtering and power factor correction) [81].
3. *Data collection*: Operational data from DERs informs control and maintenance decisions. DER monitoring allows utilities to manage power system health and establish preventative maintenance schedules (*e.g.*, cleaning of PV panels). AMR naturally facilitates the collection of consumption data which influences future system designs and market strategies through trend analysis. Monitoring sample frequency should be at least hourly in order to build load profiles of sufficient resolution for DSM strategy formulation [12].
4. *Demand Response*: Physical DR actions are taken by tertiary controllers enabling the utility to directly manipulate demand. For example, high-demand commercial loads can be scheduled for periods of high irradiance in a PV-based microgrid. Non-critical loads can be shed in periods of generation shortfall and low battery SOC. Measures can be executed to satisfy both short and longer term grid needs typically in accordance with pre-contracted agreements with customers. Market DR is accomplished through tariff structures designed to shape demand patterns. Physical DR curtailment actions and tariff schedules should be displayed to customers either through an IHD or a UEC web-based application [13].

3.1.4 Demand-side management strategies

Returning to the list of DSM strategies in Section 1.3 (SR, physical DR, market DR, and EE), the communication system gathers information, assimilates it, and executes control actions through the integrated hierarchical control structure to manipulate demand patterns. The DSM strategies are discussed in order of latency and bit rate communication requirements as outlined in Table 3.1. In a low voltage islanded

microgrid, SR actions are automated by the EMS and require the coordination of all three levels of control. Step changes in generation or demand that cause power flow imbalance and voltage or frequency fluctuations initially trigger rapid primary control responses using droop gains and converter link storage followed by coordinated secondary actions such as active or reactive power compensation from energy storage tanks [9], [90]. Such coordination must occur quickly and requires latencies less than 100 ms per node. However, data exchange is minimal and requires low bit rates of only 100 bps per node [92], [109]. This can be accomplished with simple low frequency single carrier communication methods.

Where necessary, tertiary controllers assist in SR events through physical DR by dispatching generation, shedding load, or initiating a curtailment schedule. Physical DR interventions can be planned or prompted by emergency signals of immediate or forecasted shortages. Curtailment schedules require detailed categorisation of loads. Those determined critical should not be shed or shifted while other loads deemed non-critical and flexible are subject to shedding. These shiftable loads (*e.g.*, washing machine) can be delayed or scheduled to operate during surplus periods creating virtual storage in the grid. Some loads have inertia (*e.g.*, refrigerator) and can be temporarily shed without exceeding operational tolerances [9]. In an islanded microgrid, planned or emergency blackouts to certain loads may be necessary to maintain grid stability. For example, weather forecasts could predict an abnormally long period of low irradiance in a PV microgrid prompting warnings to non-critical residential customers of an impending blackout whilst prioritizing storage assets to the community medical clinic.

Market DR is implemented through tariff protocols programmed into tertiary controllers [9]. Tariff structure limits are established to manipulate demand patterns which are enforced by primary and secondary controllers (*e.g.*, peak power and energy limits). Energy prices must be agreed by, and published to, the customer before consumption either through an IHD, web-based interface, or telecommunication. To effectively induce a customer response requires sufficient time to react in a meaningful way [150]. Market DR is therefore a longer term intervention technique.

Short term market DR is called RTP and is only effective given highly invested customers with ample time and motivation to react to price changes [150]. Since both physical and market DR are not time-critical strategies, latencies can exceed 1 s with moderate per node bit rates of 1 kbps [12], [13], [110]. Single carrier technologies can still satisfy this requirement.

EE efforts encompass utility initiatives to identify and reduce system losses and educate customers on efficient practices [9]. The former is tackled mainly through tertiary level data collection and analysis. The later occurs through customer interactions like, tariffs, IHD and energy bills, all tertiary level activities. In the most demanding of circumstances where RTP are broadcast to an IHD, communication requirements are still relatively modest. These functions can be accomplished with the same specifications listed above for DR. In the context of rural electrification, there is a bit of a paradoxical conundrum since energy use is proportional to social development and inversely proportional to energy prices. Unlike in a macrogrid where the utility encourages customers to reduce demand through efficient practices, a rural electrification microgrid manager must shape when energy is used whilst simultaneously encouraging overall energy growth.

3.1.5 Additional Services

Primary and secondary control algorithms programmed into power electronics require software updates. Such firmware updates, to fix bugs and add features, may be performed manually. But this may be infeasible or very expensive if updates are needed frequently or must be applied to many components. If updates are to be performed remotely, hardware must be designed to accommodate such downloads and the microgrid communication system needs the capacity to handle larger data transfers. Firmware updates of small microcontrollers are feasible using a medium-latency (1 s), medium-bit rate (10 kbps) connection, although more complex components containing many or large microcontrollers may have commensurately higher communication requirements. Such a feature could be

very advantageous for isolated autonomous microgrids, as it allows the utility to make design improvements remotely.

A low-latency, high-bit rate ($< 100\,\text{ms}$, $> 1\,\text{Mbps}$) microgrid communication system could deliver a bundled internet or voice service. Such a proposition would be attractive if the microgrid intrinsically required such a communication system to operate effectively. However, as demonstrated in Table 3.1, a full list of advanced microgrid services is possible using much less capable communication systems. Many of the FAN technologies (discussed in the next chapter) can theoretically support broadband-level latency and bit rates. However, to provide internet to an entire community of microgrid customers, the backhaul link must support multiple simultaneous users, significantly increasing its design specifications. The technologies necessary for such a backhaul (fibre, 4G, 5G) may not be feasible or available for the same reasons that make the microgrid remote. Furthermore, customers likely already have voice and internet access through their mobile phone and would be unwilling or unable to purchase a redundant service in their home. Although a utility company could potentially harvest additional profits from a bundled internet service, such a capability does not intrinsically amplify the capability of the power system.

3.2 Automatic Meter Reading

As a commodity, electricity is almost always metered at the point of use. Revenue from tariff collection recovers system costs and establishes profit margins. Traditionally, utility companies monitor energy consumption with electro-mechanical or simple digital meters that are read manually by utility personnel after which the customer receives a bill based on a fixed energy rate. This practice is slowly being replaced throughout the world by 'smart' meter installations which are expected to reduce costs, increase metering flexibility, and enable the smart grid [68]. The smart meter enables AMR and DSM strategies. Critically, these strategies require some form of communication between the utility and the smart meters on their network. There are three possible digital communication network links shown in Fig. 3.2 to connect the customer, smart meter, and utility:

1. field area network (FAN) with backhaul,
2. direct wide area network (direct-WAN), or
3. user-enabled communication (UEC).

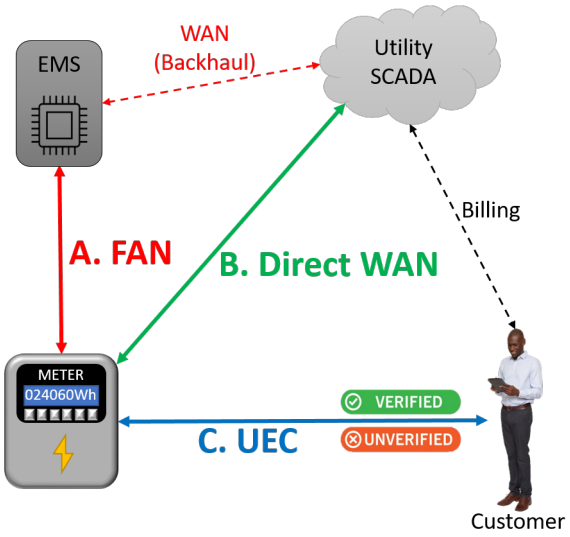

Figure 3.2: Smart meter communication links: A) FAN with backhaul B) direct-WAN, C) UEC (verified or unverified). The black dotted line indicates compulsory interactions that occur between the customer and the utility.

Additionally, Fig. 3.2 illustrates the compulsory billing link between the utility and the customer which can be accomplished through mail, voice, or electronic device.

3.2.1 Field Area Network (FAN)

A FAN links smart meters and DERs to an EMS. Fig. 1.1 provides an example of a microgird with a bus network topology. Creation of a FAN requires specific hardware, such as transceivers and interface circuitry, to be present in each smart meter. Information flow in a FAN can be unidirectional or bidirectional. If the goal of the communication system is purely AMR, only unidirectional transmission from the meter to the EMS is necessary. However, additional functions become available with two-way communication with little extra cost since a receiver typically requires similar basic hardware as found in the transmitter.

The technological requirements of the backhaul are different than the FAN and are not discussed in detail in this study. However, in general, the link necessitates

an order of magnitude higher bit rate and range since each transmission carries information from multiple customers over greater distances. For remote islanded microgrids, backhauls often utilize an internet link via satellite or cell phone networks. Fig. 1 shows a wireless backhaul such as GSM. Without a backhaul, the utility would have to extract FAN information by sending utility personnel to site, and particularly for small, remote, autonomous microgrids, removing the need for permanent or regular on-site personnel is desirable. However, field studies reveal the difficulty of eliminating this role completely since the realities of hardware deployment and customer acceptance demand access to local support [8].

3.2.2 Direct Wide Area Network (direct-WAN)

An alternative to a FAN and backhaul is a direct WAN link between each smart meter and the utility's SCADA system. Much like the backhaul, this link requires long range and is most commonly achieved by installing a cellular modem in each smart meter. Therefore, the utility depends on a third-party telecommunication contract and are constrained by its availability, data fees, data rates, and reliability. Many utilities in the developing world are upgrading manually read meters with smart meters using cellular-based direct-WANs [88], [107]. In AC macrogrids, there are normally no power electronics at the meter, there is no preexisting FAN connecting meters, and no control actions are taken at the meter level. Most homes do not have controllable loads and the direct-WAN is solely used for AMR purposes. The installation of the direct-WAN is the first step in a long term plan to create a smart grid concept. In the context of an islanded LV microgrid, a direct-WAN would likely not meet secondary and tertiary control needs and therefore would supplement an already existing FAN effectively doubling the communication system costs. It therefore makes more sense to utilize the requisite FAN for AMR.

3.2.3 User-enabled Communication (UEC)

Another method to communicate with smart meters is UEC, where the customer reports data from their meter directly to the utility. The customer could report

readings from their meter using a keypad or Bluetooth interface. Otherwise, interaction between the customer and the utility to transfer the meter data may be through text message, email, or an online account. UEC therefore depends upon the customer having semi-regular cell phone reception and/or internet access. Self-reporting could work in a remote microgrid in SSA since most customers do have cell phones and most regions have at least GSM coverage [6], [151]. The very simplest form of UEC is prepayment. The customer purchases a physical token from a local kiosk to enable a prepay meter (the meter must have a keypad interface, RFID, or magstripe reader, or similar input mechanism).

UEC allows for self-reporting where the utility requests the customer to relay unverified or verified measurements from the smart meter via voice, text message or web interface. Unverified reporting depends on the customer to reliably and honestly report a measurement, *e.g.*, kilowatt-hours consumed. Verified reporting systems first 'hash' or encrypt measurements into a self-verifying sequence of digits with which the utility can check for tampering. Such techniques can also be used to eliminate physical tokens for prepay meters.

3.2.4 Communication-less

It is possible to operate a microgrid where there is no regular communication between customer and utility, but this limits the utility to offering a flat-rate tariff only (flat-rate in this context means that there is a fixed monthly fee that does not depend on energy usage). A completely communication-less system is unlikely to be attractive to a utility: some infrequent periodic UEC to report energy consumption (*e.g.*, every 6 months) is likely to be the minimum requirement for a commercially viable system. Alternatively, periodic manual meter readings may be performed by utility personnel.

3.3 Tariff Structures

Table 3.2 breaks down metering into six basic structures and indicates if that structure can be supported by a given communication system. An important

Table 3.2: Possible tariffs vs. Type of communication link

Link Type	**Flat rate** ($/time-period)	**Fixed peak power** ($/W)	**TOU peak power** ($/W)	**Fixed energy** ($/Wh)	**TOU energy** ($/W or $/Wh)	**Real-time pricing**
No comm.	*Post-pay:* No meter hardware is required. Delinquent users are manually disconnected.	*(not feasible)*		*Post-pay:* Utility personnel manually read the meter and manually disconnect delinquent customers. Time-of-use meters require a clock.		*(not feasible)*
UEC	*Pre-pay:* The user inputs a code as proof of payment to prevent operation of the disconnect mechanism. The meter also requires a clock and a pre-programmed expiration time to determine when another payment is required.			*Pre-pay:* The user inputs a code into the meter obtained after buying credit. The pre-programmed meter decrements the credit and operates the disconnect mechanism on reaching zero. Time-of-use meters require a clock. *Post-pay*: The user regularly reports meter readings to the utility and receives a code to prevent operation of the disconnect mechanism.		*(not feasible)*
FAN	*Pre- or post-pay:* The utility controls the disconnect mechanism remotely.			*Pre- or post-pay:* The utility reads the meter and controls the disconnect mechanism remotely.		*Pre- or post-pay:* The utility updates the tariff rate in response to changing conditions, performs frequent meter readings to track customer consumption, and operates the disconnect mechanism remotely.

distinction exists between post-pay and prepay schemes. Although most utilities in the developed world charge customers after consumption (post-pay), prepay billing can be extremely effective in a remote microgrid. The rapid deployment of cell phone technology coupled with the widespread access to mobile banking applications in the developing world make prepay services a natural business model choice [4]. Prepayment provides flexibility to lower income customers with irregular cash flow to budget electricity free of the burden of recurring bills inherent of post-pay electricity contracts whilst protecting the utility from unpaid bills.

Additionally, Table 3.2 lists hardware that may be required to support the chosen tariff structure: A clock and/or a disconnect mechanism. To accurately bill the customer for consumption in a certain period, the meter must know the time. A communication system can provide time information directly or offer periodic corrections to a local real-time clock (RTC). A communication-less system cannot correct its RTC, and so, due to drift, low-cost oscillators may not be sufficient to track billing periods with acceptable accuracy. More accurate (and

expensive) advanced clocks or GPS receivers may be necessary [152]. Customers that do not pay the agreed tariff (are delinquent) must be disconnected. The disconnection/reconnection can be performed manually by utility personnel, or a contactor or other isolating mechanism can be included in the meter and operated remotely using a communication system.

The tariff structures in Table 3.2 are:

1. *Flat Rate*: Unmetered electricity access is charged at a flat rate per time-period (*e.g.*, $/month) [24]. Delinquent post-pay customers are manually disconnected. A prepay meter requires a clock to track the pay period and a contactor to disconnect meter upon delinquency.
2. *Fixed Peak Power*: In certain microgrids, it may be necessary to curtail customer peak power due to generation limitations (this is a form of physical DR known as 'peak shaving'). Despite the type of communication link, the meter monitors power and enforces the limit with a contractor, disconnecting the user if the subscription power limit is exceeded for a certain time tolerance (*e.g.*, 20 seconds) [24]. Pre-pay meters needs a clock to track the pay period.
3. *Time-of-Use Peak Power*: As for fixed peak power, but the peak power limit changes depending on the time of day.
4. *Fixed Energy*: This is the traditional method of metering. Power is measured, integrated over time, and displayed as a 4 to 6-digit energy value (Wh) [24]. Meters can be manually read by the utility technician 1-4 times per year or self-reported by the customer through UEC. AMR by a FAN requires at least a unidirectional communication link but places no stringent requirements on latency and requires very low average bit rate (only approximately 24 bits of raw data need be transmitted per reading). Sampling frequency could be as low as once per month. Prepay customers purchase energy credit and so the meter must have a contactor to disconnect access upon credit expiration. Without communication, the rate ($/Wh) must be pre-programmed into the meter.

5. *Time-of-Use Energy*: Time-of-use (TOU) energy tariffs are a form of market DR [24]. By simple example, peak demand hours could cost significantly more than off-peak times to encourage consumption during off-peak periods. Manual reading and self-reporting become more difficult since multiple counters must be read. This pragmatically limits the number of time periods to about three and 18 digits. Increasing the number of counters beyond this would likely lead to inaccurate readings and frustrated customers. Each of the TOU rates must be pre-programmed in a prepay meter. Given the complexity and the likely desire of the utility to regularly update tariff rates, the argument for AMR becomes much stronger in this scenario. The communication requirements remain the same as a fixed energy tariff except the additional need for a clock to distinguish between TOU periods. Sampling frequency depends on the TOU period but would normally be about once per hour. With hourly samples, the utility can build basic load consumption profiles for each customer. It should be noted that it is in theory possible to collect load consumption data without AMR by storing it locally on the meter and having utility personnel download it manually every few months. Such data has significant value as discussed in Section 3.1.3.
6. *Real-time pricing*: Taking market DR to its logical extreme is called real-time pricing (RTP) where the dynamic cost of electricity, dependent upon multiple variables such as weather, grid demand, generation status, storage status, and fuel prices, is relayed to the consumer. Dynamic tariffs can be for energy or peak power (*e.g.*, critical peak pricing) or both. In theory, a customer made aware of rising or falling costs will respond by making consumption pattern modifications. Time-stamped consumption data must be collected with a sample frequency at least equal to the RTP update rate. RTP requires bidirectional communication to transmit prices to the smart meter while gathering consumption data. Its requirements depend on the frequency of RTP changes, but a realistic interval would be once per hour, with no stringent latency or bit rate requirements (10 s latency, and 10 bps per meter would be

acceptable). Prepay meters cannot solely rely on UEC since the meter must receive the RTP from the utility to properly decrement the customer's energy credit or establish power ceilings.

Despite RTP offering potential benefits, widespread deployment has not yet occurred, perhaps due to marginal gains observed in pilot programs. Arguably, residential RTP lacks practicality since it depends on customers actively monitoring electricity prices. Studies demonstrate that both cost savings to the customer and desired DR magnitude changes are not proportionate to the costs and complexities of RTP implementation [153]. Many simulations and dynamic DSM algorithms have been proposed in the literature, but few field trials have proven their effectiveness with real customers [154]. Some success has been observed with large industrial customers that have dedicated staff monitoring RTPs ready to adjust load demand during peaks or dips market prices. RTP could also yield better results if utilities could remotely manage specific loads in accordance with price changes. A low voltage islanded microgrid will likely not contain such industrial customers nor many controllable loads. Furthermore, microgrids will be unlikely to rely on customers reacting to RTP to resolve short-term generation imbalances due to the inherent high latency of customer reactions. RTP may be useful in a microgrid with generation limitations if customers are afforded ample time to react to the desired trigger through day-prior forecasts targeted to prevent adverse events. Experience also shows that the price differences must be large enough to illicit a response. However, it must be noted that more effective methods are available (besides market DR) to address such situations. Physical DR solutions avoid problematic volatile prices, especially when considering low income microgrid customers who may grow to resent RTP fluctuations.

It is important to note that for all tariff structures, the customer must be aware of the tariff and be given sufficient information to verify the energy bill (this is often a statutory requirement on the utility). This can either be provided from an IHD on the meter or an UEC web-based application. Combinations of methods can target multiple desired DR outcomes.

3.4 Robust Extra-Low COst Nanogrids (RELCON) tariff case study

As isolated power systems, microgrids provide a natural canvas to implement the concepts of the smart grid. The RELCON project is an electrification field deployment consisting of a 15-customer, 24-hour service, Tier-3 islanded solar microgrid for a rural community in Kenya [19]. A case study of the RELCON project will serve as a realistic validation of a proposed CRT structure for islanded LV microgrids. The RELCON system will mimic a commercial power utility company that must establish IRR. First, the RELCON system will be described followed by a cost inventory of the grid hardware, logistical expenses, and sizing definitions necessary to deploy a PV microgrid to a remote village in SSA. Then the DER sizing assumptions are explained. Finally, the CRT structure is proposed.

3.4.1 RELCON system

At the center of the RELCON system is the generation hub consisting of a PV array, valve regulated lead acid (VRLA) battery storage bank and associated Maximum Power Point Tracking battery charging control unit illustrated in the system diagram in Fig.3.3.

DC-DC converters then step the 48 V generation bus up to the touch-safe distribution voltage of ±60 V. Individually controlled star network distribution feeders connect the hub to various customers below the extra low voltage safety threshold of 120 V DC. Feeders are buried steel wire armoured (SWA) power cables with multiple core conductors each 1.5 mm^2 cross sectional area. A satellite photo of the target village in Fig. 3.4 shows the average distribution distance of $\sim$ 100 m.

At each endpoint, the transmission cable terminates at a bidirectional multi-port DC-DC converter and smart meter (which will be referred to as a *Homebox*) pictured in Fig. 3.5. The Homebox contains a local 236.8 Wh lithium-ion battery and includes inputs for additional DC DERs (*e.g.*, PV or additional battery). The Homebox is rated at 300 W with five individually monitored 12.5 V DC output load ports. The converter compensates for any voltage drop on the transmission

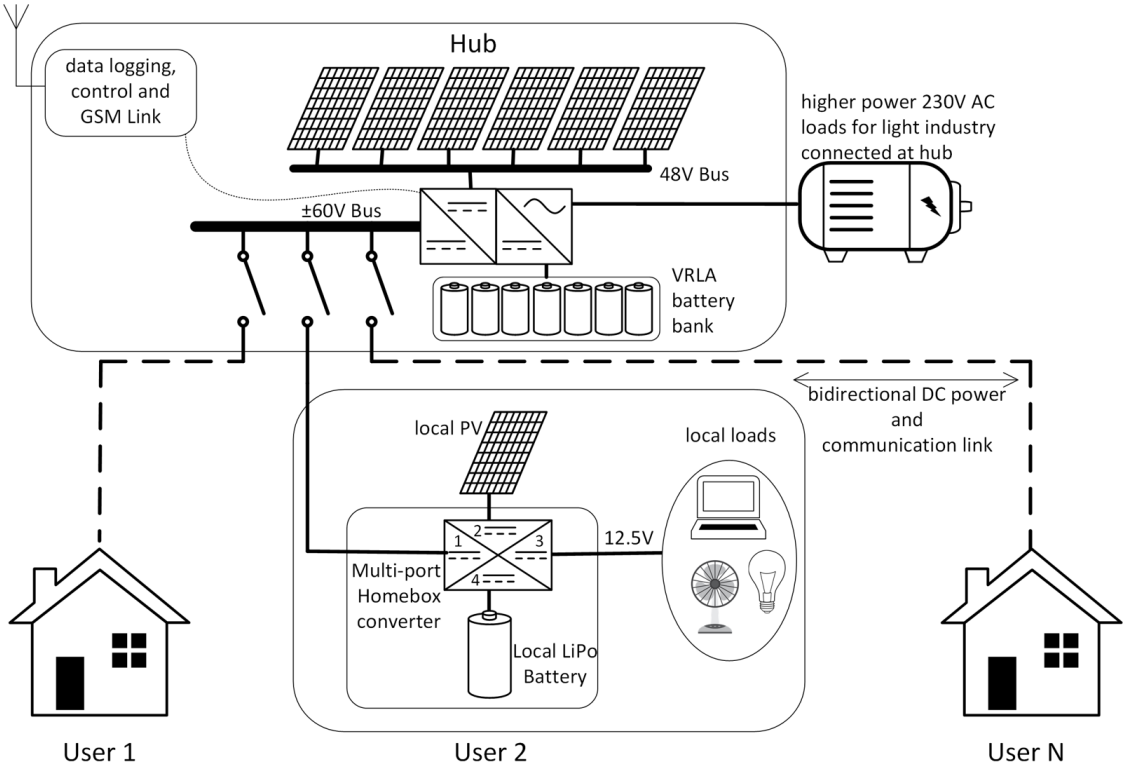

Figure 3.3: RELCON System Diagram. Central generation hub connects to N rural users (commercial/residential) through a multi-port Homebox (*i.e.*, smart meter) that communicates to an EMS with a GSM backhaul at the hub.

line, manages local DERs, regulates internal battery set points for various charging phases, and most importantly, maintains stable load supply voltage. It limits input and output currents to protect circuitry and the load whilst providing DSM capability [155]. Homeboxes communicate with the central EMS via a wireless LoRa (proprietary long range protocol) FAN (PLC technologies were also being explored at the time of deployment). The EMS connects to a web-based interface for remote control and monitoring via GSM backhaul link. The hub can also support an AC load or a grid-connection. VRLA batteries are chosen for the hub because they are the most readily available chemistry in deployment location markets.

The RELCON system was scheduled for deployment in March of 2020, but was unfortunately delayed several times and eventually cancelled due to COVID lockdowns. Still, the microgrid serves as a case study for the three main contributions of this thesis, first the validation of a CRT [19], second the cost-benefit analysis of adding digital communications to a LV microgrid [16], and lastly to validate

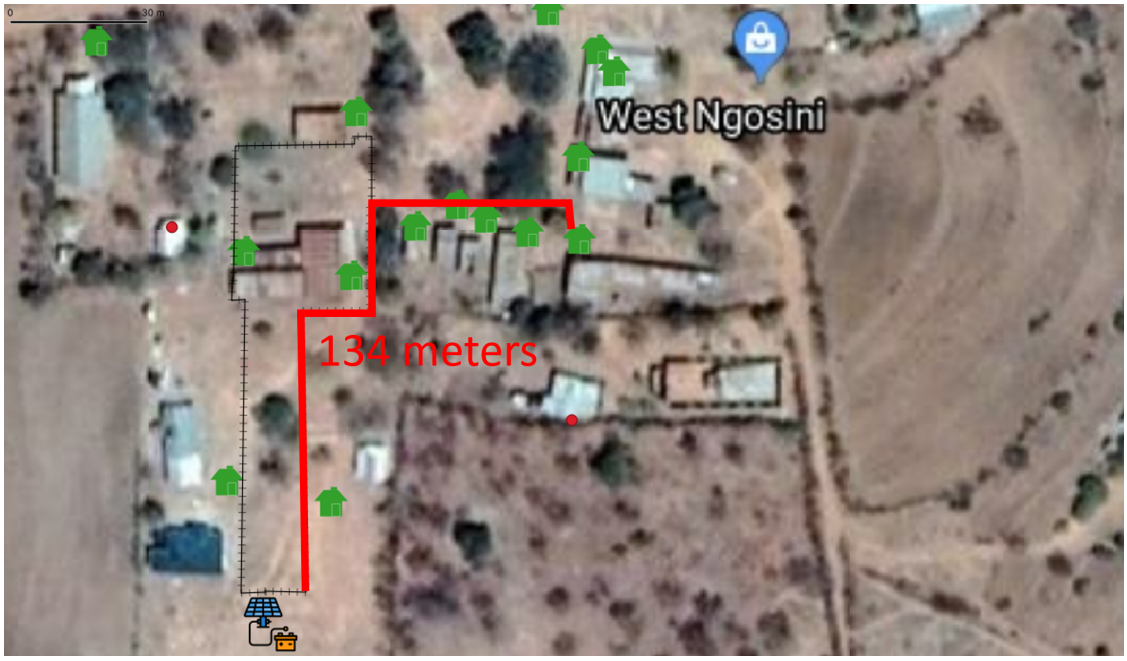

Figure 3.4: RELCON target village in Kenya.

(a) **(b)**

Figure 3.5: RELCON Homebox v1.0, bidirectional multi-port DC-DC converter, rated at 300 W, ±60 V input, 12.5 V output, contains 236.8 Wh LiPo battery. a) customer presentation, b) interior circuitry

PLC modeling and test HomePlug performance [22]. Although the microgrid was never deployed to the field, a lab-based test-bed of multiple Homeboxes was installed at the University of Oxford (Fig. 3.6) where various experiments were conducted. The physical kit serves in this chapter as a validation of the following detailed cost estimate.

Another unique feature of the RELCON system is distributed storage. This strategy can reduce sizing requirements by distributing DERs throughout the network as discussed in Section 2.1.4. One of the research objectives of the RELCON

Figure 3.6: Laboratory microgrid testbed. Eight Homeboxes are connected to a central generation hub with various lengths and configurations of SWA cable.

project was to explore the idea of distributed DERs. Each customer in Fig. 3.3 has a smart meter called a Homebox, a highly flexible multi-port DC-DC converter that allows for bidirectional power flow between customers. It also can integrate a customers local generation and additional storage such as a previously purchased SHS. The Homebox comes with a built-in lithium-ion battery. This design offers each customer a degree of independence from the central power source whilst increasing power quality by absorbing rapid load transients. Storage distribution in the RELCON network also helps alleviate conflicts in a shared network. Microgrid communities often encounter difficulties in the allocation of a CPR where some users may irresponsibly use more than their share of the centralized energy [31]. Central storage is closely monitored and low SOC triggers initiate prioritization of loads and curtailment schedules. The local lithium storage in the RELCON Homebox is not a communal resource unless the customer explicitly sells it to the grid. Therefore, each customer is guaranteed access to their personal storage in times of centralized shortage. Customers are informed of the status of the central generation hub as well as the state of the local storage through a customized IHD enabling them to make personalized energy decisions. The cost-benefit analysis of distributed vs. centralized DERs is not included in this study because the project was never deployed and data is required to measure the hypothesized benefits. This Homebox feature is mentioned here to highlight a future research opportunity. Ultimately, the goal of

DER distribution is to decrease system cost by reducing DER sizing requirements. Another strategy is through DSM, which will be the primary focus of this research.

3.4.2 RELCON cost inventory

LCOE is calculated as the sum of microgrid capital expenses (CAPEX) and operational expenses (OPEX) divided by the energy served to the grid over its lifetime.

$$LCOE = \frac{A + NB + LC + LND}{\eta ELN} \text{ [\$/kWh]} \tag{3.1}$$

There are four expense categories: A is CAPEX independent of the number of customers ($), B is CAPEX for each added customer ($/customer), C is annual OPEX independent of the number of customers ($/year), and D is annual OPEX for each added customer ($/year-customer). Although it is plausible to have shared annual OPEX, this case study has identified no operational costs independent of the number of customers making C=0. L is the lifetime of the system in years, N is the number of customers served in the microgrid, E is energy served (kWh/year-customer), and η represents technical losses as a fraction of supplied energy where: $E_{\text{supplied}} = \eta E$. Prices are validated by similar cost studies in Section 2.2.5.

CAPEX and OPEX of a Tier 3 microgrid are inventoried in Table 3.3. CAPEX values (A & B) detailed in Table 3.3 come from sizing requirements, actual invoices, and wholesale manufacturer quotations to validate estimates of photovoltaics, lead-acid battery storage, distribution cables, converters, controllers, protection hardware and all the necessary accessories to build and maintain the microgrid in a rural village. Labour costs also come from invoices and online salary estimates. They account for labourer per diem and all necessary tools and equipment. The estimated LCOE for a rural Tier-3 microgrid in SSA is $0.61/kWh.

3.4.3 RELCON load profile

Table 3.3 includes the load profile estimate for a Tier-3 community with both residential and small business customers. Average annual load profile predictions in Fig. 3.7 come from [156] and show hourly power consumption for each of 15

Table 3.3: Tier-3 PV-storage microgrid cost inventory

Variable	Quantity	Unit price	Wholesale[a]
CAPEX		**($/unit)**	**($)**
Hub converter	1.00	334.56	334.56
Installation	1.00	5377.50	5377.50
Labour (man-hrs)	432.00	5.51	2380.32
EMS	1.00	367.50	367.50
Backhaul	1.00	56.00	56.00
A			**8515.88**
CAPEX/customer		**($/unit-cust)**	**($/cust)**
Battery (Wh)	1933.14	0.10[b]	193.31
PV (W)	296.87	0.60[c]	178.12
insolation (Wh/m^2)	4000		
efficiency	0.15		
Cable (m)	100.00	0.50	50.00
Labour (man-hrs)	35.33	3.00	106.00
Protection	1.00	35.17	35.17
Homebox	1.00	276.43	276.43
Smart Meter	1.00	35.00	35.00
Digital communication	1.00	23.00	23.00
B			**897.04**
Total Customer CAPEX			**1464.76**
OPEX/customer		**($/unit-yr-cust)**	**($/yr-cust)**
CML (24 hrs/year)	0.42	0.61	0.25
O (visits/year)	0.50	1.25	0.63
M (battery life 4 years)	0.20	193.31	38.66
Mobile Money	0.33	12.00	4.00
Data	1.00	1.00	1.00
D			**44.54**
Total Customer Lifetime Cost			**2355.58**
L (years)			20.00
N (# of customers)			15.00
E Energy Served (kWh/year-customer)			152.24
E Energy Served (Wh/day-customer)			417.09
η (technical loss factor)			1.27
LCOE ($/kWh)			**0.61**

a. These values do not consider inflation.
b. Includes cost of battery rack & fuses.
c. Includes cost of PV install, MPPT controller, mounts, & connectors.

customers extracted from a full year of 15-minute resolution simulation load data. The model draws upon a combination of survey and SHS data and uses a stochastic algorithm to predict appliance usage and aggregate them to generate demand curves.

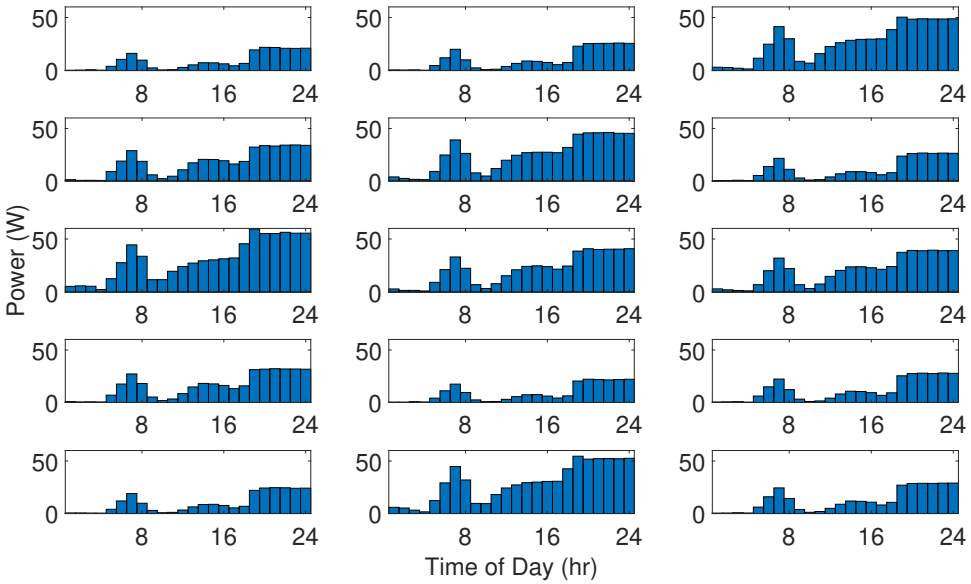

Figure 3.7: Average Tier-3 load profiles of 15 residential and small business customers used to size microgrid DER. Overall demand averages to 417 Wh/day with an average daily peak of 36 W and a max individual peak of 155 W.

Sizing of the PV and battery require the addition of 27% technical losses from the cable and converters captured by η in Table 3.3. Demand also includes NTL such as theft, unpaid bills, and CML [85]. CML is included in D as an OPEX and set to 24 hours/year [54], [59], [60]. The RELCON design includes AMR and remote disconnect which allow for rapid theft detection thus effectively eliminating theft in this case study [157], [158]. Similarly, all electricity is pre-paid using PAYG mobile money payments eliminating unpaid bills [84], [86]. Therefore, average energy served (E) is 417 Wh/day and average energy generated is $E_{\text{supplied}} = \eta E = 1.27 \cdot 417\,\text{Wh} = 530\,\text{Wh}$.

NASA climate data from [159] provides estimations of insolation at the RELCON case study site in Kenya. The assumed insolation is set to the lowest monthly average from the most recent 5 years which occurred in July 2018 at 4.0 kWh/m^2. Battery storage is sized to sustain the load without PV generation for an entire day

to provide enough storage to sustain the microgrid through a day of overcast [160]. To maximize battery life, cells are only discharged to 50% of their capacity [161], [162]. This is an industry standard. Optimizing depth of discharge, chemistry and microgrid maintenance cost was not investigated in this study but is an important topic for further research [163]–[165].

The lowest individual daily value of insolation occurred in 2014 at 1.17 kWh/m^2 and the worst multiple-day period took place in June 2019 where three consecutive days averaged 2.46 kWh/m^2. Even on the worst of cloudy days, the PV still receives over 25-50% of the worst monthly average. Furthermore, the 5-year average insolation in the target village (between 2014-2019) is 5.7 kWh/m^2, exceeding the sizing assumption, which means that, on average days, the generation will oversupply. This is the crux of microgrid design. Over-sizing the battery is a critical strategic decision to effectively build insurance for unforeseen (and inevitable) circumstance. As described in previous sections, the objective of DSM is to collect consumption and weather data to not only reduce the size of generation, but also provide a list of available tools to address shortages when they arise; thus effectively eliminating the need for insurance over-sizing. This concept will be fully explored in the next chapter. For now, these sizing assumptions are sufficient to build a realistic cost inventory and LCOE to build a tariff structure.

3.4.4 Microgrid DSM strategy

The purpose of this case study is to use a real-world microgrid deployment as context for a proposed DSM strategy with three inputs and three outputs. There is a critical balance between simplicity (to ensure customer engagement) and DSM opportunity (*i.e.*, enough levers available to shift demand). Therefore, the following DSM strategy aims to provide an extremely simple tariff structure that can be easily understood by any customer whilst facilitating realistic DSM opportunities for a remote low-voltage microgrid in a low-income rural community. It is the actual tariff structure intended for the RELCON target village in rural Kenya.

Inputs

1. Market DR: Two-pronged tariff
   (a) Peak power tariff
   (b) TOU tariff
2. Market DR: discounts
3. Physical DR

Outputs

1. demand shift,
2. flexible energy prices to guarantee access to low-income customers, and
3. CRT that guarantees IRR.

Although the specific numbers are informative and realistic, the focus is on the tariff structure itself not the numbers, since these will vary depending on design and location. The tariff is designed for a PV/battery-based microgrid, but could be modified for other DERs.

3.4.5 DSM inputs

Table 3.4 shows the simple two-pronged tariff structure.

Table 3.4: Microgrid tariff structure

Type of Connection	Power Limit	Monthly Fee (USD)
Reduced	50 W	3
Standard	100 W	5
Max	300 W	10
PAYG Night-time Energy (USD)		
	1 kWh	0.30

1. *Market DR: two-pronged tariff*
   (a) *Peak power tariff*: Each customer agrees to a pre-paid monthly subscription or connection fee that fixes the peak power usage of their Homebox. Connection fee payment guarantees unlimited energy usage during a daily 6-hour peak solar production period defined as 0900-1500 local time as shown in Fig. 3.8. Since Kenya lies near the equator, daylight hours do not vary significantly throughout the year. The definition of

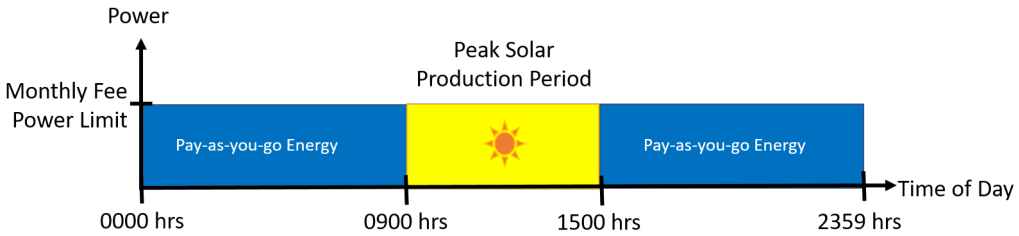

Figure 3.8: Payment timeline: The monthly connection fee limits max power usage. Day-time (0900-1500) energy use is free. Night-time energy (1500-0900) must be pre-paid. Time-of-use tariff encourages daytime consumption.

the two pay periods may be tailored for different locations or generation sources. If the connection fee is not paid by the tenth day of the month, the Homebox is remotely disabled.

(b) *TOU tariff*: *Day-time* energy (shaded yellow in Fig. 3.8) is "free" with a connection subscription. Outside of the 6-hour peak production period, *Night-time* energy (shaded blue in Fig. 3.8) is metered at \$0.30/kWh. Night-time energy is still capped at the connection fee power limit. Energy balance never expires (*i.e.*, purchased energy rolls to the next evening).

2. *Market DR discounts*: During periods of high irradiance, discounts can be offered on energy top-ups to incentivise larger payments. Similarly, during months of higher irradiance forecasts, connection fees can be discounted to encourage higher power subscriptions.
3. *Physical DR*: Since the consumers' behavior is uncertain, and weather can always negatively affect PV generation, there may be occasions when the centralized battery storage is diminished. If the hub battery state of charge is expected to dip to 10% of usable capacity, users are notified of the curtailment schedule. In the RELCON system, each subscriber still has access to their Homebox internal battery. Even when hub power is not available to the Homebox, the customer may continue using electricity until their internal battery is depleted, assuming they have an energy balance on their meter. This alleviates negative ramifications of unexpected blackouts. Curtailment

would start by baring energy top-up payments followed by load shedding procedures based on load priorities. Load shedding schedules will depend on the mix of users and community priorities. Communities should be involved in determining the order of loads. Priorities typically start with community service loads (*e.g.*, medical facilities, schools) and productive-use businesses vital to the local economy (*e.g.*, mill, egg incubator) as discussed in Section 2.1.3. In the RELCON star distribution shown in Fig. 3.3, loads can be individually isolated or throttled.

Red highlighted cells in the cost inventory in Table 3.3 indicate storage costs accounting for 41% of total microgrid lifetime costs. Average night-time consumption from Fig. 3.7 is 345.64 Wh/day or 83% of the daily consumption. If storage costs are considered a night-time cost, the LCOE of night-time energy would be \$0.30/kWh. This is the origin of the PAYG night-time energy price in Table 3.4. Therefore, remaining costs can be viewed as a day-time cost, dominated by the PV. The LCOE of day-time energy would be \$2.09/kWh. Multiplying the average day-time energy consumption of 71.44 Wh/day from Fig. 3.7 by the day-time LCOE for a 30-day month yields \$4.48/month. This is the origin of the *Standard* connection fee in Table 3.4. The *Reduced* connection option allows for lower income customer participation and the Max connection targets residents and small businesses that intend to use higher power.

Based on surveys conducted by Cooperative University of Kenya during the RELCON project, salaries in the target Kenyan village are as low as \$20/month with an average of \$65/month. Therefore, the poorest customer could, in-theory, pay only \$3/month (15% of monthly income) and still use unlimited energy during the day. It is important to remember it is likely this customer is already paying much more than \$3/month on energy based on the averages discussed in Section 2.2.1. This minimal electricity connection could displace the majority of other energy costs effectively increasing their monthly salary. Assuming Fig. 3.7 average consumption, a customer earning an average wage for the target village would

average $8/month (12% of monthly income) which includes the *Standard* connection fee and night-time PAYG payments.

3.4.6 DSM outputs

The DSM inputs provide conditions for the following outcomes:

1. *Demand shift*: The TOU energy tariff incentivises day-time usage when PV power is available. Renewable-based microgrid customers must understand the meteorological limitations of weather dependent power and the microgrid's dependence on stored energy. Although battery technologies continue to advance, storage remains one of the largest contributors to cost in an islanded microgrid. The contrast between "free" day-time and PAYG night-time energy encourages customers to both use and store as much energy during high irradiance periods, shifting night demand to the day-time. Reducing night-time demand reduces battery usage, minimizes depth of discharge, increases battery lifetime and reduces maintenance cost.
2. *Low-income customer participation*: Providing electricity to rural populations is expected to spur economic growth; however, electrical generation and transmission systems are inherently expensive. The proposed tariff distributes cost in both space and time to propagate benefits to the poorest customers. Flexible energy prices guarantee access to a range of incomes. The *Reduced* connection subscription coupled with "free" day-time energy enables even the lowest income customer while the *Max* connection allows commercial ventures the Homebox rated power for their business ventures. Flexible subscriptions incentivises economic growth by allowing customers to increase their subscription monthly. Discounts can spur growth by opening temporary opportunities to lower subscription customers. It is important to note that this tariff structure assumes Fig. 3.7 demand and does not include AC loads connected directly to the hub as in Fig. 3.3. As the village needs increase to higher tiers, the DER would need to be upgraded and tariff structure modified to add a Tier-4 or 5 subscription.

3. *CRT to guarantee IRR*: Tenable microgrid installations must have a means to recover CAPEX, cover OPEX, and establish IRR within a reasonable lifetime. The proposed tariff is designed to recover costs and secure IRR within 20 years. Prices also must be competitive compared to existing SHS and microgrid companies operating in the area. The rates in Table 3.4 are within reasonable range of the definitions of "affordable" considered in Section 2.2.1 whilst considering that the RELCON target village incomes are well below Kenyan national averages and that electrification will likely immediately increase monthly salaries due to displaced cost recovery. Additionally, WTP in SSA for electricity is as high as \$4/kWh [6] and other Tier-4 microgrid utility companies like SteamCo (\$2.34/kWh over 20 years) and PowerHive (\$0.57/kWh over 30 years) have found success at similar LCOE set point (see Section 2.2.5) [25], [41]. Rates in Table 3.4 are also competitive with SHS rates discussed in Section 2.2.2 (∼\$0.65/kWh over 20 years). SHS companies achieve success through focused marketing to convince unelectrified individuals of the displaced revenue achieved through electricity. Lease-to-own programs allow customers to achieve a Tier-2 level of energy independence, but customers require significant capital to afford the down payment and periodic payments. The RELCON DSM strategy will use the SHS marketing approach whilst increasing the power quality and quantity, lowering the periodic payments, eliminating large upfront deposits and providing communal electrification benefits.

3.4.7 DSM interactions

DSM interactions with customers occur through three methods:

1. In-home display (IHD)
2. Mobile money tariff collections
3. Text messages

Since the audience has little familiarity with electricity, each communication contributes to their energy education. Interactions occur through the Homebox

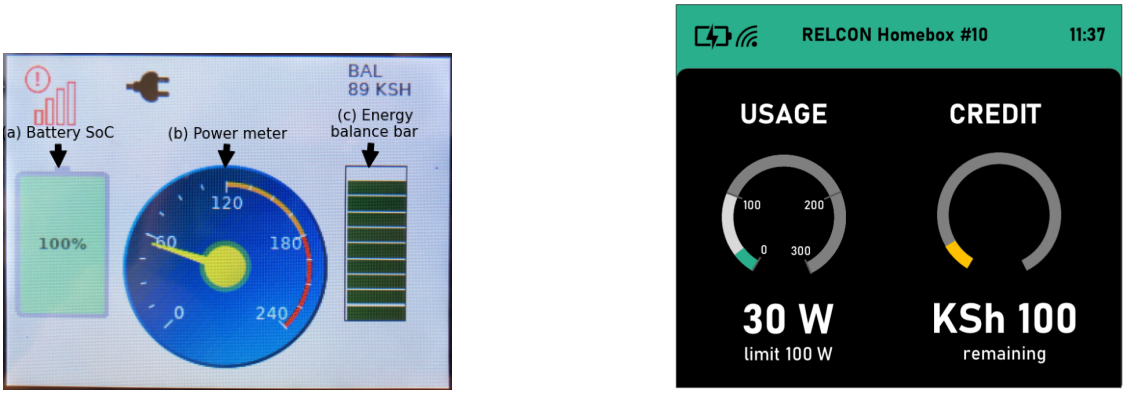

(a) (b)

Figure 3.9: Two versions of the RELCON Homebox IHD which include a SOC indicator for the local lithium-ion battery, how much power the customer is currently using, PAYG energy balance, and connection status indicators for power and communication with the hub.

IHD accompanied with audible sounds to indicate the status of the hub connection, violation of the connection power limit, SOC of the local Homebox lithium-ion battery, and the PAYG energy balance. Fig. 3.9 shows two iterations of the RELCON IHD.

Electricity is pre-paid through mobile money applications like MPESA which are ubiquitous in SSA. Since rural villagers often do not have bank accounts, the exchange of money has proven a large stumbling block to electrification efforts. Mobile money applications are now a standard method of flexible banking and are universally employed in Kenya [6]. Users can load or withdraw money to their mobile account at kiosks in commercial centers and then make payments for various services or products via SMS on their phones. Pre-paid electricity services effectively eliminate unpaid bills. Additionally, post-pay schemes often fail in low-income communities because customers fail to understand electricity as a finite resource. Pre-payment provides immediate feedback to customers when energy balances expire or when they exceed a power limitation [28]. Payments would trigger Homebox activation up to the subscription power limit. Mobile money transaction fees in Table 3.3 are estimated at \$0.05-\$0.15 per payment. Customers are assumed to make 2-3 payments monthly to maintain their subscription and

purchase energy. Discounts and curtailment schedules can be conveyed to the customer through text message either to their mobile phone or on the IHD.

3.5 Conclusion

Each of the three levels of microgrid control have specific communication requirements. Bit rate requirements tend to increase moving up the the control hierarchy while latency requirements tend to decrease. Each control level depends on lower levels, meaning a communication system capable of tertiary control must also be capable of meeting the most stringent requirements from any of the lower levels.

AMR and market DR are the primary methods to reduce microgrid costs. This case study has established a CRT balanced with rural African WTP and income thresholds whilst also guaranteeing system cost recovery and potential profit returns for microgrid developers. DSM strategies reduce overall DER sizing, increase system reliability, lengthen storage lifetime, enable energy independence, and empower consumers with the confidence to pursue productive activities. The strategies are designed to involve and educate the customer on the system's true value while engendering community stewardship and appreciation for its capacities and limitations.

4
Microgrid Communication

The primary findings of this chapter have been submitted for publication to Elsevier Renewable and Sustainable Energy Reviews: D. Neal, D. Rogers and M. McCulloch, "A Techno-Economic Analysis of Communication in Islanded Microgrids," unpublished.

Chapter 4 provides a techno-economic analysis of microgrid communication to determine if adding a digital communication system to a microgrid is worth the cost and complexity. It incorporates the communication requirements derived from Chapter 3 and conducts a thorough comparison of various wired and wireless technologies that meet those requirements. It culminates with a case study to illustrate the cost-savings achievable through microgrid communication based on the real-world RELCON project.

4.1 Field Area Network Technology Comparison

The two basic mediums for FAN communication are wired and wireless. Table 4.1 organizes various available technologies by medium. The table is not designed to define exact ranges of capability; but rather, it provides an order-of-magnitude quantifier. The list is not all-inclusive but contains many common options. Fig. 4.1 graphs the bit rate versus latency of the various digital technologies from Table 4.1

Table 4.1: Microgrid FAN digital communication technology comparison

Technology	**Medium**	**Data rate (Mbps) [110]–[113]**	**Distance (m) [110]–[113]**	**Latency (ms) [113]**	**Cost per transceiver* [166]–[169]**	**Cost per 100 m medium* [166]**	**Cost per customer***
Coaxial	Dedicated cable	100	>10,000	0.1	2	17**	19
Ethernet (twisted pair)	Dedicated cable	100	100	0.1	7	13** [170]	20
Fiber optics	Dedicated cable	1000 [171]	100,000	0.01 [172]	7	13**	20
Power electronics PLC	PLC	0.002	>1000	100	0	0	0
NBPLC (G3 or Prime)	PLC	0.05	800	50 [173]	24	0	24
HPGP	PLC	10	300	5	33 [174]	0	33
HPAV	PLC	100	300	2	20 **	0	20 **
GSM †	Wireless	0.014	>10,000	300 [175], [176]	10	2 ‡	12
LPWAN (LoRa)	Wireless	0.05 [177]	>1000 [93]	50 [178]	20	0	20
Zigbee	Wireless	0.25 [171]	100	100 [179], [180]	31	0	31
Wifi	Wireless	50	100	20 [181], [182]	14	0	14

* Costs in USD and reflect the market as of May 2022.
** Similar price available from suppliers in Kenya [183], [184]
† GSM considered because it has the widest coverage in SSA and most likely technology available for remote microgrids [185].
‡ Includes 3rd party data costs: hourly 1 kB data transfer at average cost of data in SSA ($8.4/GB) [186].

and graphically situates them in comparison to the microgrid requirements from Table 3.1. Dot size is scaled according to cost-per-customer from the last column of Table 4.1. Both non-digital communication metering methods (manual meter reading and UEC) from Chapter 3 are included as contrast. Manual meter reading has the same fundamental bit rate and latency as UEC since ∼24 bits of data are be being read by either a utility technician or customer manually less often than once per month which equates to less than 1 μbps.

4.1.1 Dedicated cables

Communication cables can be laid at the same time as the power cable, either buried or hung on poles. Dedicated cable networks are normally organized into a star topology (Fig. 3.1a) but can also use bus network (Fig. 1.1 or Fig. 3.1b) or ring (Fig. 3.1c) topologies [141], [142]. Network routers or switches are normally required at junctions in bus or ring topologies. Wired communication systems are mature technologies, very reliable and typically outperform wireless technologies. High data rates, long range and low latencies are readily attainable. Although Ethernet over twisted pair is fast and very inexpensive, distances are limited. Coaxial cable offers a good balance of capacity, distance, and affordability for wired solutions. Wired solutions are also commonly used for backhaul links. However, if a community of loads is in close enough proximity for a wired backhaul, it is likely also feasible

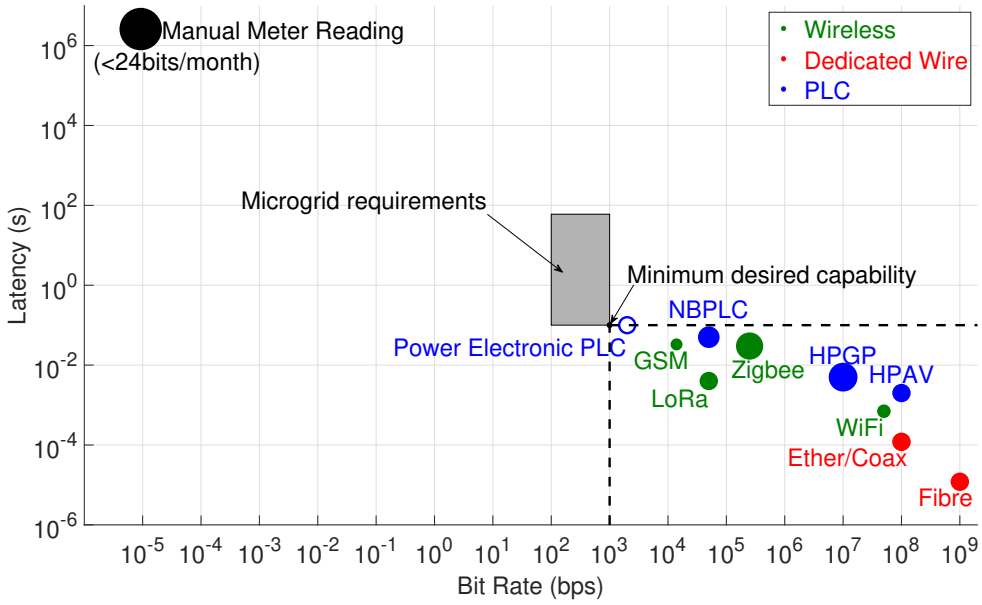

Figure 4.1: Microgrid FAN communication technology bit rate versus latency comparison. The filled dot area is scaled to reflect cost-per-customer (Power Electronics PLC is 'free' and so is an open dot). The grey rectangle shows the specification region that satisfies all three levels of hierarchical microgrid control. All the digital technologies from Table 4.1 exceed these requirements. The non-digital case of manual meter reading is included for comparison.

to connect the community to a macrogrid rather than installing a microgrid, so this situation may be rare in practice.

4.1.2 Powerline communication (PLC)

PLC is also a wired technology but uses the existing power cables rather than dedicated wires. The network topology is therefore determined by the power grid topology from Fig. 3.1. High-frequency data signals are coupled onto the powerline (high compared to the power frequency of 50-60 Hz). PLC technology is mature and is widely used by utility companies to coordinate protection systems. In large grids, it is a very attractive option because no new cables need to be laid. Utility companies have full control of the communication medium and must only purchase and install PLC modems throughout the power network. NB PLC that utilize the G3 or Prime ODFM protocols in the CENTELEC A frequency bands (< 100 kHz) is currently being deployed throughout Europe for smart meter upgrade programs

[173]. However, this niche technology is not widely available [174]. HomePlug is a BB protocol occupying a higher frequency band (1-30 MHz) that delivers higher bit rates [119]. The AV was HomePlug's first iteration of indoor internet distribution modems that use pre-existing building cabling with data rates of 200 Mbps. In 2010, HomePlug developed the GP technology created as a low-power solution for smart grids such as electric vehicle (EV) charging stations [118]. Despite its intention of being a 'trimmed-down' and cheaper version of AV, the smaller manufacturing scale of GP make it more expensive than the more-capable AV. Standby power saving techniques used in the GP were then incorporated in the next generation AV2 that occupies a wider band (1-86 MHz) and achieves advertised data rates up to 2 Gbps. AV modules are mass-produced, widely available around the world, and relatively cheap compared to both the GP and NB options. A full description of the HomePlug technology will follow in Chapter 5.

Power Electronics PLC refers to a wide range of other bespoke PLC techniques that advertise much lower bit rate but at little to no cost. For example, secondary control load sharing enhancement is proposed in [187] through modulating the DER loading condition into a variable pulse width modulation switching frequency that can be interpreted by neighbouring DERs. In [188], data is modulated by perturbing the switching frequency achieving data rates of 3.8 kbps. In [189], a software-based amplitude modulation scheme encodes data on a DC link at 2 kbps by perturbing the duty cycle of the converter switches. This implementation requires zero-additional-hardware and so, in theory, has no hardware costs.

4.1.3 Wireless

Wireless systems are flexible, modular, and do not require extra cabling. There are many mature wireless systems on the market. However, in the field, they can suffer from unexpected blind spots or interference leading to reliability issues [190]. The theoretical bit rates are often not realised in practice because of congestion and low signal strength. However, despite these obstacles, wireless networks have proven to be successful in many microgrid deployments. Basic protocols typically use star-like

topologies that rely on line-of-sight between transmitter nodes and a centralized receiver, but more sophisticated techniques can form ring or mesh topologies to extend range. Included in Table 4.1 are two main wireless categories, low power wide area network (LPWAN) that support lower bit rate over long range such as LoRa and GSM, and higher bit rate home area network (HAN) options with short range like Wi-Fi and Zigbee. High manufacturing volumes make cellular technologies an attractive economic choice [177]. Furthermore, extensive GSM coverage in Sub-Saharan Africa make it a strong candidate for remote rural microgrids [185], [186]. However, a FAN that uses cellular technology is dependent upon a third-party telecommunication company. Data prices, network congestion, and contract terms may prove limiting. These technologies also make strong candidates for backhaul links. HAN options may not have sufficient range for all microgrid FANs but are still a very capable option for smaller grids or with the inclusion of repeater nodes or mesh networking techniques.

4.1.4 Latency

In this thesis, latency refers to the round-trip time for a message to propagate between the smart meter and the EMS over a distance of 100 m. Latency in wired or wireless solutions at this geographic scale depend primarily on the protocols and modulation techniques used. The delay due to signal propagation in the medium is comparatively negligible. For wired technologies, the values in Table 4.1 are the time it takes a standard TCP exchange of 1500 bytes to occur at the given bit rate. The latency values for wireless technologies are taken from literature experiments. Latency of the Power Electronics PLC technique in [189] is measured using a 32 byte message (sufficient to send an AMR). Both HomePlug latencies are measured. For manual meter reading (utility sends technician to read the meter), the 'latency' is literally the time between readings: once per month, which yields a data rate of < 24 bits/month (derived from reading six numerical digits on a meter display). It is important to note that although UEC significantly reduces cost and complexity of manual meter reading, it still has the same fundamental bit

rate and latency as manual meter readings. The only difference is the customer is reading the meter rather than utility personnel.

4.1.5 Cost per customer

'Cost per customer' is the cost of implementing a communication technology using a commercially available module ready for plug-and-play integration. This cost includes 100 m of cable (for wired technologies), the modem microchip or transceiver, antennas (for wireless), and interface hardware (*e.g.*, PCB and supporting components, connectors). Prices are calculated at wholesale quantities based on quotations from major suppliers. Shipping costs are not included. Some of the mainstream technologies are available from suppliers (*e.g.*, TDK Solutions in Kenya) in the developing world at competitive prices. The cost of a solution is strongly dependent on the maturity and manufacturing capacity associated with the technology. As a result, *e.g.*, Ethernet and Wi-Fi are very price competitive. Dedicated-cable technologies are attractive for geographically small microgrids (transmission distances less than 100 m), but cable cost quickly becomes prohibitive at larger distances.

Fig. 4.1 and the data in Table 4.1 reveal that all the evaluated technologies exceed the communication requirements defined in Table 3.1. The minimum desired capability from Table 3.1 to satisfy the three levels of hierarchical microgrid control is a bit rate of 1 kbps and latency less than 100 ms. The remaining delineating factor is cost, in which case Power Electronics PLC is the superior candidate. However, unlike the other technologies, this option is not an off-the-shelf product, but rather entails a bespoke software algorithm that has developmental costs. Furthermore, the prices in Table 3.1 are all of the same order of magnitude and can easily be afforded when amortised over long periods of time. Therefore, the engineering decision becomes somewhat subjective, influenced by multiple site specific factors such as geography, physical obstacles, distance between nodes, soil characteristics, cell phone coverage, local product availability, manpower, and future upgrade requirements, to name a few.

4.2 Communication cost-benefit Analysis

The following cost-benefit analysis synthesises Chapters 3 and 4 to quantify the service value added to an islanded LV microgrid through the addition of an increasingly capable communication link. First, a communication-less baseline is established using the RELCON cost inventory from Table 3.3. Second, a minimally capable FAN is added to the power system. Then, the FAN bit rate is incrementally increased while observing the effect on the cost of energy. LCOE best captures the cost-benefit outcome of adding a digital communication system since it accounts for all microgrid costs over the microgrid's lifetime [50]. It demonstrates the unsubsidised energy tariff amortised by the customer and reveals savings gained through digital communication. Eq. (4.1) expands upon Eq. (3.1) from the previous chapter. Each of the four expense categories are multiplied by a discount factor. Additionally, LCOE is normalized to the communication-less baseline for comparison effect.

$$\mathrm{LCOE_p} = \frac{\frac{A\hat{\alpha_\mathrm{p}}+BN\hat{\beta_\mathrm{p}}+CL\hat{\gamma_\mathrm{p}}+DLN\hat{\delta_\mathrm{p}}}{ELN\hat{\eta_\mathrm{p}}}}{\mathrm{LCOE_{base}}} \text{ [\$/kWh]} \tag{4.1}$$

Hatted Greek letters represent discount factors that change in reaction to the installation of a communication system with a particular bit rate. The subscript p specifies the communication service bit rate level. All other normal lettered variables A, B, C, D, E, and N are fixed baseline costs and assumptions for a communication-less microgrid and are catalogued in Table 4.2. These variables represent the same things as in Table 3.3 but will be slightly different since the baseline microgrid has no communication system. For ease of reading, the variable definitions are included here: A is CAPEX independent of the number of customers (\$), B is CAPEX for each added customer (\$/customer), C is annual OPEX independent of the number of customers (\$/year), and D is annual OPEX for each added customer (\$/year-customer). Again $C = 0$ since no annual OPEX costs are identified for the Tier 3 RELCON case study. L is the lifetime of the system in years, N is

the number of customers served in the microgrid, E is energy served (kWh/year-customer), and η represents technical and non-technical losses as a fraction of supplied energy where: $E_{\text{supplied}} = \eta E$.

4.2.1 Manual Meter Reading $p = 1$

The baseline for the cost-benefit analysis is a communication-less islanded rural microgrid based on the RELCON cost inventory from Section 3.4.2. Note that all the communication related costs are set to zero. Sizing is based on the same load profile estimations featured in Fig. 3.7 meaning energy served (E) remains the same. However, since the microgrid does not have secondary or tertiary control and no means of curtailment, DERs must be conservatively oversized to prevent outages. Therefore, the insolation is set to the worst 3-day average from last decade, 2.46 kWh/m^2 to accommodate all loads in bad weather while also supporting peak demand. This increases annual CAPEX (B).

Baseline annual OPEX per customer (D) encompasses battery replacement every four years and a monthly visit from a utility technician, primarily to manually read the meter and collect cash payments from customers. Monthly cash payment collection schedules are typical in a rural microgrid to minimize payment size and maximize collection success [24]. This visit could also be used to perform any needed maintenance. Each visit costs \$1.25 [191], [192]. (This is lower than the \$2.60 estimate in the UK smart meter study in [88] due to market differences between the UK and Kenya.) Such a visit is, of course, a form of communication with a latency of one month and a bit rate of approximately 24 bits per month. Other OPEX that must be amortised are unpaid bills (10% of energy served) and customer minutes lost (CML) due to outages [54]. The national grid in Kenya experiences well over 200 hours/year of CML [193]. However, microgrids significantly reduce CML and a modest 24 hours/year is assumed for the case study [60].

Technical losses (*e.g.*, cables, converters) are lower without communication since communication hardware uses power [88]. Non-technical losses due to theft are set to 5% of load [53]. Losses are encompassed by $\hat{\eta}_{\text{p}}$. The baseline LCOE in

Table 4.2: Communication-less microgrid baseline costs and assumptions

Variable	**Quantity**	**Unit price**	**Wholesale**[a]
CAPEX		**($/unit)**	**($)**
Hub converter	1.00	334.56	334.56
Installation	1.00	5377.50	5377.50
Labour (man-hrs)	432.00	5.51	2380.32
EMS	0	367.50	0
Backhaul	0	56.00	0
A			**8092.06**
CAPEX/customer		**($/unit-cust)**	**($/cust)**
Battery (Wh)	1841	0.10[b]	184.08
PV (W)	458	0.60[c]	274.76
insolation (Wh/m^2)	2460		
efficiency	0.15		
Cable (m)	100.00	0.50	50.00
Labour (man-hrs)	35.33	3.00	106.00
Protection	1.00	35.17	35.17
Homebox	1.00	276.43	276.43
Zero-communication meter	1.00	9.00	9.00
Digital communication	0	23.00	0
B			**935.44**
Total Customer CAPEX			**2212.37**
OPEX/customer		**($/unit-yr-cust)**	**($/yr-cust)**
Unpaid tariff (kWh/year)	15.22	0.75	11.42
CML (kWh/year)	0.42	0.75	0.31
O (utility visits/year)	0.50	1.25	0.63
M (battery replacement/year)	0.20	184.08	36.82
Mobile Money	0	12.00	0
Data	0	1.00	0
D			**63.55**
Total Customer Lifetime Cost			**2745.86**
L (years)			20.00
N (# of customers)			15.00
E Annual energy served (kWh/year-customer)			152.24
E Daily energy served (Wh/day-customer)			417.09
$\hat{\eta_0}$ (baseline losses)			1.21
$\mathbf{LCOE}_{\text{base}}$($/kWh)			**0.75**

a. These values do not consider inflation.
b. Includes cost of battery rack & fuses.
c. Includes cost of PV install, MPPT controller, mounts, & connectors.

Table 4.2 is \$0.75/kWh which reflects the true cost of unsubsidised communication-less Tier 3 PV microgrid electricity in rural Kenya [25], [30], [50]. All energy costs are compared to this baseline; therefore, the normalized LCOE for manual meter reading is \$1.00/kWh.

4.2.2 Cost-benefit table

Having established a communication-less baseline, Table 4.3 shows how the addition of communication to the microgrid will change CAPEX, OPEX, and losses. The first row of the table shows the manual meter reading communication-less baseline where all the discount factors are set to 1 except for the loss factor $\hat{\eta_0}$ which shows 21% losses in the baseline system due to technical and non-technical losses (*i.e.*, theft).

Table 4.3 contains seven communication levels ($p = 0$ to 6): manual meter reading (baseline, $p = 0$), UEC ($p = 1$), AMR ($p = 2$), secondary control ($p = 3$), tertiary control ($p = 4$), high fidelity (HiFi) monitoring ($p = 5$), and bundled internet ($p = 6$). The vector of discount factors $\hat{x_{\mathrm{p}}} = (\hat{\alpha_{\mathrm{p}}}, \hat{\beta_{\mathrm{p}}}, \hat{\gamma_{\mathrm{p}}}, \hat{\delta_{\mathrm{p}}}, \hat{\eta_{\mathrm{p}}})$ is calculated by:

$$\hat{x_{\mathrm{p}}} = \prod_{i=1}^{q} x_{\mathrm{i}} \tag{4.2}$$

where q is the highest counter within the communication level row and expense column of interest. The model is built in MATLAB. Communication levels are made possible through hardware additions (inputs) which trigger cost changes (outputs). Baseline expenses (A, B, D) are modified within the model according to the inputs. Outputs change expenses as well. But they also affect sizing assumptions and losses. Each change is quantified by a discount factor. The product of those discount factors produces the discount vector $(\hat{x_{\mathrm{p}}})$ for a given communication level. For example, referencing the annual OPEX column and the UEC row in Table 4.3:

$$\hat{\delta_1} = \prod_{i=1}^{q=2} \delta_{\mathrm{i}} = \delta_1 \delta_2 = 0.76 \times 0.78 = 0.59 \tag{4.3}$$

Table 4.3: Cost-benefit analysis baseline costs and assumptions

FAN type	Communication Service		Input→Output→LCOE	Shared CAPEX $\hat{\alpha_p}$		Annual CAPEX per Customer $\hat{\beta_p}$		Annual OPEX per Customer $\hat{\delta_p}$		Losses $\hat{\eta_p}$	
No digital communication	Manual Reading	Baseline	Meter (No comm) +9 ($/customer) [88]							η_1	1.21
		$LCOE_0$	**1.00**	$\hat{\alpha_0}$	**1.00**	$\hat{\beta_0}$	**1.00**	$\hat{\delta_0}$	**1.00**	$\hat{\eta_0}$	**1.21**
	UEC	Inputs	Meter (Prepaid) +43 ($/customer)[1] [88]			β_1	1.05				
		Outputs	Prepaid meters reduce frequency of utility visits to 1 visit/2 years. [88]					δ_1	0.76		
			Prepaid meters eliminate non-technical losses from unpaid tariffs. [84], [86]					δ_2	0.78		
		$LCOE_1$	**0.83**	$\hat{\alpha_1}$	**1.00**	$\hat{\beta_1}$	**1.05**	$\hat{\delta_1}$	**0.59**	$\hat{\eta_1}$	**1.21**
Low-bit rate FAN (<1 kbps) with GSM backhaul	AMR	Inputs	Backhaul link +35 ($)	α_1	1.00[2]						
			Meter (Smart) -8 ($/customer)[3] [88]			β_2	0.99				
			Digital comm +23 ($/customer)			β_3	1.02				
			Mobile money fees +4 ($/yr-customer) [194]					δ_3	1.11		
			Data fees <+1 ($/yr-customer) [186]					δ_4	1.00[2]		
		Outputs	Smart meter increases technical losses by 10%. [88]			β_4	1.04	δ_5	1.08	η_2	1.10
			Data collection analysis increases accuracy of sizing reducing PV size by 39%.			β_5	0.89				
			AMR decreases theft by 10%. [85], [195]			β_6	1.00[2]	δ_7	1.00[2]	η_3	1.00[2]
			AMR decreases CML 20%. [87], [88]					δ_6	1.00[2]		
		$LCOE_2$	**0.79**	$\hat{\alpha_2}$	**1.00**	$\hat{\beta_2}$	**0.98**	$\hat{\delta_2}$	**0.71**	$\hat{\eta_2}$	**1.32**
	Secondary Control	Inputs	EMS +82 ($) [19]	α_2	1.01						
			Control sensors +12 ($/customer) [19]			β_7	1.01				
		Outputs	Secondary control eliminates theft. [157], [158]			β_8	0.99	δ_8	0.97	η_4	0.97
			Secondary control increases efficiency of converters and controllers by 1%. [102], [196]			β_9	0.98	δ_9	0.99	η_5	0.99
			Secondary controllers better manage SOC increasing battery life by 10%. [197], [198]					δ_{10}	0.90		
			Secondary controllers better prevent outage decreasing CML another 5%. [87], [88]					δ_{11}	1.00[2]		
		$LCOE_3$	**0.78**	$\hat{\alpha_3}$	**1.01**	$\hat{\beta_3}$	**0.97**	$\hat{\delta_3}$	**0.61**	$\hat{\eta_3}$	**1.26**
	Tertiary Control	Inputs	IHD +18 ($/customer) [88] δ			β_{10}	1.02				
			Data fees <+1 ($/yr-customer) [186]					δ_{12}	1.00[2]		
		Outputs	DR capability allows for battery size reduction of 10%. [69], [71], [88], [199]			β_{11}	0.96	δ_{13}	0.91		
			DSM measures result in 10% demand shift from night to day further reducing battery size by 10%. [77], [78], [81], [88]			β_{12}	0.97	δ_{14}	0.91		
			Data enhanced tertiary controllers better protect batteries increasing their life another 20%. [76], [197]					δ_{15}	0.83		
			Tertiary controllers better prevent outage decreasing CML another 5%. [87], [88]					δ_{16}	1.00[2]		
		$LCOE_4$	**0.68**	$\hat{\alpha_4}$	**1.01**	$\hat{\beta_4}$	**0.92**	$\hat{\delta_4}$	**0.42**	$\hat{\eta_4}$	**1.26**
Broadband FAN (>1Mbps) with 4G backhaul	HiFi Monitoring & RTP	Inputs	Backhaul upgrade +21 ($) [88]	α_3	1.00[2]						
			Load sensors +15 ($/customer) [19]			β_{13}	1.02				
			Data fees +1 ($/yr-customer) [186]					δ_{17}	1.03		
		Outputs	DSM measures result another 10% demand shift from night to day further reducing battery size by 10% [88], [200], [201]			β_{14}	0.97	δ_{18}	0.91		
			High resolution battery data improves battery health maintenance increasing their life another 10%. [149]					δ_{19}	0.93		
			Remote firmware update reduces frequency of utility visits to 1 visit/5 years. [88]					δ_{20}	0.98		
			High resolution load data prevents outages decreasing CML another 5%. [87], [88]					δ_{21}	1.00[2]		
		$LCOE_5$	**0.65**	$\hat{\alpha_5}$	**1.02**	$\hat{\beta_5}$	**0.91**	$\hat{\delta_5}$	**0.36**	$\hat{\eta_5}$	**1.26**
	Bundled Internet	Inputs	Backhaul upgrade +100 ($) [183], [184]	α_4	1.01						
			Data fees +55 ($/yr-customer) [186]					δ_{22}	3.41		
		$LCOE_6$	**1.04**	$\hat{\alpha_6}$	**1.03**	$\hat{\beta_6}$	**0.91**	$\hat{\delta_6}$	**1.24**	$\hat{\eta_6}$	**1.26**

[1] Costs and percentages are cumulative and include all costs and changes from previous row.
[2] Change is less than 1%.
[3] The smart meter is $8 cheaper than a prepaid meter.

After completing similar calculations for $\hat{\alpha_1}$, $\hat{\beta}_1$, and $\hat{\eta_1}$, they are input into Eq. (4.1) to find LCOE_1 for the UEC communication level. Benefits are assumed cumulative; therefore, calculations include all discounts from previous rows (*i.e.*, the counter i in Eq. (4.2) always starts with 1).

The resultant model can be used by microgrid developers by entering initial values for A, B, C, D, E, L, N, and η and then applying the discount factors for the desired level of communication from Table 4.3. Reduction in LCOE occurs through the installation of a digital communication FAN with an increasing bit rate capability. Hardware installations will directly increase the CAPEX but will yield cost savings through efficiency gains.

Percent savings are extracted from estimates in the literature and are selected carefully and modestly to not exaggerate the effects of digital communication. Unreferenced values in Table 4.3 come from Table 4.1 or they are explained below. Although the literature clearly shows digital communication (specifically, DSM measures) can reduce demand, this case study assumes demand (E) to be constant [69]. This assumption was made for two reasons. First, in the context of a rural islanded microgrid where energy consumption is initially very low, a demand reduction actually increases the cost per unit of electricity. Therefore, microgrid developers targeting unelectrified communities will be encouraging an increase in demand to make energy cheaper to low-income customers. Second, first-time electricity communities experience slow but steady increases in consumption [46], [48]. By keeping E constant, the case study accounts for these realities while also avoiding exaggerated or misleading results. This cost analysis can be compared to estimates in a UK-based macrogrid smart meter upgrade analysis [88] which validates the underlying assumptions of the case study while tailoring the results to an islanded LV microgrid. This is an important distinction since the literature primarily deals with smart grid modeling and experimentation in grid-tied Tier 5 systems. The following sections will discuss each communication level.

4.2.3 User Enabled Communication (UEC) $p = 1$

Prepay meters are more expensive than traditional post-pay meters, but still bring large savings by eliminating unpaid bills and reducing the frequency of utility personnel visits to once every two years for meter maintenance [84], [86], [88]. Instead of monthly visits for manual meter readings, the customer purchases either physical or digital tokens to charge the prepay meter. This drastically slashes OPEX by 41% and reduces total cost by 17% lowering the normalized LCOE to \$0.83/kWh.

4.2.4 AMR $p = 2$

Slightly cheaper smart meters replace prepaid meters and an average bidirectional digital communication system from Table 4.1 (\$23) is installed at each smart meter. As demonstrated in Fig. 4.1, any of the technologies explored in Chapter 3 satisfy the modest AMR requirement defined in Table 3.1. It is therefore also assumed that the installed AMI communication system inherently satisfies the requirement for secondary and tertiary control with a medium latency of 100 ms and a bit rate of at least 1 kbps. The cost estimate of \$23 is less than the \$33 estimate in [88] because the UK-based study assumes a slightly more expensive cellular-based direct-WAN transceiver that also contains extra home area network hardware. Each customer must also absorb the fractional cost of adding an additional transceiver (\$23) at the hub and a GSM backhaul as defined in Table 4.1 (\$12). Backhaul data fees are set at \$8.40/GB (the average rate in Sub-Saharan Africa [186]). Customers still prepay for electricity but do so via a mobile money banking application on their cell phone (*e.g.*, MPESA, a Kenyan mobile money application) which incurs transaction fees of \$0.33/month per customer [19], [194].

Despite the increase in CAPEX, OPEX and losses from the addition of AMI, an additional 4% reduction in LCOE is achieved primarily through more accurate DER sizing facilitated by hourly AMR data. It is assumed that the microgrid developer has load profile data from other similar microgrids to inform a more accurate sizing of the DER. To capture this, insolation is increased to 4 kWh/m^2, the worst monthly average from last decade [159]) versus the worst 3-day average used in the

communication-less baseline. AMR data reduces DER size by 39%. With hourly demand measurements, the utility can more rapidly identify shortages and repair them, thus reducing the CML by 20% [87], [88]. Electricity theft typically occurs by bypassing the meter. Consumption monitoring can better identify such anomalies reducing theft by 10% [85], [88], [195]. Normalized LCOE for AMR is \$0.79/kWh.

4.2.5 Secondary Control $p = 3$

Secondary control requires an EMS at the hub and additional control sensors. Cost benefits are negligible (1% decrease in LCOE), but secondary control provides a much more reliable grid and a foundation for tertiary benefits. Secondary control algorithms also can quickly recognize theft, triggering the EMS or smart meter to isolate the customer. It is assumed that secondary control software together with the AMR hourly data can effectively eliminate theft [157], [158]. The extent of savings possible with secondary control varies widely and depends heavily on the microgrid design, available data, and sophistication of the algorithm. This case study is based upon a star configured DC microgrid where theft detection is relatively simple. However, theft detection and isolation can be significantly more challenging on radial feeders. Microgrid-wide signalling and the resulting control actions improve electrical efficiency by 1% [102], [196] and further reduce CML by another 5% [88]. State of charge management extends battery lifetime by 10% [197], [198]. Normalized LCOE for AMR is \$0.78/kWh.

4.2.6 Tertiary Control $p = 4$

An IHD is added to the smart meter to inform the customer about their consumption and facilitate their participation in DSM measures. Physical DR actions that curtail demand when necessary to preclude outages and protect storage assets enables a 10% reduction in battery size and another 5% decrease in CML [69], [71], [88], [199]. TOU tariffs incentivise daytime usage shifting 10% of night-time usage to day-time during periods of solar production [77], [78], [81], [88]. These DSM measures also reduce the grid evening peak demand usually drawn from the batteries [76]. Battery

management algorithms that combine secondary control mechanisms with data collection allow for detailed battery health monitoring further extending battery life by 20% [197]. The communication system selected from Table 4.1 for the microgrid FAN enables AMR, secondary, and tertiary control reducing total cost by 32% primarily through DER-size minimisation and reductions in OPEX. Tertiary control brings normalized LCOE down to $0.68/kWh.

4.2.7 High Fidelity Monitoring and Real-Time Pricing $p = 5$

This scenario assumes 15-minute resolution load-specific monitoring, RTP, and load-targeted physical DR summarizing the 'state-of-the-art' case scenario as promised by the literature on smart grids [69], [202], [203]. It is also assumed that each customer contractually agrees to a high level of remote control of five specific loads of special interest. Using the Homebox smart meter design from Section 3.4, each of the load ports can be powered, monitored, and controlled independently by the utility. The smart meter IHD displays curtailment schedules and notifications. Data is sent and received every 15 minutes from each smart meter containing information about the customer's total consumption and specific data on each of the five loads. Studies suggest a maximum of 30% of the load is potentially flexible to DSM measures. Therefore, RTP is assumed to shift another 10% of demand shift beyond the tertiary case [200], [201]. RTP combined with load-specific physical DR measures can extend battery life another 10% and reduce CML another 5% [88], [149]. Remote firmware updates (assumed to be 1 MB every 2 years) together with four times more samples increase data fees but simultaneously decrease the number of visits by utility personnel to once every five years [88].

As explained in Section 3.3, RTP and load-specific DR are unrealistic expectations for an islanded rural microgrid because they too heavily depend on customer consent and participation. The literature on RTP smart grids contains mostly theoretical-based simulations and is only included in this case study to illustrate the hypothetical additional savings possible presuming the simulations could be implemented. Table 4.3 shows, even in this optimistic model, LCOE reduction is

3% beyond tertiary control. Load-specific DSM may require even more hardware (*e.g.*, Bluetooth transmitter, microcontroller, clock, contactor, and display installed at each load of interest) further increasing CAPEX negating the potential cost benefits. Normalized LCOE for high fidelity monitoring and RTP is \$0.65/kWh.

4.2.8 Bundled Internet $p = 6$

Providing bundled internet (or voice services) through each customer's smart meter is technically possible but it requires additional hardware such as Ethernet ports and routers both at the smart meter and at the EMS. The backhaul link estimation comes from the price of a 4G router and network switch to handle much higher bit rates for multiple customers [183], [184]. This scenario assumes a modest 1 Mbps connection and 0.55 GB/month usage for each customer [204]. Providing internet to microgrid customers through the FAN does not improve LCOE; and internet service would require a separate tariff to cover the additional incurred cost. However, from a commercial utility perspective, a bundled internet service may not be worth pursuing in a rural context for the reasons discussed in Section 3.1.5. It seems plausible to offer such a service where demand exists assuming the data fees associated with internet transmission can be collected from participating customers. However, it must be emphasized that the added hardware to facilitate internet or voice does not provide any additional reductions to LCOE beyond the HiFi scenario. Bundled internet lifts the normalized LCOE to \$1.04/kWh.

4.3 Conclusion

Fig. 4.2 plots LCOE versus bit rate of an increasingly capable communication network. Values on the x-axis come from Table 3.1 and the y-axis shows normalized LCOE (\$/kWh) from Table 4.3. UEC-provided meter reading can reduce the LCOE by 17% simply through the installation of a prepay meter or the implementation of self-reporting. However, UEC alone cannot provide the control and monitoring services summarized in Table 3.1. AMI, secondary and tertiary microgrid control systems will reduce and shape demand, increase hardware efficiency, and lengthen

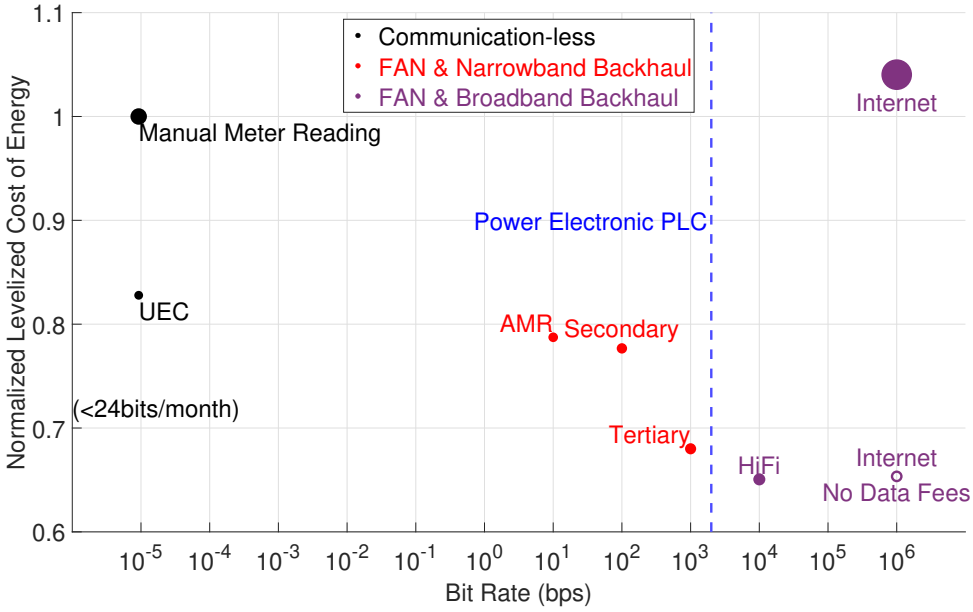

Figure 4.2: Quantification of the service value added to a microgrid through the installation of a communication system. As the capability of the communication system (expressed in bit rate) increases, the LCOE decreases. LCOE is normalized to a communication-less microgrid. Dot area is scaled to reflect cost of the required communication system. The dotted blue line marks the bit rate capability of Power Electronic PLC to convey the services available with less than 2 kbps. Bundled internet service is shown both accounting for the necessary data fees (solid dot) and neglecting those data fees (empty dot) assuming the customer is paying internet access data fees separately.

service life. Fig. 4.2 reveals that secondary control does not significantly reduce the price of energy which is why many microgrid ventures only pursue savings from UEC and AMR. However, to harvest the cost savings from tertiary control made possible with DSM, secondary control is requisite. Upon investment in a minimally capable communication system (< 100 ms latency, > 1 kbps), multiple high impact services become possible, reducing the LCOE by 32%. However, as the capability of the communication system increases above 10 kbps there occurs a point of diminishing returns where the capability of the communication system does not yield further reductions in LCOE. The additional 3% savings portrayed in the HiFi scenario is possible but unlikely and depends on the implementation design and hardware costs associated with individual load control.

The choice of communication technology and the reductions in LCOE in any

particular system will, of course, depend on many factors, but this cost-benefit analysis has shown that there are two large step changes in LCOE reductions. First, through pre-payment and the second, through tertiary control to implement DSM.

5
Transmission Line Model

The primary findings of this chapter have been submitted for publication to IEEE Transactions on Power Delivery: D. Neal, D. Rogers and M. McCulloch, "Broadband Powerline Communication for Low-Voltage Microgrids," unpublished.

Chapter 5 overviews transmission line theory and s-parameters. These are used to build a bottom-up analytical powerline model from the cross sectional geometry of the cable. The model incorporates proximity effects learned from multiconductor transmission line theory and frequency dependent dielectric material behaviour to accurately predict signal attenuation at high frequency. The model is validated with s-parameter measurements taken with a 2-port VNA on the RELCON laboratory testbed.

5.1 Introduction

Having established the costs and benefits of adding a digital communication FAN to a microgrid, this chapter assumes the selection of PLC as the chosen technology. Since available technologies all exceed the required bit rate and latency for microgrid control as shown in Fig. 4.1, and the lack of variance in amortised cost fails to differentiate them, the engineering choice becomes much more nuanced. In the context of rural electrification, PLC was selected for further study for various

reasons. This study was prompted in part by the HomePlug GP, a BB PLC technology designed as a robust low-power alternative to its more capable relative the AV for smart grid applications, specifically EV charging networks [118]. First, applying the technology to a rural microgrid seems a natural fit. Second, the HomePlug technology offers a plug-and-play solution for microgrid developers. They utilize IP protocols that are easy to use and integrate into other layers of the SCADA. The HomePlug AV became widely available as an indoor internet networking tool in the 2000s [119]. Although indoor networks are slightly different than microgrids networks, their similarities in length and topology render the former a useful proxy for studying communication within microgrids. Third, PLC offers a wired solution without extra cabling. This offers reliability like other wired technologies without the cost of added cable. Since wired solutions have been shown to be cost-prohibitive beyond 100 m, PLC can potentially reduce capital costs. Wireless solutions sometimes have reliability issues caused by obstacles (*e.g.*, tin roofs in [190]). When deploying to an unknown environment like a remote village, wireless solutions introduce engineering uncertainties. Lastly, bespoke PLC solutions offer low bit-rate communications sufficient for microgrid control with zero-added hardware using power electronics converters [189]. Since modern microgrid designs heavily depend on power electronics, the prospect of forming a "free" FAN is an exciting prospect. This last reason is not investigated in depth in this study, but is mentioned here as additional motivation for exploring and understanding how power distribution cables behave as a communication medium.

5.2 Two-wire Transmission Line Model (TLM)

As the length of the transmission line approaches the communication signal wavelength (*i.e.*, line length>tenth of the wavelength), the channel must be modelled as a distributed element transmission line to account for wave propagation behaviour [205]. The distributed element TLM in Fig. 5.1 considers an infinitesimally small section of cable with two conductors where z is the position on the line.

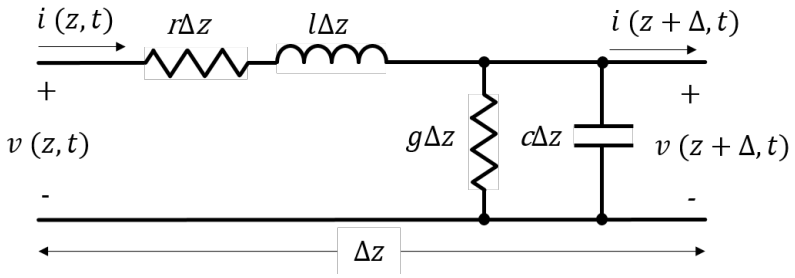

Figure 5.1: Distributed element model of two-wire transmission line where Δz is an infinitely small length of cable and voltage and current behave like propagating waves. Reproduced from [205]

The transmission line conductor is modelled with a series resistance (r) and shunt admittance (g) that cause frequency dependent signal attenuation. Series inductance (l) and shunt capacitance (c) are determined by the dielectric and affect signal propagation. This model is commonly referred to as the *two-wire* model with per-unit parameters $rlcg$. Per-unit parameters can be mathematically derived from the cable cross sectional dimensions from Fig. 5.2.

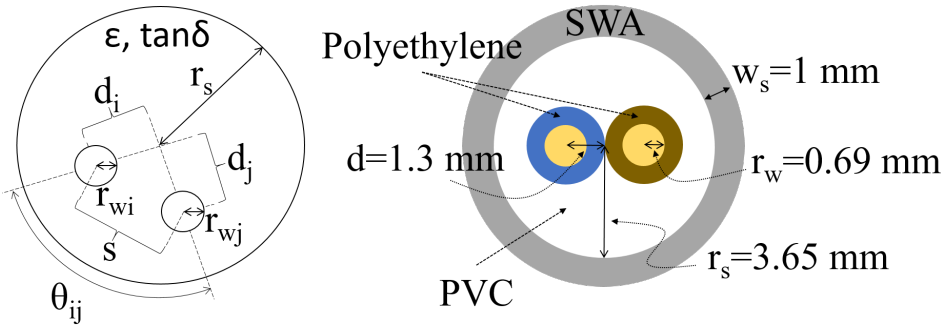

Figure 5.2: Cross sectional geometry of a) generic shielded multiconductor cable reproduced from [205] b) 1.5 mm^2 SWA 2-core power cable.

The starting point for modeling will be the simple two-wire scenario in Fig. 5.2(a) where a set of parallel wires with conductivity σ and permeability μ is surrounded by a homogeneous medium with permittivity ε and loss tangent $\tan\delta$.

5.2.1 Per-unit parameters

Frequency dependence of the ac resistance is included anytime the radius of the conductor is greater than twice the skin depth [205]:

$$\delta_{skin} = \frac{1}{\sqrt{\pi f \mu \sigma}} \text{ [m]} \tag{5.1}$$

where f is frequency in Hz, μ is the magnetic permeability of the conductor and given by $\mu_0\mu_\text{r}$ ($\mu_\text{r} = 1$ for copper). The conductivity of copper at room temperature is $\sigma = 58.13$ (MS/m). Using the dimensions in Fig. 5.2, the two-wire per-unit $rlcg$ equations are as follows:

$$r_\text{two-wire} = \frac{1}{2\pi r_\text{w} \sigma \delta_\text{skin}} \text{ [}\Omega\text{/m]} \tag{5.2}$$

$$l_\text{two-wire} = \frac{\mu}{\pi} \text{acosh}\left(\frac{d}{r_\text{w}}\right) \text{ [H/m]} \tag{5.3}$$

$$c_\text{two-wire} = \frac{\pi\varepsilon}{\text{acosh}\left(\frac{d}{r_\text{w}}\right)} \text{ [F/m]} \tag{5.4}$$

$$g_\text{two-wire} = 2\pi f c_\text{two-wire} \tan\delta \text{ [S/m]} \tag{5.5}$$

where the dielectric material surrounding the conductors is characterised with the permittivity ($\varepsilon = \varepsilon_0\varepsilon_\text{r}$) and the loss tangent ($\tan\delta$) both of which will be discussed later. Both l and c decrease slightly with frequency but are considered constant in this model.

5.2.2 Wave equations

Circuit analysis of Fig. 5.1, assuming steady state conditions in the time domain, yield the traveling wave equations that express voltage and current at any point z along the line:

$$V(z) = V^+ e^{-\gamma z} + V^- e^{\gamma z} \text{ [V]} \tag{5.6}$$

$$I(z) = \frac{1}{Z_0}(V^+ e^{-\gamma z} - V^- e^{\gamma z}) \text{ [A]} \tag{5.7}$$

where V^+ and I^+ are the incident (or forward) traveling waves and V^- and I^- are the reflected (or reverse direction) waves. The characteristic impedance Z_0 is the ratio of voltage to current for a traveling wave on a transmission line.

$$Z_0 = \frac{V^+}{I^+} = \frac{-V^-}{I^-} = \sqrt{\frac{r + j\omega l}{g + j\omega c}}\ [\Omega] \tag{5.8}$$

The propagation constant γ consists of α (Np/m), the attenuation constant that communicates the per-unit decay of the signal, and β (radians/m), the phase constant that expresses the amount of phase change per unit length of transmission line or how fast the signal's phase varies as it moves along the line (phase velocity $v_p = \frac{\omega}{\beta}$) [205].

$$\gamma = \alpha + j\beta = \sqrt{(r + j\omega l)(g + j\omega c)}\ \left[\mathrm{m}^{-1}\right] \tag{5.9}$$

These two variables (Z_0 and γ) characterise a transmission line and form the foundation of the two-wire TLM.

5.3 Scattering Parameters (s-parameters)

S-parameters are derived from the wave equations and are an effective tool for transmission line analysis primarily because they are directly measurable at the terminations (*i.e.*, ports) of any network. This allows for characterisation of any network as a closed system without access to, or knowledge of, the network itself. The transmission line in Fig. 5.1 can be thought of as a 2-port network. The scattering matrix in Fig. 5.3 relates the incident voltages to the reflected voltages at each port.

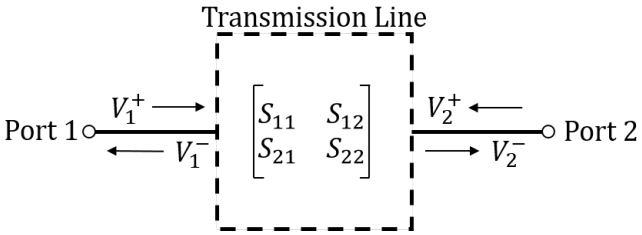

Figure 5.3: One line diagram of 2-port network defined by its s-parameters.

If the incident signal on Port 2 is set to zero ($V_2^+ = 0$), then S_{11} is defined as the ratio of the reflected (or exiting) voltage to the incident (or entering) voltage at Port 1 while S_{21} is the ratio of the reflected voltage at Port 2 to the incident voltage at Port 1.

$$S_{11} = \frac{V_1^-}{V_1^+} = \Gamma \tag{5.10}$$

$$S_{21} = \frac{V_2^-}{V_1^+} \tag{5.11}$$

S_{11} is called the reflection coefficient (Γ) and S_{21} the transmission coefficient *i.e.*, the forward voltage transfer function of the transmission line. When the load connected to Port 2 matches the characteristic impedance of the transmission line, S_{21} is analogous to the transfer function of the 2-port network where Port 1 is input and Port 2 is output.

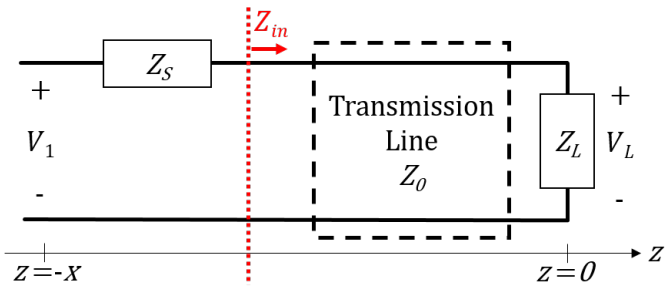

Figure 5.4: Relationship of impedances on a transmission line with characteristic impedance Z_0. The load is located at $z = 0$ whilst the source V_1 is at $z = -x$. The source has output impedance Z_L and the load has impedance Z_L.

Scattering parameters (s-parameters) are complex numbers and are always less than unity for passive devices. They are most often graphed in decibels (dB) as a function of frequency. S_{21} will be the primary tool in this study to evaluate the frequency response of a given network and the corresponding PLC channel performance.

Solving for the voltage at the load port of the transmission line in Fig. 5.4 where $z = 0$, simplifies the wave equations.

$$\begin{aligned} V_\mathrm{L} &= V_1^+ + V_1^- \text{ [V]} \\ I_\mathrm{L} &= \frac{1}{Z_0}(V_1^+ - V_1^-) \text{ [A]} \end{aligned} \tag{5.12}$$

Since $V = IZ_\mathrm{L}$:

$$Z_{\mathrm{L}} = Z_0 \frac{V_1^+ + V_1^-}{V_1^+ - V_1^-} \ [\Omega] \tag{5.13}$$

Solving for the ratio of reflected to incident voltage ($\frac{V_1^-}{V_1^+}$) yields S_{11} *i.e.*, reflection coefficient (Γ).

$$S_{11} = \frac{V_1^-}{V_1^+} = \Gamma = \frac{Z_{\mathrm{L}} - Z_0}{Z_{\mathrm{L}} + Z_0} \tag{5.14}$$

When $Z_{\mathrm{L}} = Z_0$, the reflection coefficient equals zero implying a "matched" load. The traveling wave is fully absorbed by the load and no energy reflects towards the transmitter. Said another way, all the wave energy is flowing in one direction. Coincidentally, this is also the maximum power transfer condition where the transmission line behaves as if it were infinitely long and the signal does not vary with distance. Any non-zero reflection coefficient means some energy reflects back towards the transmitter. Reflected waves add to incident waves at each point on the line creating standing wave conditions. When $Z_{\mathrm{L}} = 0$ or $Z_{\mathrm{L}} = \infty$ producing a reflection coefficient of 1 or -1, the entire signal is reflected producing standing waves with amplitudes double that of the signal voltage and current amplitudes equal to 0 A (or vice versa), *i.e.*, zero-power transfer.

5.3.1 Measuring s-parameters

The 2-port s-parameter matrix in Fig. 5.3 is measured with a VNA according to Fig. 5.4 by injecting a range of radio frequency signals (V_1) into a device under test (DUT). In this case, the DUT is a section of cable of length x with characteristic impedance Z_0 connected as in Fig. 5.5.

Port 1 of the DUT is connected to VNA Port A and Port 2 of the DUT is connected to VNA Port B. This is done by connecting the two core conductors of the SWA cable seen in Fig. 5.2 to the two conductors of the VNA, one as the signal conductor and the other as the reference conductor. VNA Ports A and B both have a fixed impedance of $Z_{\mathrm{L}} = Z_{\mathrm{L}} = 50\,\Omega$. This is a differentially coupled single-ended measurement, *i.e.*, the measurement is taken across the core conductors of the cable,

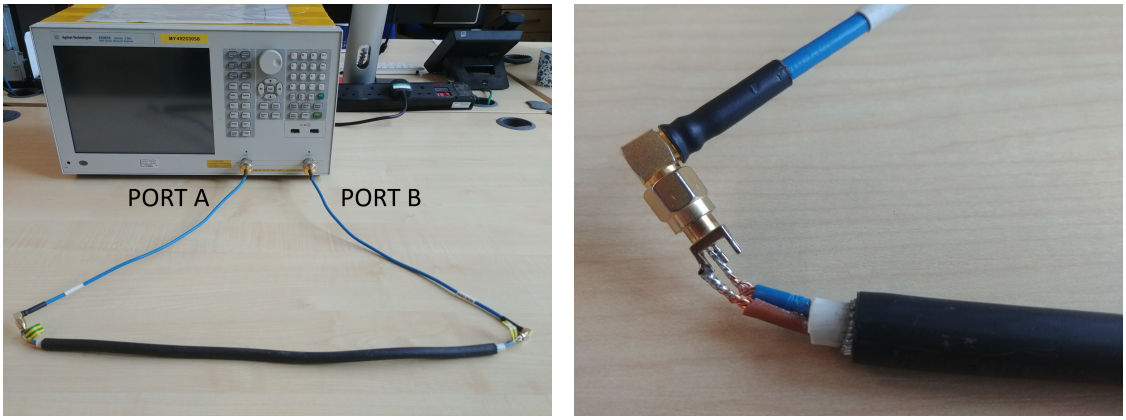

(a) (b)

Figure 5.5: VNA s-parameter experimental setup for a differentially coupled single-ended measurement of the two core conductors of a 1.5 mm^2 SWA cable.

one connected to the VNA signal conductor and the other connected to the VNA ground reference as in Fig. 5.5(b). A differential measurement can only be made using a 4-port VNA or through ground isolating balum filters [206]. The shield and any other unused conductors in a multiconductor cable are left floating. It is possible to reference the PLC signal to the shield instead of the core conductor. However, in this study, all PLC signals will be differentially coupled on core conductors since it has been shown to create a cleaner channel due to common-mode rejection. This is primarily due to the blocking effect of the shield that helps protect signals from EMI, cross talk, and common mode noise [136], [207], [208].

The resulting s-parameters for a 50 m section of cable are compared to the two-wire TLM in Fig. 5.6. Only S_{11} and S_{21} are shown since the DUT is symmetrical, meaning $S_{11} = S_{22}$ and $S_{21} = S_{12}$. The model accurately predicts impedance mismatch reflection oscillations seen in S_{11} indicating a satisfactory estimation of per-unit inductance and capacitance. However, the model drastically overestimates attenuation at high frequency as seen in S_{21} which would lead the model to underestimate PLC functionality on long cables. S_{21} overestimation arises from ignoring both the frequency dependence of the dielectric material and proximity effects. Improvements to the model will be discussed in Sections 5.5-5.6.

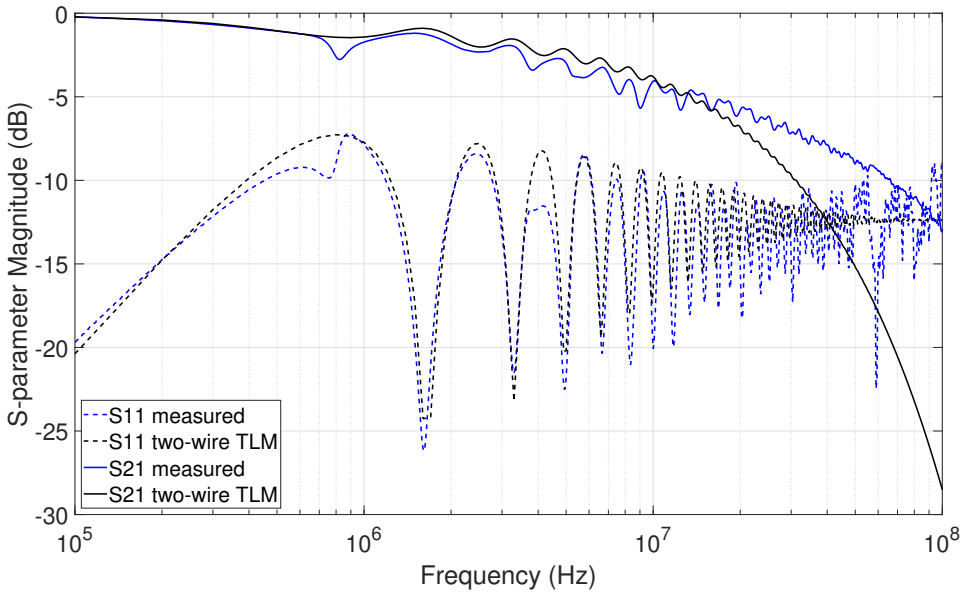

Figure 5.6: Differentially coupled single-ended VNA s-parameter measurement of a 50 m section of 1.5 mm^2 SWA cable compared to the two-wire TLM.

5.3.2 Open circuit/short circuit cable characterisation

Looking out of VNA Port A into the network is the impedance Z_{in} (designated with a red line in Fig. 5.4) defined as the ratio of voltage to current at the port terminals.

$$Z_{\text{in}}(z) = \frac{V(z)}{I(z)} = Z_0 \frac{V_1^+ e^{-\gamma z} + V_1^- e^{\gamma z}}{V_1^+ e^{-\gamma z} - V_1^- e^{\gamma z}} = Z_0 \frac{Z_{\text{L}} + Z_0 \tanh \gamma z}{Z_0 + Z_{\text{L}} \tanh \gamma z} \ [\Omega] \tag{5.15}$$

When measuring s-parameters with a 50 Ω VNA, the DUT is matched when its characteristic impedance also equals 50 Ω. In this situation, there are no reflections, $S_{11} = 0$, and $S_{21} = 1 = 0$ dB. Otherwise, there will be reflections that can be used to characterise the DUT using the *open/short* method. The open/short method takes advantage of a simplification of Eq. (5.15) when the transmission line terminates in an open circuit (oc, *i.e.*, $Z_{\text{L}} = \infty$) or a short circuit (sc, *i.e.*, $Z_{\text{L}} = 0$).

$$\begin{aligned} Z_{\text{in-oc}} &= Z_0 \coth \gamma z \ [\Omega] \\ Z_{\text{in-sc}} &= Z_0 \tanh \gamma z \ [\Omega] \end{aligned} \tag{5.16}$$

From the perspective of the VNA injected signal V_1^+ behind its $50\,\Omega$ source impedance, Z_{in} becomes the perceived load impedance Z_{L}. The VNA applies equation Eq. (5.14) to calculate S_{11}.

$$S_{11\text{-VNA}} = \Gamma_{\text{VNA}} = \frac{Z_{\text{in}} - Z_{\text{S}}}{Z_{\text{in}} + Z_{\text{S}}} = \frac{Z_{\text{in}} - 50\,\Omega}{Z_{\text{in}} + 50\,\Omega} \tag{5.17}$$

Now, instead of connecting Port 2 of the DUT to VNA Port B, the DUT is left either open or shorted to measure ($S_{11\text{-oc}}$) and ($S_{11\text{-sc}}$) to calculate ($Z_{\text{in-oc}}$) and ($Z_{\text{in-sc}}$) from Eq. (5.17). Then the characteristic impedance and propagation constant can be found from Eq. (5.16 and thereafter, each of the per-unit parameters from Eqs. (5.8)-(5.9).

$$Z_0 = \sqrt{Z_{\text{in-sc}} Z_{\text{in-oc}}}\ [\Omega] \tag{5.18}$$

$$\gamma = \frac{1}{x}\text{atanh}\sqrt{\frac{Z_{\text{in-sc}}}{Z_{\text{in-oc}}}}\ \left[\text{m}^{-1}\right] \tag{5.19}$$

$$r = \text{Re}\{\gamma Z_0\}\ [\Omega/\text{m}] \tag{5.20}$$

$$l = \frac{1}{\omega}\text{Im}\{\gamma Z_0\}\ [\text{H/m}] \tag{5.21}$$

$$c = \frac{1}{\omega}\text{Im}\Big\{\frac{\gamma}{Z_0}\Big\}\ [\text{F/m}] \tag{5.22}$$

$$g = \text{Re}\Big\{\frac{\gamma}{Z_0}\Big\}\ [\text{S/m}] \tag{5.23}$$

Open/short measurements of a 50 m section of SWA cable is shown in Fig. 5.7.

The phase velocity for this cable relates to the conductivity of the copper conductor and the permittivity of the dielectric.

$$v_p = \frac{2\pi f}{\beta} = \frac{c_{\text{light}}}{\sqrt{\mu_{\text{r}}\varepsilon_{\text{r}}}}\ \left[\frac{\text{m}}{\text{s}}\right] \tag{5.24}$$

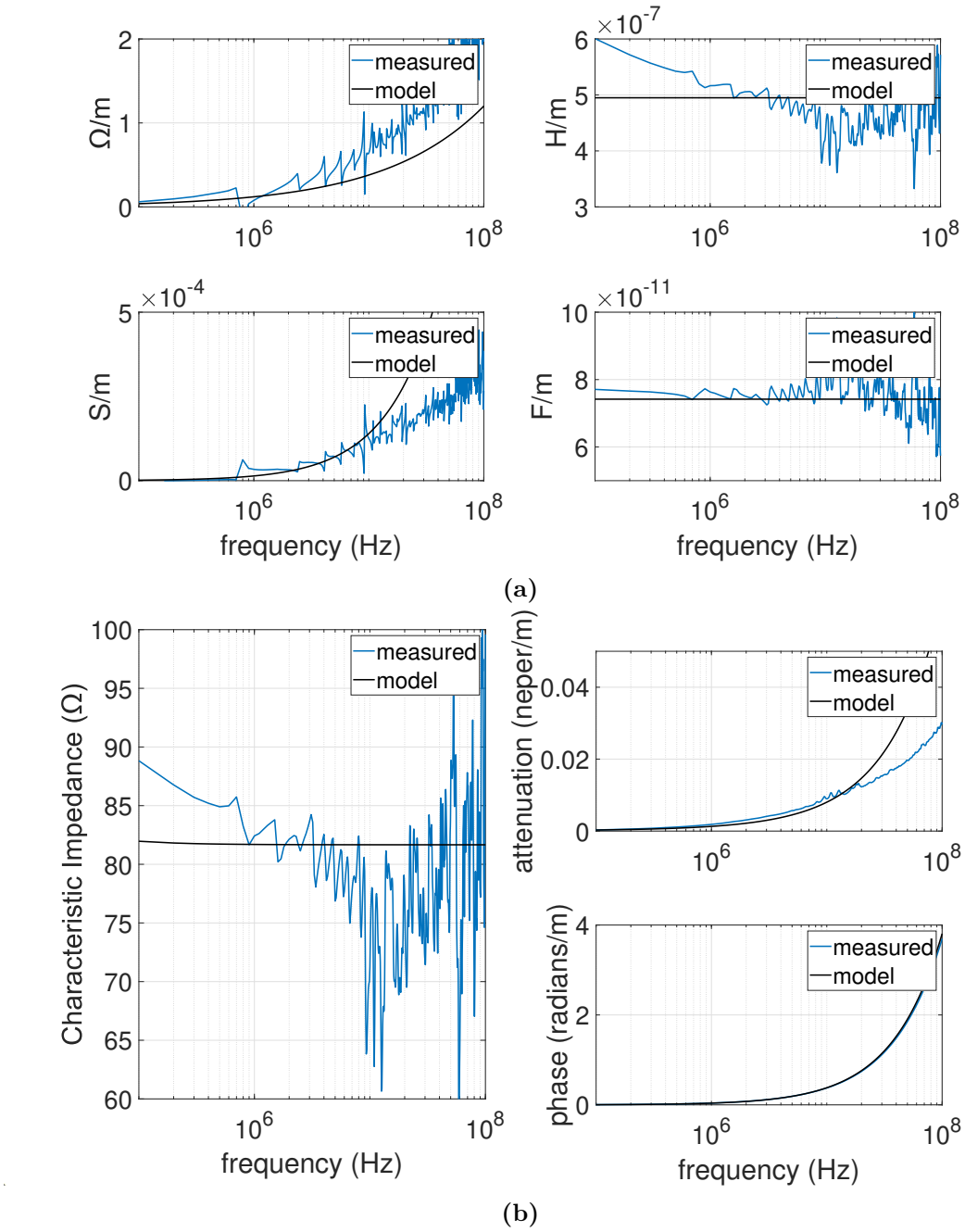

Figure 5.7: Measured per-unit parameters compared to the two-wire TLM for a 50 m section of 1.5 mm^2 SWA power cable a) *rlcg* b) characteristic impedance and propagation constant.

$$\lambda = \frac{v_p}{2\pi f} \text{ [m]} \tag{5.25}$$

Phase velocity for the SWA cable is approximately 1.65×10^8 (m/s) and the wavelength at 30 MHz is 5.6 m. A 50 m DUT will have its first resonant oscillation

at $\sim 80\,\text{kHz}$ as notable in Fig. 5.7. To avoid reflections and the oscillatory nature of the measurements, the DUT would need to be less than the quarter wavelength (1.4 m at 30 MHz). However, the smaller the DUT, the more accentuated measurement errors become and although the curves look smoother, they are not as accurate.

The overestimation of the S_{21} signal attenuation seen in Fig. 5.6 is echoed in the attenuation constant curve in Fig. 5.7(b). As observed in Fig. 5.7(a), the attenuation error is rooted in the underestimation of the per-unit resistance and the overestimation of the per-unit conductance. Error in the per-unit resistance arises from neglecting proximity effects of other conductors and the per-unit conductance error is from frequency dependence of the dielectric insulation material. High frequency attenuation is critical in this study because it is the main determinant of PLC functionality when approaching its limitations. Therefore, the rest of the chapter is dedicated to accounting for these two errors.

5.4 Internal inductance

Before addressing the two main errors in attenuation, internal inductance is going to be incorporated into the model. Since internal inductance contributes very little, it is usually ignored. Nevertheless, it will be included here as it will be important later when extracting *rlcg* per-unit values from multiconductor measurements. Measurable per-unit inductance is the sum of external inductance and internal inductance [205]:

$$l = l_{\text{ext}} + l_{\text{int}}\ [\text{H/m}] \tag{5.26}$$

$$l_{\text{int}} = \frac{1}{4\pi r_{\text{w}}}\sqrt{\frac{\mu}{\pi f \sigma}}\ [\text{H/m}] \tag{5.27}$$

$$l_{\text{ext}} = l_{\text{two-wire}}\ [\text{H/m}] \tag{5.28}$$

The internal (or self) inductance is frequency dependent whilst external inductance is not. It is important to remember that measured inductance will include both.

5.5 Dielectric frequency dependence

The 1.5 mm^2 steel-wire armoured (SWA) cable in Fig. 5.2(b) provides an example to address the errors in the two-wire TLM. Although the equations above provide a general idea of the frequency response of a transmission line, they do not provide sufficient accuracy of attenuation at high frequency. Capacitance and admittance are heavily dependent upon the dielectric constants. The dielectric constants are both normally considered constant and can either be measured or estimated with lookup tables [209]. However, the example SWA cable has more than one dielectric material. Inhomogeneous materials can be assumed homogeneous using fractional cross-sectional areas to estimate an effective homogeneous constant:

$$\xi_{\text{r-homogenous}} = \sum_{n=1}^{N} \frac{a_{\text{n}}}{a_{\text{T}}} x_{\text{rn}} \tag{5.29}$$

where ξ is the dielectric constant of interest (*i.e.*, ε_{r} or $\tan\delta$), n is the dielectric material, N is the total number of dielectric materials, a_{n} is the cross-sectional area of the n^{th} dielectric, and a_T is the total cross-sectional area of the insulation medium [210]. The conductors in Fig. 5.2(b) are surrounded by polyethylene and those are enveloped in PVC. For the range between 1 MHz and 100 MHz, PVC has average constants $\varepsilon_{\text{r-PVC}} = 3.9$, $(\tan\delta)_{\text{PVC}} = 0.04$ and polyethylene values are $\varepsilon_{\text{r-poly}} = 2.3$, $(\tan\delta)_{\text{poly}} = 3 \times 10^{-4}$ [211]. Using the dimensions of Fig. 5.2(b) and Eq. (5.29) yield effective homogeneous constants: $\varepsilon_{\text{r}} = 3.3$ and $\tan\delta = 0.03$. The advantage of look-up table estimates is they require no cable measurements. These constants are used in the two-wire model from Section 5.2.

In reality, both dielectric constants decrease with frequency. Measurements of the SWA cable in Fig. 5.8 show the frequency dependent behaviour compared to the effective homogeneous estimate from look-up tables.

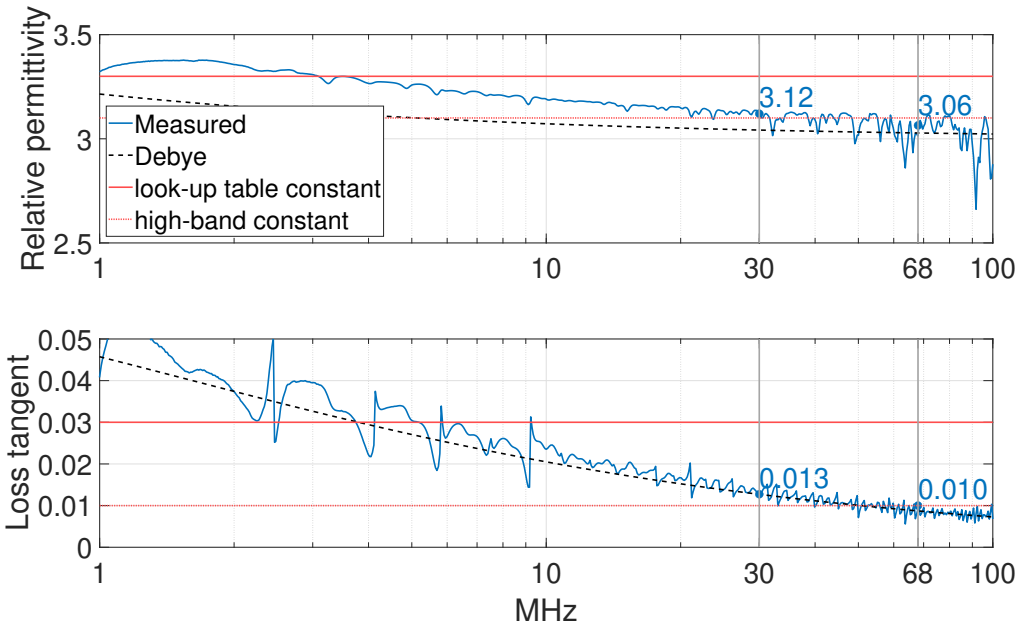

Figure 5.8: Measured dielectric properties of 1.5 mm^2 SWA power cable vs constant approximations and the Debye approximation.

Because the estimates are averages over a wide band, they do not accurately predict attenuation at the upper envelope of operation. One way to address this is to instead choose constants that better predict attenuation at high frequency. In this case, the HomePlug GP operates up to 30 MHz and the AV up to 68 MHz. Using the measured values at these two frequencies, a reasonable approximation for this upper range would set $\varepsilon_{\mathrm{r}} = 3.1$ and $\tan\delta = 0.01$. Although this method causes errors at lower frequencies, it works very well to predict high-band attenuation. It is likely a microgrid developer would not be able to measure the dielectric constants of the power cable. In this case, the recommendation is to choose values from look-up tables that favour the upper end of the frequency band of interest, which means typically choosing the lower number given for a frequency range, since the constants decrease with frequency.

The frequency dependence of the dielectric can be more accurately represented using the Debye function with the Cole-Cole modification [212], [213]:

$$\varepsilon_{\mathrm{r}}(\omega) = \varepsilon_{\mathrm{r}}^{'}(\omega) + j\varepsilon_{\mathrm{r}}^{''}(\omega) = \varepsilon_{\infty} + \frac{\varepsilon_{\mathrm{DC}} - \varepsilon_{\infty}}{(1 + j\omega\tau)^{\phi}} \tag{5.30}$$

$$\tan\delta = \frac{\varepsilon_{\mathrm{r}}''}{\varepsilon_{\mathrm{r}}'} \tag{5.31}$$

where $\varepsilon_{\mathrm{DC}}$ is the permittivity at DC, ε_{∞} is the settling value at high frequency, τ is the dielectric relaxation time constant which defines the frequency around which the dielectric constant relaxes to a different value, and ϕ is a stretching factor determining the width of frequency range over which the relaxation occurs. Values for $\varepsilon_{\mathrm{DC}}$ and ε_{∞} are best observed from measurement but could be estimated from look-up tables [210], [211]. The following solution is obtained from curve fitting the Debye equation to the measurement in Fig. 5.8 and will be used moving forward.

$$\varepsilon_{\mathrm{r}}(\omega) = 3 + \frac{4-3}{(1+j\omega 1.5\times 10^{-6})^{0.5}} \tag{5.32}$$

5.6 Multiconductor transmission line theory

In order to tackle proximity effects, the model must include elements of multiconductor transmission line theory.

The multiconductor model expands Fig. 5.1 to account for the mutual interactions between conductors shown in Fig. 5.9. Per-unit calculations for *rlcg* include both self terms on the diagonal of the matrices in Eqs. (5.33)-(5.36) and mutual terms on the off-diagonals [205]. Matrices are denoted with bold capital letter variables.

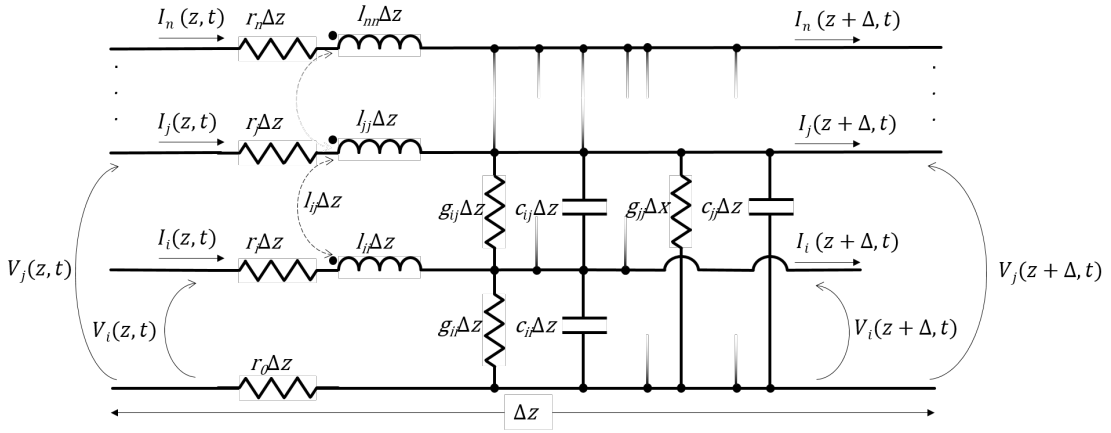

Figure 5.9: Distributed element model of multiconductor transmission line with n conductors (all referenced to the 0^{th} conductor) where Δz is an infinitely small length of cable and voltage and current behave like propagating waves. Adapted from [205].

$$\mathbf{R} = \begin{bmatrix} r_{\mathrm{i}} + r_0 & r_0 & \dots & r_0 \\ r_0 & r_{\mathrm{j}} + r_0 & \dots & r_0 \\ \vdots & \vdots & \ddots & \vdots \\ r_0 & r_0 & \dots & r_{\mathrm{n}} + r_0 \end{bmatrix} \ [\Omega/\mathrm{m}] \tag{5.33}$$

$$\mathbf{L} = \begin{bmatrix} l_{\mathrm{ii}} & l_{\mathrm{ij}} & \dots & l_{\mathrm{in}} \\ l_{\mathrm{ji}} & l_{\mathrm{jj}} & \dots & l_{\mathrm{jn}} \\ \vdots & \vdots & \ddots & \vdots \\ l_{\mathrm{ni}} & l_{\mathrm{nj}} & \dots & l_{\mathrm{nn}} \end{bmatrix} \ [\mathrm{H/m}] \tag{5.34}$$

$$\mathbf{C} = \begin{bmatrix} \sum_{k=1}^{n} c_{\mathrm{ik}} & -c_{\mathrm{ij}} & \dots & -c_{\mathrm{in}} \\ -c_{\mathrm{ji}} & \sum_{k=1}^{n} c_{\mathrm{jk}} & \dots & -c_{\mathrm{jn}} \\ \vdots & \vdots & \ddots & \vdots \\ -c_{\mathrm{ni}} & -c_{\mathrm{nj}} & \dots & \sum_{k=1}^{n} c_{\mathrm{nk}} \end{bmatrix} \ [\mathrm{F/m}] \tag{5.35}$$

$$\mathbf{G} = \begin{bmatrix} \sum_{k=1}^{n} g_{\mathrm{ik}} & -g_{\mathrm{ij}} & \dots & -g_{\mathrm{in}} \\ -g_{\mathrm{ji}} & \sum_{k=1}^{n} g_{\mathrm{jk}} & \dots & -g_{\mathrm{jn}} \\ \vdots & \vdots & \ddots & \vdots \\ -g_{\mathrm{ni}} & -g_{\mathrm{nj}} & \dots & \sum_{k=1}^{n} g_{\mathrm{nk}} \end{bmatrix} \ [\mathrm{S/m}] \tag{5.36}$$

For the cable in Fig. 5.2(a), the 0^{th} reference conductor is the shield. In this case, the signal is applied to a core conductor $(i, j, ..., n)$ with a return path through the shield. Most multiconductor cable models neglect proximity effects by assuming the conductors are sufficiently separated ($s > 4r_{\mathrm{w}}$). Numerical derivations of per-unit resistance that account for the proximity effects of the n^{th} conductor are extremely complex and can be found in [214], [215]. This study will focus on the two-core SWA case in 5.2(b). The conductors are not sufficiently separated to ignore the proximity effects at the frequency range of interest. Assuming all the conductors have the same radius, the per-unit resistances for shielded parallel conductors with dimensions of Fig. 5.2 are [216]:

$$r_{\mathrm{i}} = r_{\mathrm{j}} = \frac{1}{\pi r_{\mathrm{w}} \sigma \delta_{skin}} \left[1 + \frac{1 + 2\left(\frac{d}{r_{\mathrm{w}}}\right)^2}{4\left(\frac{d}{r_{\mathrm{w}}}\right)^4} \left(1 - 4\left(\frac{w}{2r_{\mathrm{s}}}\right)^2 \right) \right] \ [\Omega/\mathrm{m}] \tag{5.37}$$

$$r_0 = \frac{1}{\pi r_{\mathrm{s}} \sigma_{\mathrm{s}} \delta_{\text{skin-s}}} \left[1 + \left(\frac{w}{2r_{\mathrm{s}}}\right)^2 - \frac{1 + 4\left(\frac{d}{r_{\mathrm{w}}}\right)^2}{8\left(\frac{d}{r_{\mathrm{w}}}\right)^4} \right] \ [\Omega/\mathrm{m}] \tag{5.38}$$

where the conductivity of carbon steel $\sigma_{\mathrm{s}} = 70$ (MS/m). For unshielded conductors, the equations must be modified to reference either one of the n^{th} conductors or a ground plane [205]. These equations account for the proximity effects of both the neighboring conductor and the shield.

Per-unit external inductance terms are [205]:

$$l_{\mathrm{ii}} = \frac{\mu}{2\pi} \ln\left(\frac{r_{\mathrm{s}}^2 - d^2}{r_{\mathrm{s}} r_{\mathrm{w}}}\right) \text{ [H/m]} \tag{5.39}$$

$$l_{\mathrm{ij}} = \frac{\mu}{2\pi} \ln\left(\frac{d_{\mathrm{j}}}{r_{\mathrm{s}}} \sqrt{\frac{(d_{\mathrm{i}} d_{\mathrm{j}})^2 + r_{\mathrm{s}}^4 - 2 d_{\mathrm{i}} d_{\mathrm{j}} r_{\mathrm{s}}^2 \cos\theta_{\mathrm{ij}}}{(d_{\mathrm{i}} d_{\mathrm{j}})^2 + d_{\mathrm{j}}^4 - 2 d_{\mathrm{i}} d_{\mathrm{j}} d_{\mathrm{j}}^3 \cos\theta_{\mathrm{ij}}}}\right) \text{ [H/m]} \tag{5.40}$$

After populating the inductance matrix, the capacitance and admittance matrices can be found [205]:

$$\mathbf{C} = \mu\varepsilon \mathbf{L}^{-1} \text{ [F/m]} \tag{5.41}$$

$$\mathbf{G} = \mu\sigma \mathbf{L}^{-1} = \frac{\sigma}{\varepsilon}\mathbf{C} \text{ [S/m]} \tag{5.42}$$

Series impedance and shunt impedance matrices are:

$$\mathbf{Z} = \mathbf{R} + j\omega\mathbf{L}' = \mathbf{R} + j\omega\mathbf{L}_{\mathrm{int}} + j\omega\mathbf{L} \text{ [}\Omega\text{/m]} \tag{5.43}$$

$$\mathbf{Y} = \mathbf{G} + j\omega\mathbf{C} \text{ [S/m]} \tag{5.44}$$

where $\mathbf{L}_{\mathrm{int}}$ is the product of Eq. (5.27) and the identity matrix [217]. The product of series and shunt impedances yields the eigenvector $\mathbf{T}$ and eigenvalues (Λ) whose square root is the propagation constant matrix $\mathbf{\Gamma_P}$ (not to be confused with the reflection coefficient Γ). The propagation constant matrix and eigenvector provide the means to calculate the characteristic impedance matrix [218]:

$$\mathbf{ZY} = \mathbf{T}\mathbf{\Lambda}\mathbf{T}^{-1} \tag{5.45}$$

$$\mathbf{\Gamma_P} = \sqrt{\mathbf{\Lambda}}\ [\mathrm{m}^{-1}] \tag{5.46}$$

$$\mathbf{Z_0} = \mathbf{T\Gamma_P^{-1}T^{-1}Z}\ [\Omega] \tag{5.47}$$

The matrices $\mathbf{Z_0}$ and $\mathbf{\Gamma_P}$ characterise a multiconductor cable and form the foundation of the multiconductor model.

5.6.1 Measuring multiconductor cables

The following procedure follows methods described in [217], [219] to take single-ended measurements of a multiconductor cable with a 2-port VNA. All single ended measurements are taken with respect to the shield reference plane which is connected to the VNA ground reference. Conversions of single-ended measurements yield differential measurements that can be compared to the two-wire model results in Fig. 5.7.

Each conductor termination is considered its own port to form an $n \times n$ s-parameter matrix, where n are the number of ports as numbered in Fig. 5.10(a). The cable shield is not included in the number of ports but acts as the reference conductor and is mounted to metal plates using glands pictured in Fig. 5.10(b). One SMA per port is mounted to the same metal plate such that all outer conductors of the SMA connectors share electrical connection with the cable shield. Each core of the cable is then connected to the inner conductor of a SMA connector.

Singled-ended measurements are taken in groups, two ports at a time, to build 2x2 submatrices [220]. The total number of submatrices is $n(n-1)/2$. All unused SMA connectors must be terminated with the same impedance as the VNA ports, in this case $50\,\Omega$. If ports are terminated in an impedance that is different than the VNA, the measured s-parameters must be corrected according to the normalization procedure outlined in [217]. This sequence continues until populating all $n \times n$ measurements. Any repeat measurements (*e.g.*, multiple S_{11} measurements) can be averaged. For example, the two-core SWA cable from Fig. 5.10(a) has four

ports and a reference shield. A cable of length x m is mounted for measurement as depicted in Fig. 5.10(a).

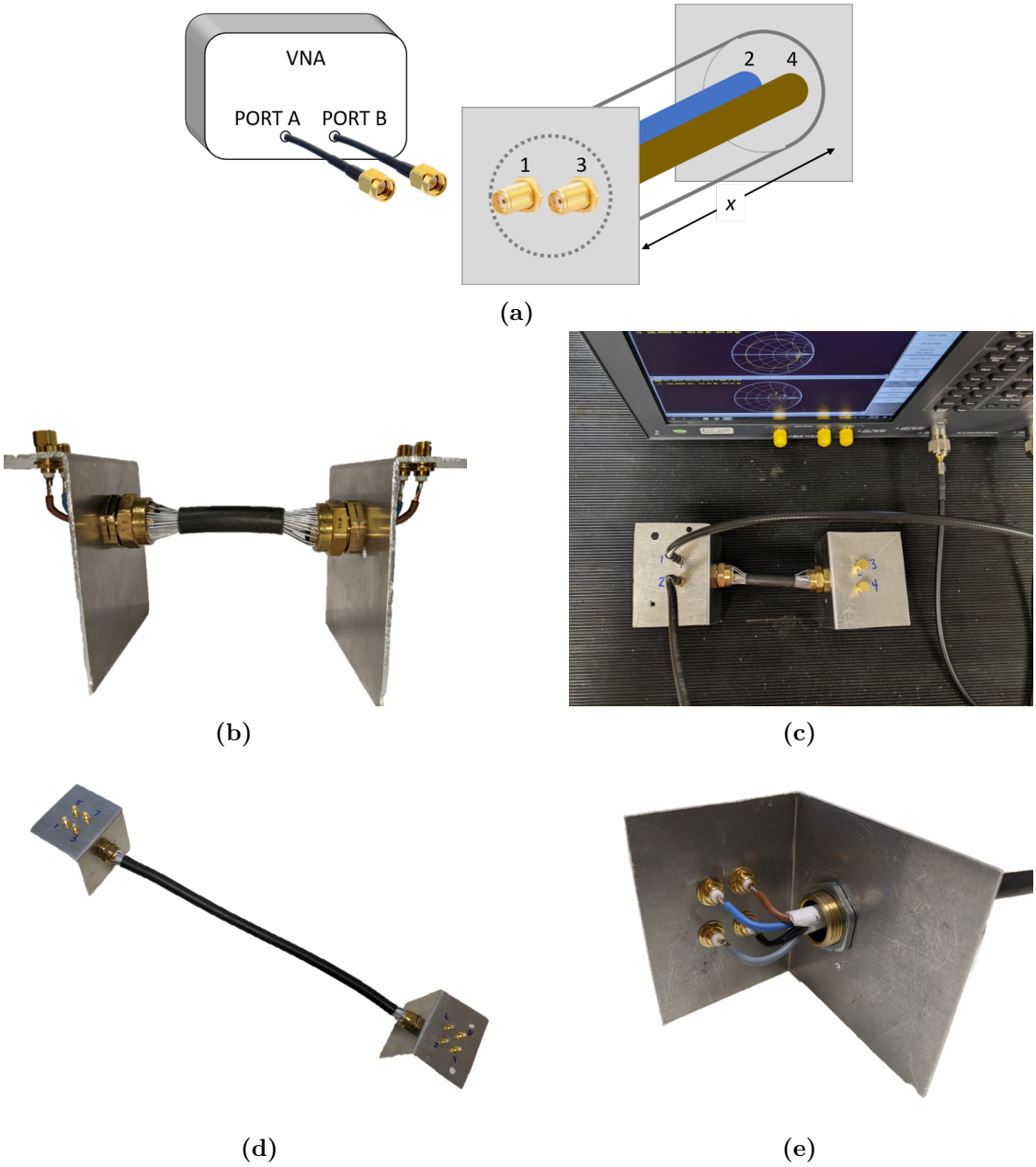

Figure 5.10: Multiconductor cable characterisation experimental setup: a) Diagram shows a two-core cable with odd conductors on one side and even on the other. Cable shielding and the outer conductor of the SMA connectors are electrically connected to metal reference plates. SMA inner conductor is connected to cable conductor. b) Example of a 2-core cable mounted to aluminium reference plates using SWA cable glands. c) Open/short characterisation of 2-core cable with one end connected to VNA and the other side shorted with SMA shorting caps. d) Example of a 4-core cable mounted to aluminium reference plates using SWA cable glands. e) Under-side of small section of four-core cable to illustrate the cable core connection to the SMA inner conductor.

The measurement sequence proceeds hence:

1. VNA Port A is connected to DUT Port 1 and VNA Port B to DUT Port 2.
2. Ports 3 and 4 are both terminated with a 50 Ω cap.

This measurement populates the first 2x2 submatrix with $S_{11}, S_{12}, S_{21}, \text{and} S_{22}$. For the next measurement, VNA Port A remains on DUT Port 1 while VNA Port B is moved to DUT Port 3. The summarized list of connection combinations is A1-B2, A1-B3, A1-B4, A2-B3, A2-B4, A3-B4. Each connection combination produces another 2x2 submatrix. The six submatrices are assembled to create the 4x4 matrix in Eq. (5.48). Assuming the DUT has perfect symmetry, only one row or one column is needed since same coloured s-parameters are, in theory, equal.

$$S_{single} = \begin{bmatrix} S_{11} & S_{12} & S_{13} & S_{14} \\ S_{21} & S_{22} & S_{23} & S_{24} \\ S_{31} & S_{32} & S_{33} & S_{34} \\ S_{41} & S_{42} & S_{43} & S_{44} \end{bmatrix} \tag{5.48}$$

Conceptually, the values in black are all reflection coefficients, green are transmission coefficients, blue are nearside crosstalk (NEXT) coefficients, and red are far-side crosstalk (FEXT) coefficients [221]. The first row of values in Eq. (5.48) for a 50 m section of two-core 1.5 mm^2 SWA cable are shown in the same corresponding colours in Fig. 5.11.

Although PLC signals can be coupled between a core conductor and the shield, better performance can be guaranteed by using two of the core conductors in a differential manner [222]. This reduces common-mode noise and decreases attenuation since the copper cores conduct better than the shield. The single-ended matrix in Eq. (5.48) can be mathematically transformed to a mixed mode matrix:

$$\mathbf{M} = \frac{1}{\sqrt{2}} \begin{bmatrix} 1 & 0 & -1 & 0 \\ 0 & 1 & 0 & -1 \\ 1 & 0 & 1 & 0 \\ 0 & 1 & 0 & 1 \end{bmatrix} \tag{5.49}$$

$$\mathbf{S_{mixed}} = \mathbf{M}\mathbf{S_{single}}\mathbf{M^{-1}} = \begin{bmatrix} S_{d1d1} & S_{d1d2} & S_{d1c1} & S_{d1c2} \\ S_{d2d1} & S_{d2d2} & S_{d2c1} & S_{d2c2} \\ S_{c1d1} & S_{c1d2} & S_{c1c1} & S_{c1c2} \\ S_{c2d1} & S_{c2d2} & S_{c2c1} & S_{c2c2} \end{bmatrix} \tag{5.50}$$

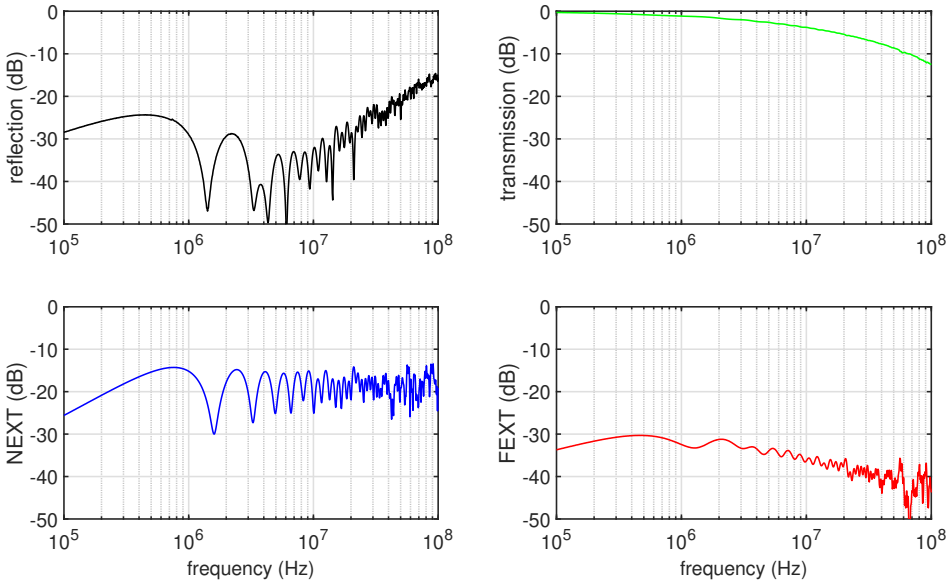

Figure 5.11: Single-ended coefficients of a 50 m section of 1.5 mm^2 two-core SWA. a) reflection (S_{11}), b) transmission (S_{21}), c) NEXT ($S13$) and d) FEXT ($S14$).

where the top left quadrant yields a 2x2 differential signal submatrix analogous to the two-wire measurements taken in Fig. 5.5 [219]. The other quadrants labelled "dc" and "cd" show what common mode signal arises from differential injection or vice versa. The bottom right quadrant, "cc", defines the common mode behaviour on a differential pair and will be equal to the differential quadrant for a passive symmetrical power cable [221].

5.6.2 Multiconductor open/short cable characterisation

A full characterisation of a multiconductor cable can be performed in a similar fashion as described in Section 5.3.2 using the open/short method. Using the DUT in Fig. 5.10(a) (2-core SWA) as an example, the first measurement is taken by connecting VNA Port A to DUT Port 1 and VNA Port B to DUT Port 3 just like the photo in Fig. 5.10(c). DUT Ports 2 & 4 are either kept open or shorted to the reference metal plate with shorting caps to create two separate 2x2 submatrices [217].

$$\mathbf{S_{OC}} = \begin{bmatrix} S_{11} & S_{13} \\ S_{31} & S_{33} \end{bmatrix} \;\&\; \mathbf{S_{SC}} = \begin{bmatrix} S_{11} & S_{13} \\ S_{31} & S_{33} \end{bmatrix} \tag{5.51}$$

Following the same calculation from Eq. (5.17), the open and short circuit matrices from Eq. (5.51) are used to calculate open and short circuit $\mathbf{Z}_{\text{in}}$ matrices:

$$\mathbf{Z_{in:OC,SC}} = (\mathbf{I} - \mathbf{S_{OC,SC}})^{-\mathbf{1}}(\mathbf{I} + \mathbf{S_{OC,SC}})(50\mathbf{I})\ [\Omega] \tag{5.52}$$

where $\mathbf{I}$ is the identity matrix and $50\,\Omega$ is the VNA source impedance. From there, due to the relationship established in Eq. (5.15), $\mathbf{Z}_{\text{in}}$ can be used to solve for the characteristic impedance, propagation constant, and each of the per-unit parameters [217], [223].

$$\mathbf{Z_{in:OC}} = (\cosh \mathbf{\Gamma_P} z)\mathbf{Z_0}\ [\Omega] \tag{5.53}$$

$$\mathbf{Z_{in:SC}} = (\tanh \mathbf{\Gamma_P} z)\mathbf{Z_0}\ [\Omega] \tag{5.54}$$

$$\mathbf{Z_0} = (\mathbf{Z_{in:SC}}\mathbf{Z_{in:OC}^{-1}})^{-\frac{\mathbf{1}}{\mathbf{2}}}\mathbf{Z_{in:SC}}\ [\Omega] \tag{5.55}$$

$$\mathbf{\Gamma_P} = \frac{1}{x}(\text{atanh}[\mathbf{Z_{in:SC}}\mathbf{Z_{in:OC}^{-1}}]^{\frac{1}{2}})\ [\text{m}^{-1}] \tag{5.56}$$

$$\mathbf{R} = \text{Re}\{\mathbf{\Gamma_P}\mathbf{Z_0}\}\ [\Omega/\text{m}] \tag{5.57}$$

$$\mathbf{L'} = \frac{1}{\omega}\text{Im}\{\mathbf{\Gamma_P}\mathbf{Z_0}\}\ [\text{H/m}] \tag{5.58}$$

$$\mathbf{C} = \frac{1}{\omega}\text{Im}\{\mathbf{Z_0^{-1}}\mathbf{\Gamma_P}\}\ [\text{F/m}] \tag{5.59}$$

$$\mathbf{G} = \text{Re}\{\mathbf{Z_0^{-1}}\mathbf{\Gamma_P}\}\ [\text{S/m}] \tag{5.60}$$

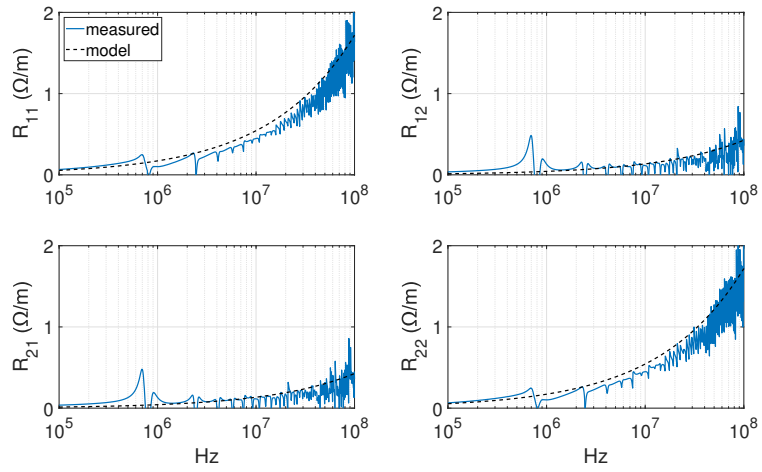
measured
model
R11 (Ω/m)
R12 (Ω/m)
R21 (Ω/m)
R22 (Ω/m)
Hz

(a)

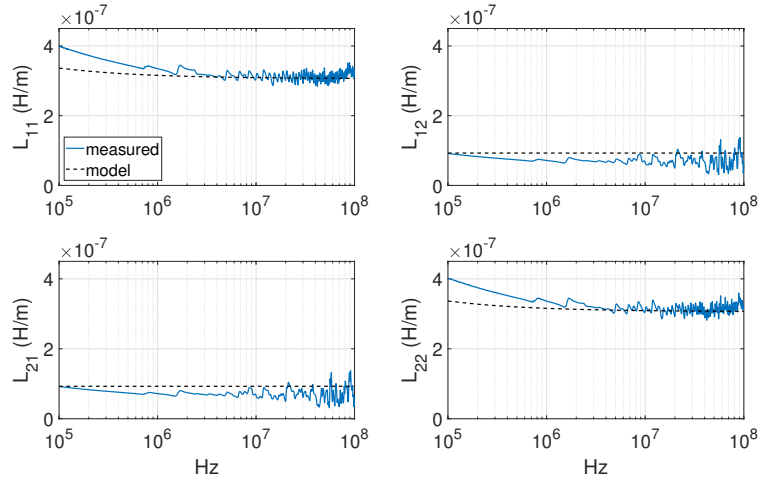
×10-7
measured
model
L11 (H/m)
L12 (H/m)
L21 (H/m)
L22 (H/m)
Hz

(b)

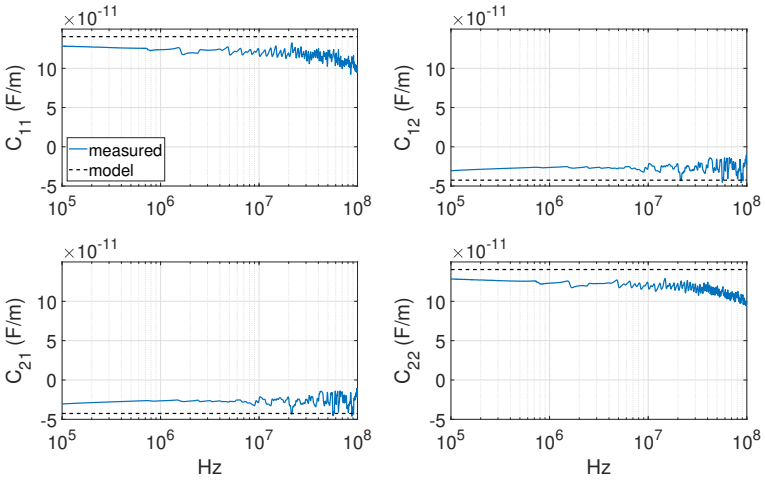
×10-11
measured
model
C11 (F/m)
C12 (F/m)
C21 (F/m)
C22 (F/m)
Hz

(c)

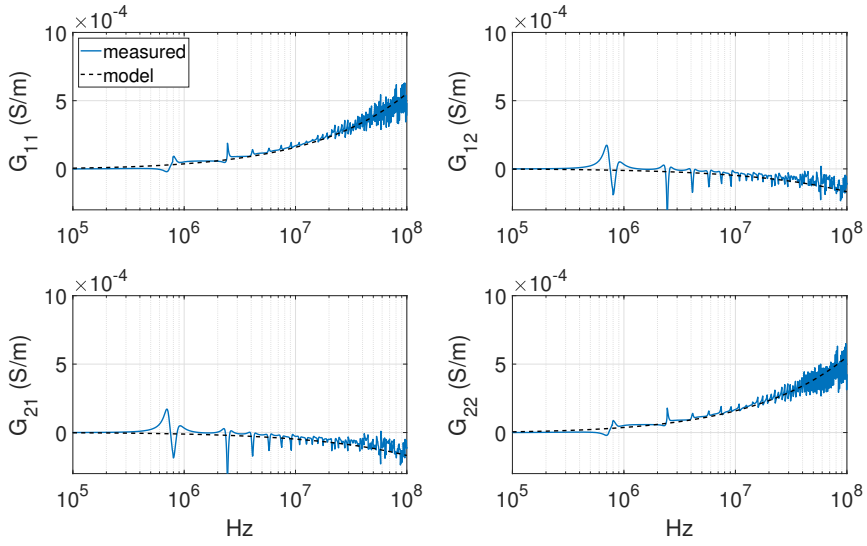

(d)

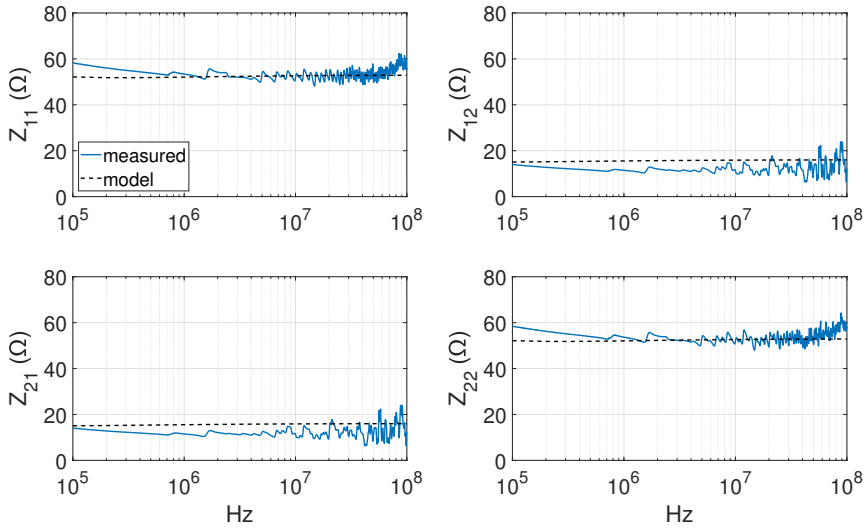

(e)

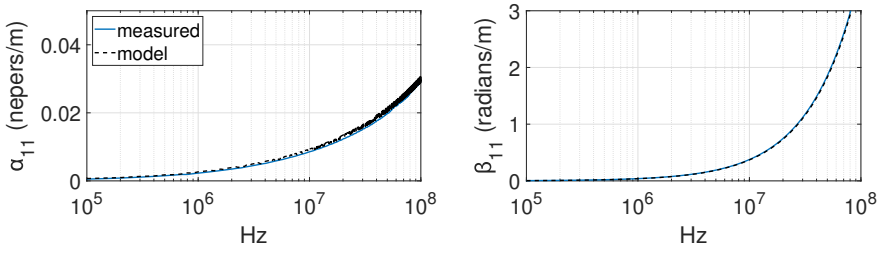

(f)

Figure 5.12: Measured multiconductor per-unit matrices compared to the multiconductor model for 50 m section of two-core 1.5 mm^2 SWA power cable a) $\mathbf{R}$ b) $\mathbf{L}$ c) $\mathbf{G}$ d) $\mathbf{C}$ e) $\mathbf{Z_0}$ and f) $\mathbf{\Gamma_P}$. Only the self-terms of the propagation constant are shown since the off-diagonal terms are zero.

Fig. 5.12 illustrates the results from a multiconductor characterisation of a 50 m section of two-core 1.5 mm^2 SWA cable. The multiconductor model accurately represents the cable by incorporating both the Debye dielectric model in Eq. (5.32) and the proximity effects from Eq. (5.37-5.38).

The same process using a 2-port VNA can be followed for a cable with even more conductors. For example, the 4-core cable pictured in Fig. 5.10(d) would produce an 8x8 single-ended matrix for Eq. (5.48) requiring many more 50 Ω termination caps. The open/short characterisation for the same cable starts by creating 2x2 submatrices like those in Eq. (5.51). Remaining odd DUT ports must be terminated with a 50 Ω cap while even ports are either left open or shorted to the reference plate. All necessary connection combinations are summarized with this sequence: A1-B3, A1-B5, A1-B7, A3-B5, A3-B7, A5-B7. Any repeat measurements (*e.g.*, multiple short circuit S_{11} measurements) can be averaged. The six 2x2 submatrices are assembled to build two 4x4 matrices: one for open circuit and the other for short circuit [217].

$$\mathbf{S_{OC,SC}} = \begin{bmatrix} S_{11} & S_{13} & S_{15} & S_{17} \\ S_{31} & S_{33} & S_{35} & S_{37} \\ S_{51} & S_{53} & S_{55} & S_{57} \\ S_{71} & S_{73} & S_{75} & S_{77} \end{bmatrix} \tag{5.61}$$

5.7 Modified two-wire model

Despite the accuracy gained with the multiconductor model, the full model is unnecessary to accurately represent the PLC channel. Multiconductor simulations are complex, and measurements require cumbersome procedures or an expensive multiport VNA. Microwave engineering software tools typically have built-in model blocks for various types of transmission lines such as coaxial, microstrip and the two-wire used in this study. However, the model blocks only have 2-ports and use the basic equations that neglect the factors discussed in this chapter. Two adjustments can be made to the two-wire TLM to address the attenuation errors seen in Fig. 5.7: overestimation of per-unit admittance from neglecting the frequency dependence of the dielectric constant, and underestimation of per-unit resistance

due to proximity effects. The first is resolved using the Debye approximation in Eq. (5.32). The second error is addressed by incorporating the multiconductor model of per-unit resistance into the two-wire model. Instead of Eq. (5.2), the modified model will use two times Eq. (5.37) which accounts for the presence of the shield, the proximity of the other core, and the differential return path. Since the PLC signal is differentially coupled across the two core conductors, the per-unit resistance is $r_\mathrm{i} + r_\mathrm{i}$ rather than the common mode coupled term $r_\mathrm{i} + r_0$ from the diagonal in the multiconductor per-unit resistance matrix of Eq. (5.33).

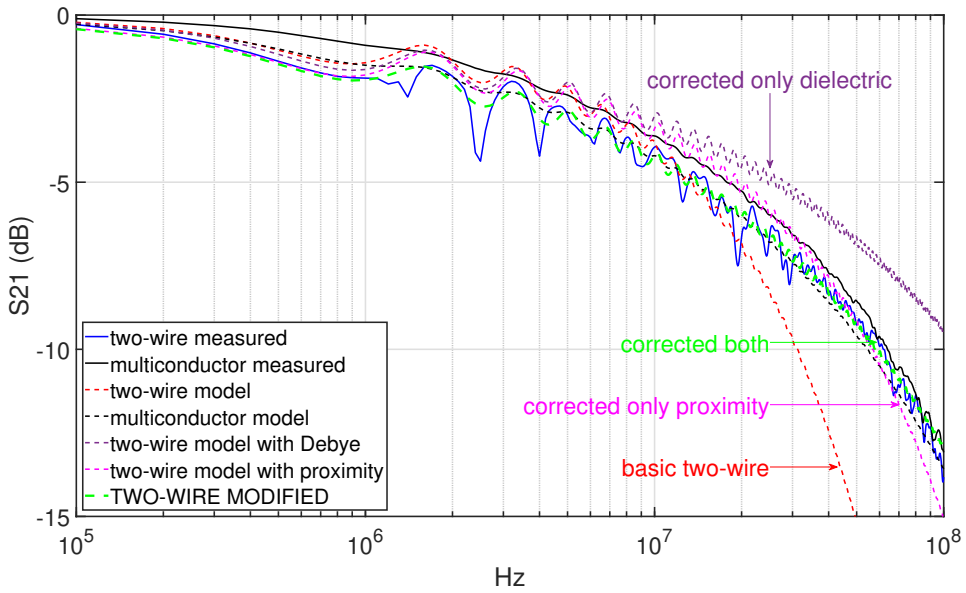

Figure 5.13: S_{21} measured versus model of a 50 m section of two-core 1.5 mm^2 SWA power cable. Measured values are solid lines and models are dashed. All curves are compared to the multiconductor measurement in black which offers the most accurate representation of the true PLC frequency response. The most complex and accurate model is the multiconductor model based on Fig. 5.9. The basic two-wire model in red ignores both the dielectric frequency dependence and proximity effects. Other curves are added to show the effect of each individual correction. The two-wire modified model in green closely approximates the multiconductor model.

Fig. 5.13 compares transmission coefficient (S_{21}) measurements of the various models. The differential measurements S_{d1d1} and S_{d2d1} from the differential quadrant of the mixed mode matrix in Eq. (5.50), derived from the single-ended multiconductor measurement matrix in Eq. (5.48), are the most accurate representation of the differentially coupled PLC signal frequency response. The multiconductor model uses

Section 5.6 to build a 4-port transmission line following the "Lossy Multiconductor Transmission Line Circuit" example in the RF Toolkit of MATLAB [224]. Then single-ended s-parameters are extracted using the `sparameters` command and then converted to mixed mode parameters as in Eq. (5.50) using the `s2sdd` command. The basic two-wire model uses Section 5.2 and the `rfckt.twowire` command which requires cross sectional inputs from Fig. 5.2 and scalar inputs for the dielectric constants. The `rfckt.rlcgline` command, on the other hand, accepts vector inputs for *rlcg* allowing for the incorporation of a frequency dependent dielectric constant and a modification of the per-unit resistance to account for proximity effects. The effect of each correction by itself is shown in Fig. 5.13 as well as the modified two-wire model which corrects for both.

5.8 Conclusion

This modified two-wire model is advantageous because it can be easily used in GUI-based software programs that only have 2-port building blocks (*e.g.*, Simulink, LTspice, AWR Microwave Office). AWR Microwave Office by Cadence has a simple user-friendly GUI designed specifically for s-parameter analysis that will be used in the next chapter to rapidly create complex branched networks using the modified two-wire TLM [225]. This software tool along with the modified two-wire TLM is recommended for microgrid developers considering BB PLC as a communication technology in order to rapidly predict PLC performance on a given grid architecture.

Since the cable lengths used in a microgrid approach the wavelengths of PLC signals, the TLM must be used to accurately represent the communication channel. Although PLC signals only require two conductors, elements of the multiconductor TLM must be considered since proximity effects increase high frequency attenuation. Additionally, dielectric constants must be frequency dependent to avoid attenuation errors. The modified two-wire model now forms the fundamental building block to simulate networks of power cables.

6
Powerline Communications

The primary findings of this chapter have been submitted for publication to IEEE Transactions on Power Delivery: D. Neal, D. Rogers and M. McCulloch, "Broadband Powerline Communication for Low-Voltage Microgrids," unpublished.

Chapter 6 contains the experimental results of BB HomePlug GP and AV performance tests on various network structures. The modified two-wire TLM from Chapter 5 is validated by VNA s-parameter measurements and used to predict PLC performance on various networks. It is proposed as a quick and simple tool for microgrid developers to determine the functionality of BB PLC on a given network topology. Suitability of BB PLC for microgrid communication is stated.

6.1 HomePlug Technology Overview

Both the HomePlug GP and AV use the same OFDM technology, an efficient high bandwidth transmission modulation technique that maps digital data to orthogonally spaced sinusoidal subcarriers. In the frequency domain, data modulated on each subcarrier peak is free from spreading interference because the signal power from neighbouring subcarriers is at zero as portrayed in Fig. 6.1 [224]. This technique avoids the necessity of guard bands in between subcarriers thereby increasing the

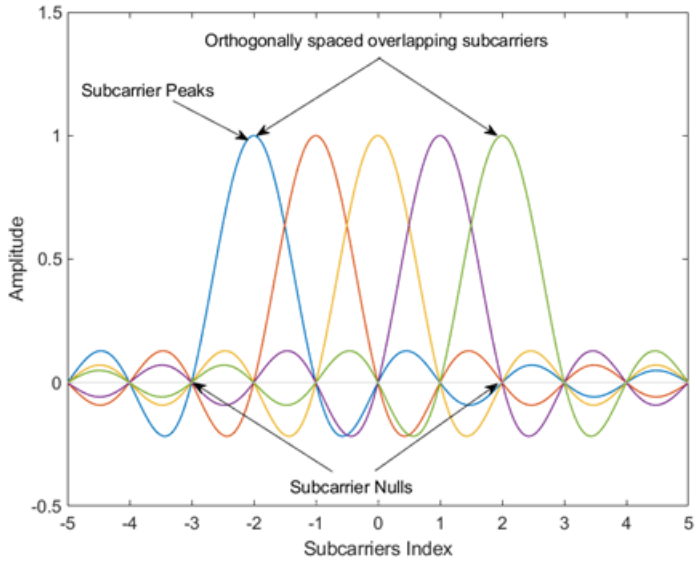

Figure 6.1: Sample OFDM frequency spectrum. Reproduced from [226]

amount of data that can be transmitted within a given bandwidth [222]. HomePlug technology separates subcarriers by 24.414 kHz.

Digital information is modulated onto each subcarrier using phase shift keying (PSK) where the phase of the subcarrier sinusoid is shifted by certain phase quantities to encode the binary data. The GP is limited to quadrature PSK (QPSK) where the carrier's phase is shifted to encode two bits of data as shown in Fig. 6.2(a) [118]. More data can be encoded per subcarrier using more complex phase shift maps or even combining amplitude changes with phase shifts like in the case of quadrature amplitude modulation (QAM) as in Fig. 6.2(b).

The AV also incorporates ABL, which is a process where the transmitter pings the channel, evaluates the quality of each subcarrier, and maps the signal-to-noise ratio (SNR) of each subcarrier to create a tone map like the one for a 50 m SWA cable in Fig. 6.3 [119]. The number of bits-per-subcarrier are adjusted according to the SNR tone map [227]. Notches of subcarriers can be effectively turned off to avoid transmitting on poor quality channels. Subcarrier bit loading varies from level 0 to 10 depending on the tone map which includes a pre-programmed list of masked carriers that are permanently blocked to deconflict with legacy applications (*e.g.*, amateur radio) [119]. The higher the bit loading level, the more complex the

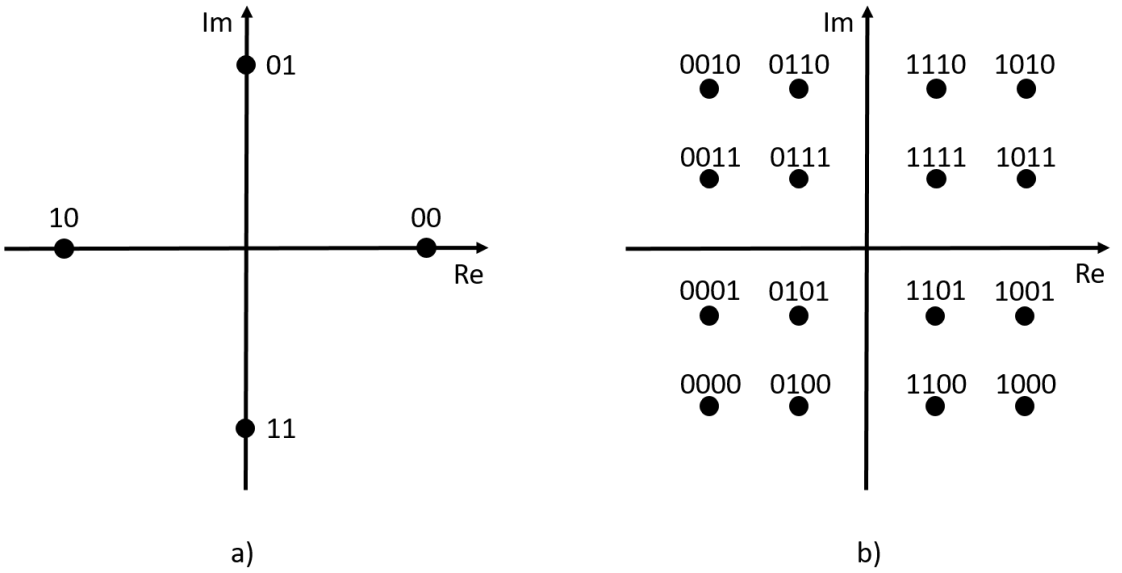

Figure 6.2: PSK techniques: a) HomePlug GP is limited to QPSK where two bits of data are encoded in the phase of the subcarrier. b) HomePlug AV uses up to 1024 QAM. This is an example 16 QAM map that enables encoding of four bits of data encoded using 16 unique amplitude and phase combinations.

modulation technique, starting with simple QPSK up to 1024 QAM. The tone map is also used to calculated the physical data rate capacity of the channel in Mbps. Some of the notches in Fig. 6.3 are masked due to EMI regulations while others are reduced due to channel quality. Pre-masked bands depend on the geographic region of retail. The bands for North America are published in [228]. The AV2 devices used in this study were purchased in the UK and have slightly different mask bands.

Forward error correction binary codes (called Turbo codes) are added to the modulated data stream to detect bit errors. When the channel quality is poor, QPSK modulation is boosted using Robust ODFM (ROBO) techniques where 2-5 redundant copies of each packet are sent to increase reception probability [228]. The GP does not employ ABL and only relies on QPSK with ROBO [118]. Although repetitions reduce throughput, it has been proven to increase reliability when operating in noisy channels (such as powerlines). In the ROBO mode, all subcarriers are used indiscriminately.

The GP utilizes 1155 subcarriers between 1.8-30 MHz, while the most advanced AV (AV2) increases the number of possible carriers up to a maximum of 4096

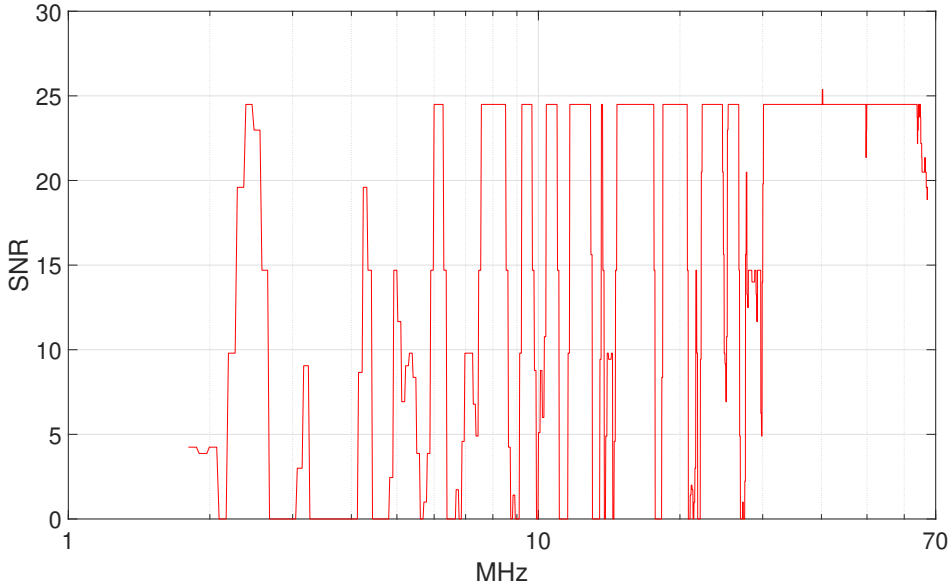

Figure 6.3: HomePlug AV2 unitless SNR tone map for a 50 m SWA cable.

and widens the potential bandwidth to 86.13 MHz [15]. The AV2 devices used in this study use 2096 carriers up to 68 MHz.

6.2 Experimental Setup

The HomePlug products are tested on the RELCON system from Section 3.4. The experimental setup in Fig. 6.4 is used to evaluate PLC performance on a given cable network. In this test, microgrid power flows from a generator to a load via power electronic converters. Those converters are mostly capacitive in nature and present a low impedance path for PLC frequencies. Therefore, low pass filters (LPF), placed between the converters and the powerline, are necessary to present a high impedance to PLC signals. The distribution network consists of various lengths and branching configurations of SWA power cable modeled with the modified two-wire TLM from Chapter 5.

Following Fig. 6.4 from bottom left, internet protocol (IP) test data originates at the Linux computer. The data is addressed to a `namespace`, a self-contained partition that tunnels data to the USB-ethernet output such that communication occurs down wire vs internally in the Linux machine [229], [230]. Moving up the

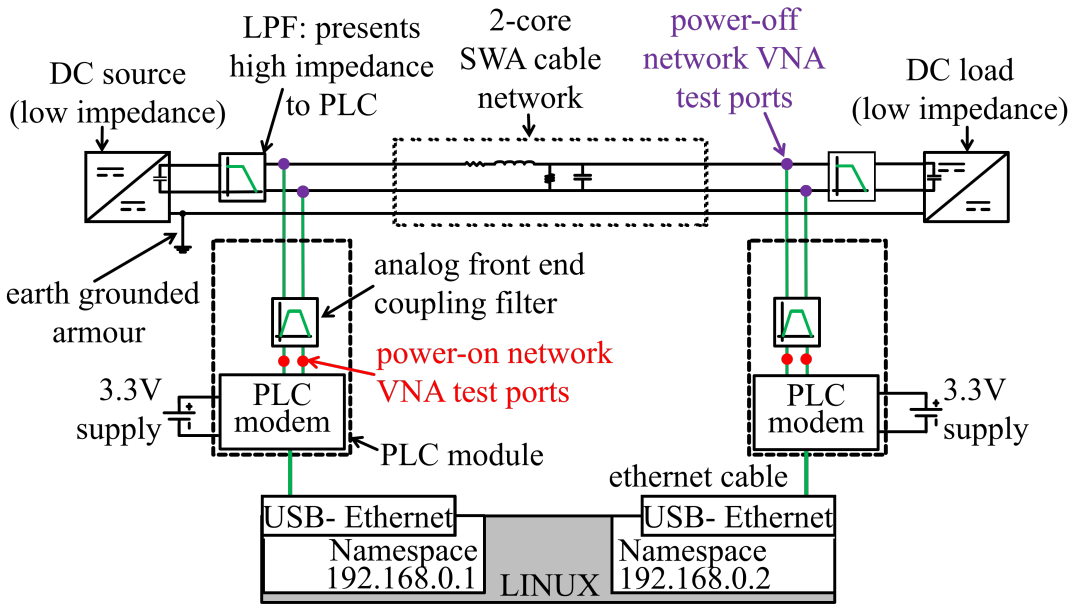

Figure 6.4: Network performance test setup.

diagram, the HomePlug PLC modem modulates the IP test data into a time domain OFDM symbol that is transmitted as a differential voltage signal and coupled to the powerline through the analog-front-end (AFE) filter circuit. After traveling through the powerline distribution network the signal is received by another PLC modem at the opposing node, demodulated by another PLC modem, and passed to the receiving Linux `namespace` IP address.

VNA measurements are taken of both *dead* (microgrid power off) and *live* (microgrid power on) powerlines. Direct VNA measurements of the distribution network are taken at the purple network ports in Fig. 6.4 whilst the network is dead. Live measurements are taken behind the AFE at the red ports to observe the full PLC path from transmitting modem to receiving modem. Two software utilities are used to generate internet IP test data on the Linux machine. `Ping` measures network latency by calculating roundtrip time for an IP message to travel from transmitter to receiver and back. The Linux processing contributes 0.4 ms. The powerlines contribute (based on approximately 1.65×10^8 m/s transmission speed) less than 0.003 ms latency due to the PLC modem pair. When a reliable PLC connection is established, latencies are consistently around 10 ms for the GP and

4 ms for the AV meaning the majority of latency comes from modulation protocols. These numbers do not vary with network structure since the modulation techniques operate to guarantee latency consistency.

The `iPerf` utility similarly produces a stream of IP data from client (transmitter) to server (receiver) at channel max capacity to measure throughput, jitter, and packet loss or retries [231]. Jitter is latency deviation and tends to rise with channel degradation. Data can be packaged in transmission control protocol (TCP) or user datagram protocol (UDP) format. The main difference is TCP's need for a transmission receipt. When the client does not receive a receipt from the server, the client retries. UDP, on the other hand, transmits indiscriminately which can lead to packet loss. HomePlug modulation techniques also sacrifice throughput to maintain acceptable thresholds of packet loss and retries. That leaves throughput as the main variable to evaluate PLC performance. There is a clear relationship between the data rate capacity calculated by the tone map, the actual throughput measured by `iPerf`, and channel quality.

In addition to the Linux utilities, the HomePlug modems made by Qualcomm Atheros (QCA) have software tools called the Open Powerline Toolkit that can be used to evaluate performance. These tools are open source [227]. Each modem chip has a unique MAC address which is used to interrogate the chip for various parameters. Three commands were used in the PLC tests:

1. `int6k`: interrogates the modem and prints the network configuration. It identifies which chip address has established itself as Central Coordinator (CCo) and which are its subordinate stations [228]. Any chip can act as either. The program is used to quickly assess if two or more modems have established a network.
2. `plctone`: prints SNR tone map. The chip exchanges investigative packets with network neighbours to assess the channel quality to create a tone map as in Fig. 6.3. The tone map also incorporates pre-masked carriers and is then used for ABL protocols. This feature only works on the AV chip.

3. `plcrate`: polls all modems on network and prints physical data rates in Mbps. This is the maximum transmission rate capability of the modem for a given tone map. This feature only works on the AV chip. Data rate is only based on the physical layer and establishes the ceiling capability whereas throughput is the actual bit rate achieved after software and hardware overhead. Throughput calculated by `iPerf` will always be lower than the data rate reported by `plcrate`.

6.3 Analog-front-end (AFE) PLC coupling circuit

Measurements of live networks are taken at the red illustrated ports in Fig. 6.4 through the AFE coupling circuit on the dLAN Green PHY Evaluation Board made by devolo and purchased from Codico [232]. The evaluation board provides access to the PLC modem [14] and the AFE coupling circuit. To best compare VNA measurements to the network model, an s-parameter model of the AFE is required. The coupling circuit is modeled in AWR Microwave Office and illustrated in Fig. 6.5. It includes a three-winding transformer (devolo UT11359) to step up the PLC signal both upon transmission and reception [233]. In parallel with the transformer is a capacitive low pass filter to block frequencies above the band of interest (1-30 MHz). The transformer is modelled as an ideal three-coil mutually coupled inductor with leakage inductance modelled as an additional inductor placed in series with the transmit coil per the transformer data sheet [232]. Coil 1 is the receiver, coil 2 the transmitter, and coil 3 connects to the impedance matching resistor of 96 Ω (impedance option on the evaluation board closest to the cable's characteristic impedance seen in Fig. 5.7(b)) before connecting to the powerline.

AWR was chosen because of the user-friendly GUI designed for rapid 2-port network design and s-parameter graphical analysis. The software comes with the basic two-wire model, but also allows for bespoke *rlcg* per-unit values to accommodate the modifications made in Chapter 5. Fig. 6.6 shows S_{21} measured from a GP transmitter, through the AFE, down a 10 cm coaxial cable, to another

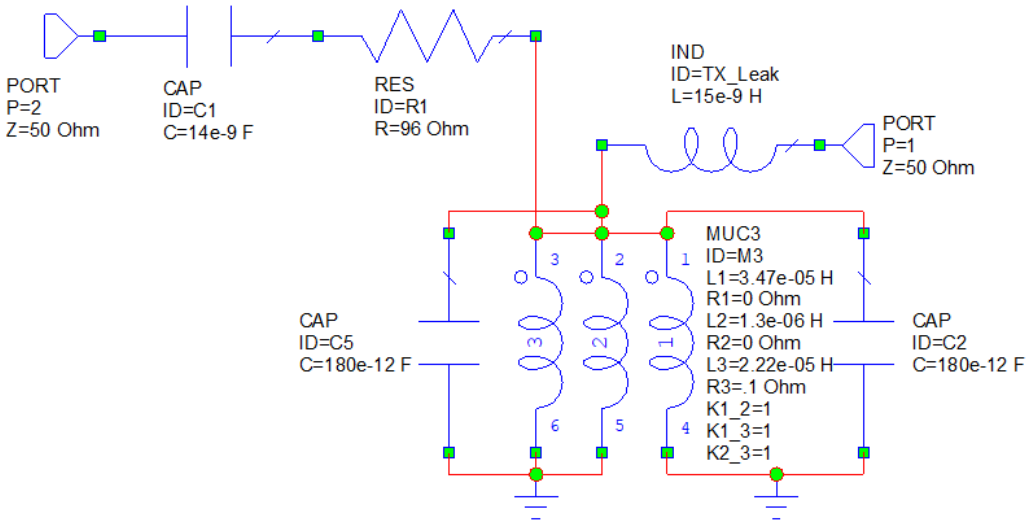

Figure 6.5: Network performance test setup.

GP receiver showing a "direct connection" frequency response. The s-parameters for the passband of an ideal transformer is determined by (20):

$$S_{xfmr}(n) = \frac{1}{n^2+1}\begin{bmatrix} n^2+1 & 2n \\ 2n & n^2+1 \end{bmatrix} [\mathbf{dB}] \tag{6.1}$$

where n is the number of turns [234]. The GP transformer has a 1:4:5 (TX:powerline:RX) ratio and therefore n=5 from transmit to receive [233].

$$S_{xfmr}(n) = \begin{bmatrix} -0.7 & -8.3 \\ -8.3 & -0.7 \end{bmatrix} [\mathbf{dB}]$$

Fig. 6.6 shows the 8.3 dB attenuation from the transformer plus approximately 2 dB more due to the non-ideal realities of the circuit. This bandpass filter shape will dominate the network VNA measurements.

6.4 PLC performance on microgrid networks

Microgrid power network architectures follow one of two basic structures: star or radial as in Fig. 3.1. Star feeders are direct dedicated connections from a central generation bus to a load. Radial feeders consist of a main cable with several ancillary branches. Even though radial feeders must be larger to support higher currents,

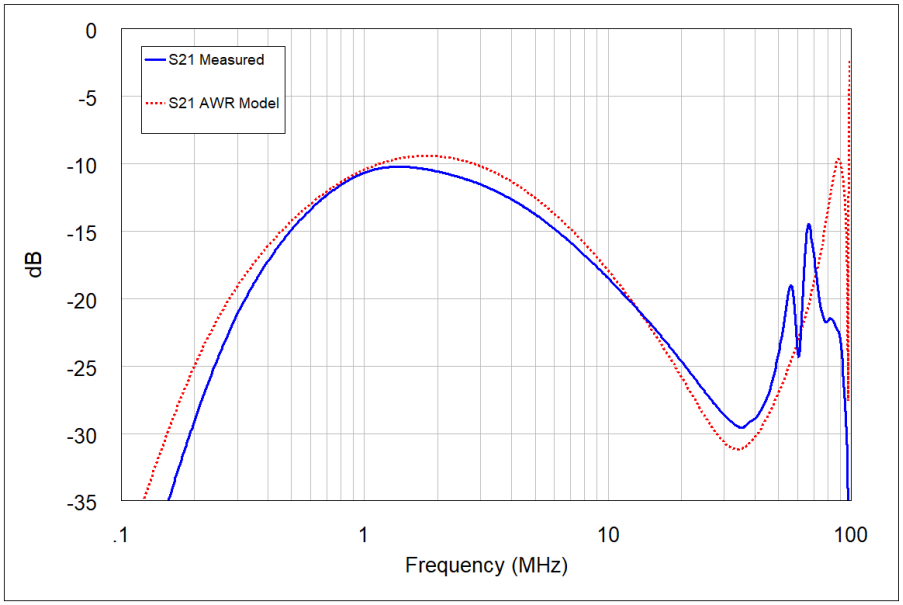

Figure 6.6: Network performance test setup.

radial networks tend to use less cable length, often making them cheaper and therefore more common. BB PLC modulation techniques were originally designed for complex radial indoor networks with random lengths, multiple branches, and dynamic unknown load impedences. There are three main causes of attenuation that impede PLC connectivity: cable length, noise, and notches from branches or impedance discontinuities.

6.4.1 Star Feeders

Attenuation due to cable length is shown in Fig. 6.7. These measurements are of the dead feeder only. They do not include the AFE. This is to establish an attenuation functionality threshold based on cable length.

The published reach of HomePlug products is 300 m; however, the GP can function up to 700 m and the AV up to 800 m on dead star feeders. Functionality decreases on live feeders because of converter switching noise. Blue VNA measurements in Fig. 6.7 become unreliable below −80 dB due to the VNA noise floor [235]. The threshold for GP operation on live star feeders is −60 dB of attenuation at 30 MHz. This equates to a 450 m range with microgrid power on.

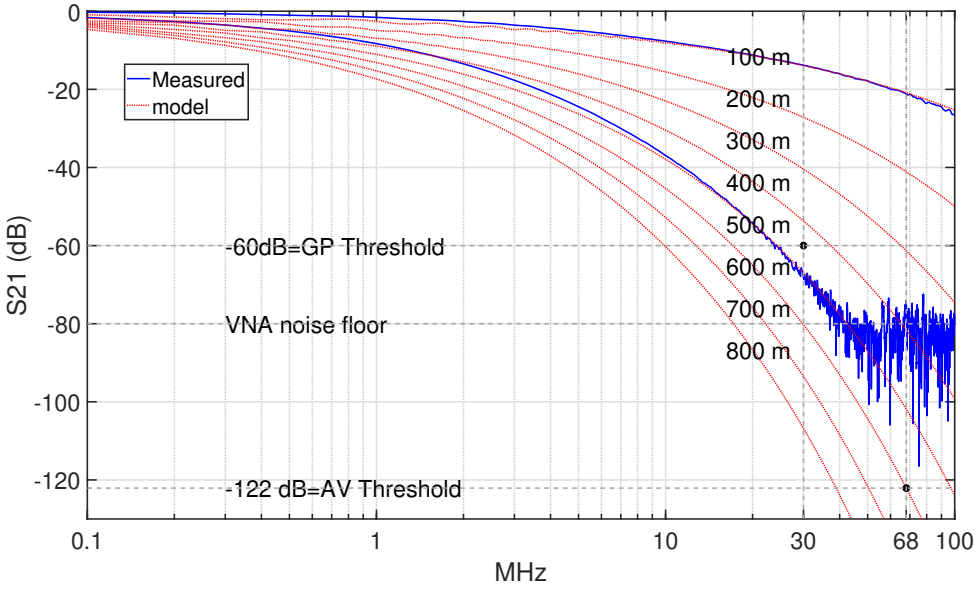

Figure 6.7: S_{21} vs. cable length. VNA measurements are in blue. Measurements become unreliable at $-80\,\mathrm{dB}$ due to the VNA noise floor. Grey lines show the limit of PLC functionality on a live star feeder. The GP requires cable attenuation $> -60\,\mathrm{dB}$ at 30 MHz to establish reliable connectivity corresponding to a 450 m live star feeder. For the AV, cable attenuation $> -122\,\mathrm{dB}$ at 68 MHz corresponding to 600 m.

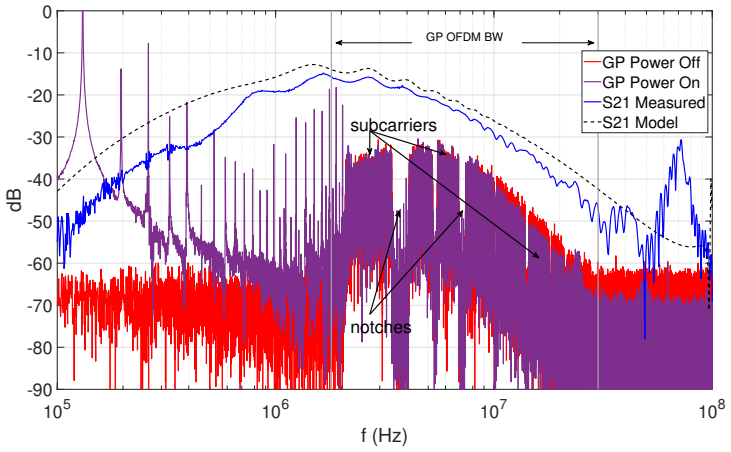

(a)

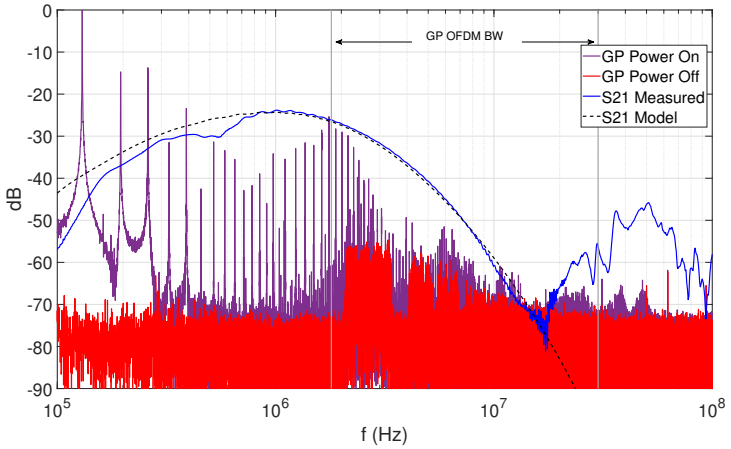

(b)

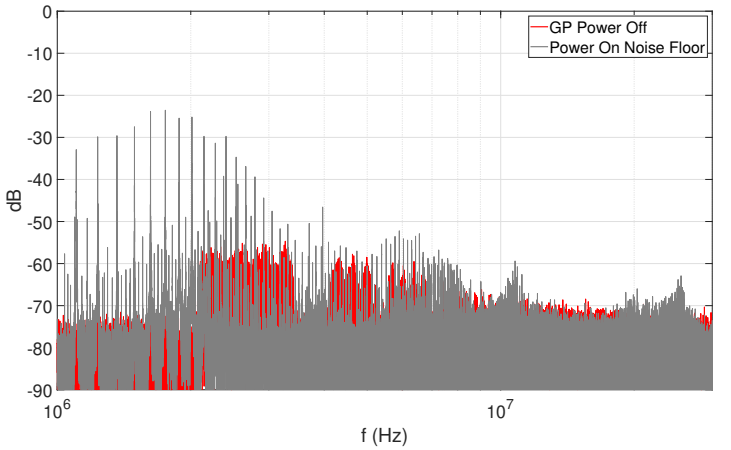

(c)

Figure 6.8: FFT of oscilloscope measurements of received GP TCP OFDM symbols on a) 50 m and b) 500 m of SWA cable star feeder. Red shows reception with a dead feeder (microgrid power off) while purple shows reception with a live feeder (microgrid power on) with the associated converter noise on the line. The FFT is compared to the S_{21} measurement and model of the same length. The FFT shows the OFDM symbol between 1.8-30 MHz tapering with the attenuation of the line as expected from the S_{21} curve. c) Zoom-in of the received GP TCP message at 500 m in red. The noise floor in grey debilitates the message making GP connection unreliable at 500 m with microgrid power on.

The GP functionality limit is further illustrated in Fig. 6.8 which presents the fast Fourier transform (FFT) of time domain oscilloscope measurements of received GP TCP messages at 50 m and 500 m. The frequency plot includes the noise associated with a dead feeder (microgrid power off in red) compared to a live feeder (microgrid power on in purple). There is an increase in the overall noise floor with distinct harmonic spikes in the lower frequencies caused by the switching power converters. Amongst the noise in Fig. 6.8(a) are clear PLC subcarrier groupings in the band between 1.8-30 MHz from the GP OFDM symbol. Pre-programmed notches are also visible. GP transmission power is fixed; therefore, the amplitude of each received carrier is determined by the amount of attenuation caused by the length of the star feeder. Hence, the OFDM symbol follows the shape of S_{21}. S_{21} measurements in Fig. 6.8 are made looking through the GP AFE coupling circuit as modelled in Section 6.3. Performance at 500 m is unreliable when microgrid power is on because the received strength of the OFDM is exceeded by the noise as shown in Fig. 6.8(c).

Since the GP does not use ABL, it relies on the ROBO technique of sending multiple copies of each data packet. To maximize the GP reach during performance tests, the ROBO setting is programmed at the most conservative level which sends five repeat copies of each packet [118]. With this setting, the GP range is maximized, but data PHY rates are limited to 3.8 Mbps and throughputs of approximately 1.5 Mbps. These rates did not change with cable length or channel quality. There is no gradual decrease in performance. The GP either meets the connection threshold or it does not.

Table 6.1: Star feeder power-off & power-on functionality vs. distance

	Cable length (m)					
	300	**400**	**500**	**600**	**700**	**800**
GP (power off)	✓	✓	✓	✓	✓	
GP (power on)	✓	✓				
AV (power off)	✓	✓	✓	✓	✓	✓
AV (power on)	✓	✓	✓	✓		

Table 6.1 summarizes PLC functionality on star feeders for both the GP and AV when microgrid power is off or on. In contrast to the GP, AV bit rate varies

with channel quality. The relationship between cable length and data rate is illustrated in Fig. 6.9(a). Data rate (in red) is extracted using the QCA toolkit `plcrate` command whilst throughput (in blue) is measured using the `iPerf` network performance utility. AV throughput is limited to 100 Mbps due to the RJ45 Ethernet connectors used on the AV device. The mean SNR of the entire spectrum (1.8-68 MHz) in Fig. 6.9(b) is extracted from the QCA toolkit `plctone` command. From experimentation, it is determined that average SNR must be above 1.0 to achieve AV connectivity. Due to the hardware ceiling on AV throughput, both data rate (`plcrate` command) and SNR (`plctone` command) reported by the QCA modem are the best predictors of channel performance.

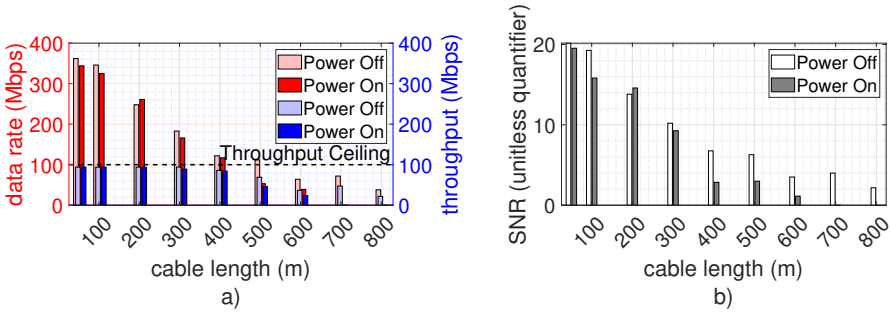

Figure 6.9: Performance vs distance for the HomePlug AV. Light colours indicate microgrid power is off and dark colours show power is on. a) data rate and throughput vs. distance b) SNR vs. distance

From Fig. 6.9 and Table 6.1, the AV functionality on a star feeder with microgrid power on is 600 m. This equates to -122 dB attenuation at 68 MHz due to the cable length as depicted in Fig. 6.7. Fig. 6.10 echoes this limitation showing how noise effects SNR at various cable lengths. SNR maps are compared to S_{21} measurements and models looking through the GP coupling circuit (under the assumption that the GP and AV coupling circuits are very similar).

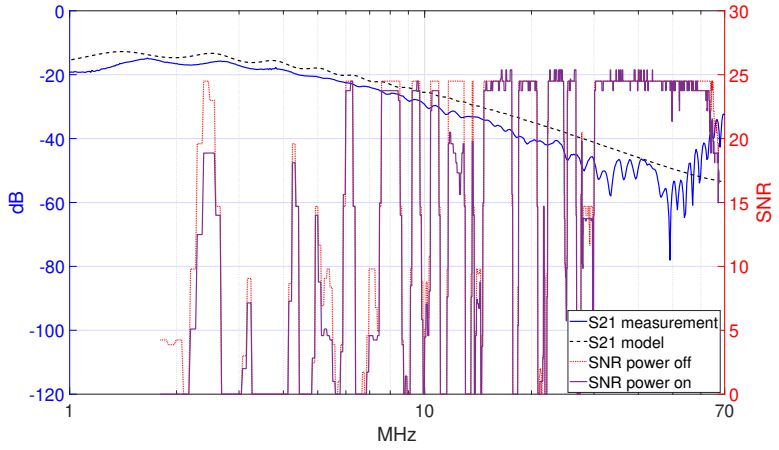

(a)

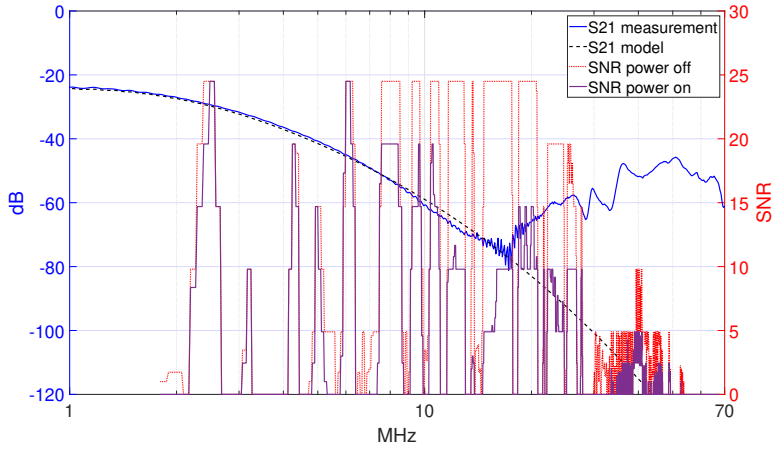

(b)

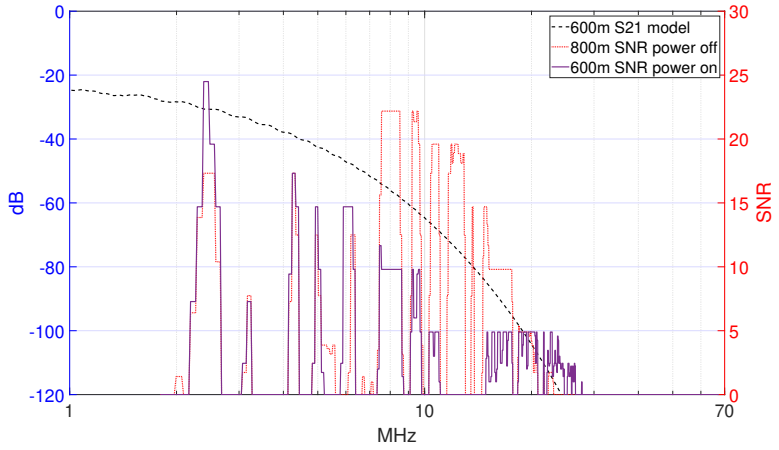

(c)

Figure 6.10: SNR compared to S_{21} on a) 50 m b) 500 m c) 600 m star feeder comparing the difference between microgrid power off and on. Dotted red lines show a dead network and solid purple lines show a live network. At 50 m, noise has very little effect on subcarrier load whereas at 500 m, not only are higher frequency subcarriers attenuated by cable length, but higher frequencies are also more susceptible to microgrid power converter noise since it operates closer to the noise floor. In c), the live 600 m SNR is compared to a dead 800 m to illustrate how much power flow cripples the tone map.

At 50 m, converter noise does not change SNR except for a small reduction in usage of the lower band subcarriers due to harmonic spikes. As cable length increases, the top of the band is most affected due to signal attenuation where the noise has greater impact. The ABL algorithm reduces data loads on higher frequency carriers. The carriers and connectivity success depends on the lower band. The highest frequency of use at the AV operational envelope, a live 600 m feeder, is 27 MHz with an average SNR of 1.13 yielding a data rate capacity of 39 Mbps and throughput of 24 Mbps. This is still ample bandwidth for microgrid communications.

6.4.2 Radial Feeders

Branches on radial feeders cause multipath reflections and standing waves that create notches in the frequency response. The severity of the notches is determined by the branch length and branch termination. In this case, the branches terminate in a large LPF in front of a DC-DC converter as in Fig. 6.4. Therefore, at PLC frequencies, the load termination appears as an open circuit which improves the frequency response as demonstrated in Fig. 6.11. The filter helps shield the PLC network from the problematic switching noise, load dynamics, and capacitive loading of the power converters.

Two radial test networks are shown in Fig. 6.12 that serve as the DUT for VNA and PLC performance measurements. PLC signals are injected at the microgrid generation hub, indicated with a source in Fig. 6.12, and then received at one of the branch terminations, indicated with a lettered home. The lettered home represents the LPF and power converter at the feeder termination.

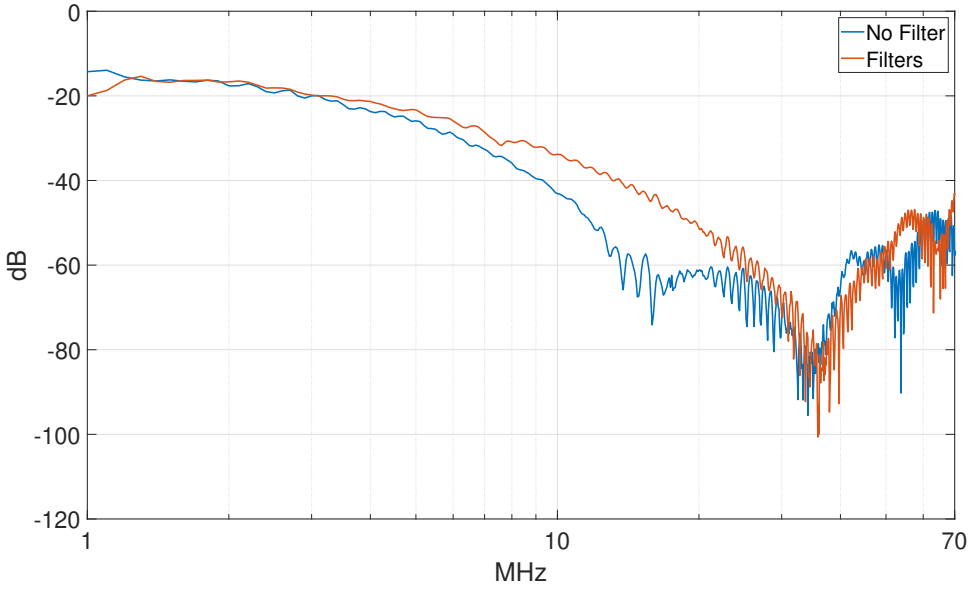

Figure 6.11: S_{21} of 200 m star feeder with and without an inductive LPF in between the DC-DC converter and the PLC modem. The filters block the low impedance path of the capacitive load and reduce attenuation throughout the PLC bandwidth.

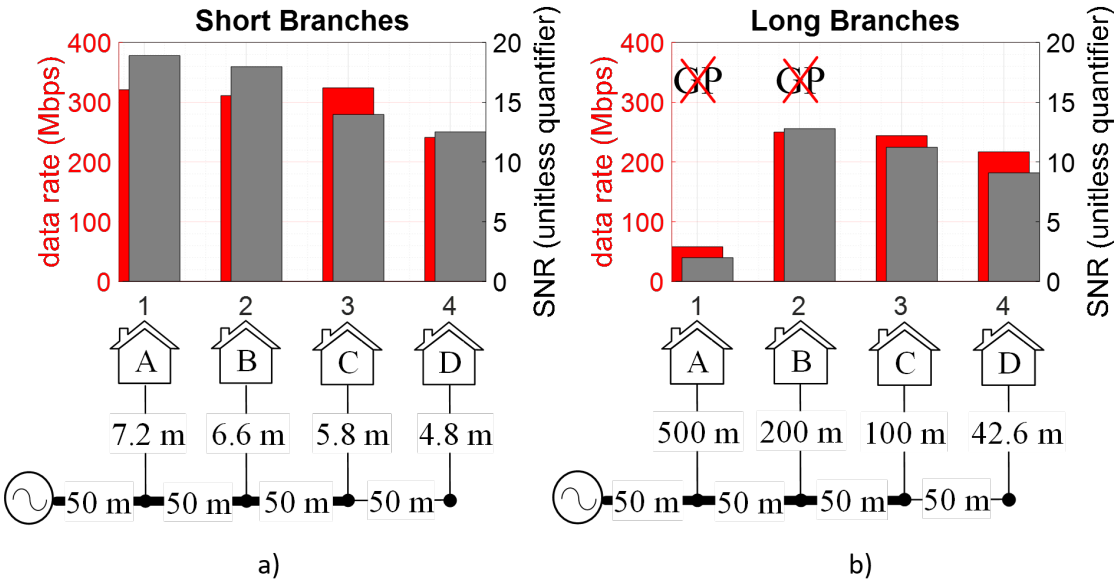

Figure 6.12: Experimental radial feeder networks with a) short branches and b) long branches. The PLC transmitter is placed at the microgrid hub indicated by a source. Receivers are placed at the end of each branch as designated by homes A-D. Each branch is labelled with its respective length in meters. Cables represented by thick lines are SWA cables with 6 mm^2 cores while thin lines have 1.5 mm^2 cores. The bar plots show the AV functioned well on all branches with solid data rates and SNR. The GP was also tested for functionality on the same branches. It achieved connectivity on all branches except A and B of the long branch network mostly due to cable length limitations.

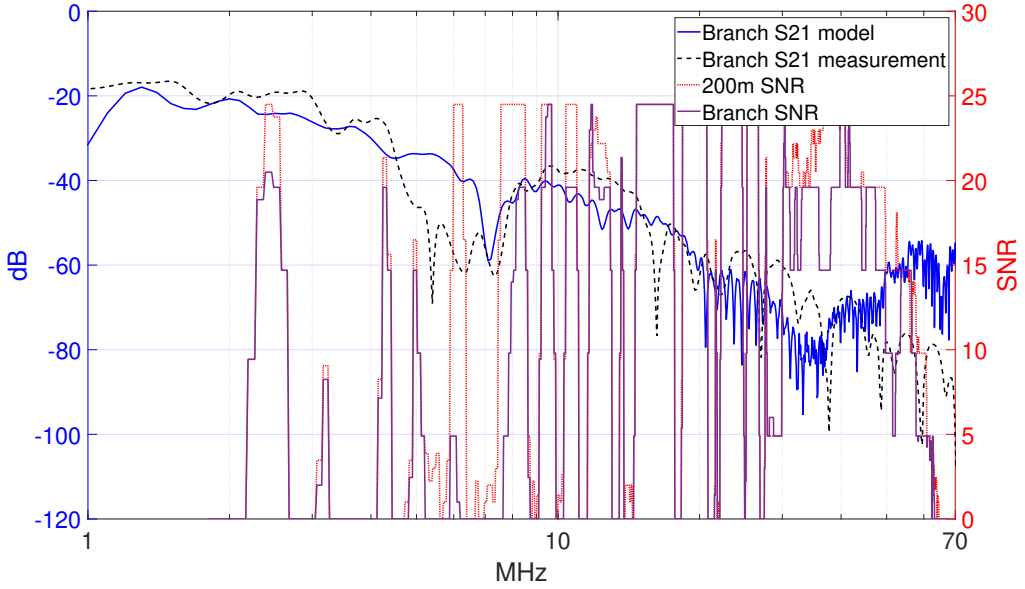

(a)

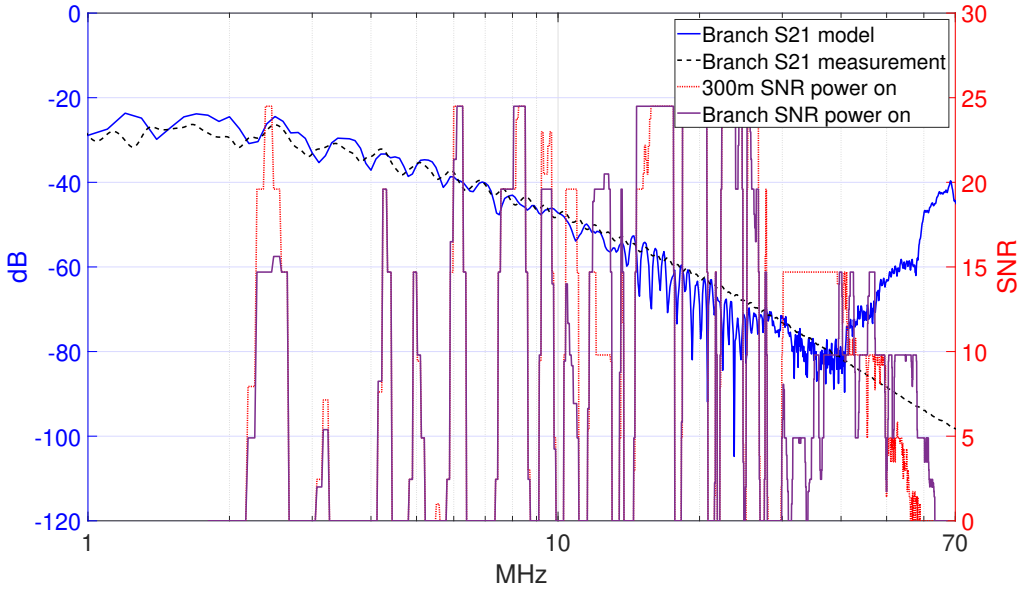

(b)

Figure 6.13: SNR compared to S_{21} on Home 'D' of a) short branch network and b) long branch network. Branch SNR is compared to a similar length of star feeder. Short branches create notches which are especially problematic for the GP that relies on information on all subcarriers. The branch lengths in the short network create a notch around between 5-8 MHz and the AV reduces the data loading on those subcarriers. Long branches do not create deep notches.

Both the GP and AV establish connectivity at every load with two exceptions: the GP does not function on homes A and B on the long branch network. This is

to be expected since A exceeds the GP cable length limit and B is very close to that limit. Comparisons of the S_{21} and SNR of houses D are reported in Fig. 6.13.

Branches that approach the length of the quarter wavelength of a particular PLC subarrier cause resonant notches like the one seen at 7 MHz in Fig. 6.13(a) (in blue). Hence, shorter branches tend to be more problematic, especially for the GP. The SNR plot in red shows a 200 m star feeder tone map. The purple SNR plot shows house D from the short branches network in Fig. 6.12(a) which is just over 200 m in length. Note the AV ABL adjusts the subcarrier loading between 5-8 MHz due to the notch created by short branches. However, since the GP does not use ABL, it cannot reduce or eliminate the use of certain bands that may have deep notches. This notch only dips to −60 dB because the branches are of slightly different lengths effectively widening the notch. The GP still achieves connectivity. As the lengths of the branches become very similar in length, the notches narrow and deepen. The depth of the notch increases even more when two short branches extend from the same junction. Long branches do not cause notching as manifested by the lack of difference between the red (star feeder) SNR plot and the purple (radial feeder with long branches) plot in Fig. 6.13(b). Three additional test networks in Fig. 6.14 illustrate the short branch issue.

The AV establishes connectivity on every branch in each of the three networks. The lowest performing branch with microgrid power on is Fig. 6.14(c) Home B with SNR=0.5, data rate of 15 Mbps, and throughput of 5 Mbps. With microgrid power off, the GP established connection in all branches except the same mentioned above. But with microgrid power on, the GP on several branches failed to connect as indicated with a red X in Fig. 6.14. VNA measurements are not available for these test cases, but network models made in AWR are used to approximate the channel which show deep notches that extend below −70 dB causing GP failure. These notches are most likely to occur in conjunction with either multiple short branches of similar length and/or due to multiple short branches hanging from the same junction.

One last test network in Fig. 6.15 helps define the threshold for the GP. When all the branches are connected, the GP cannot connect between the microgrid hub

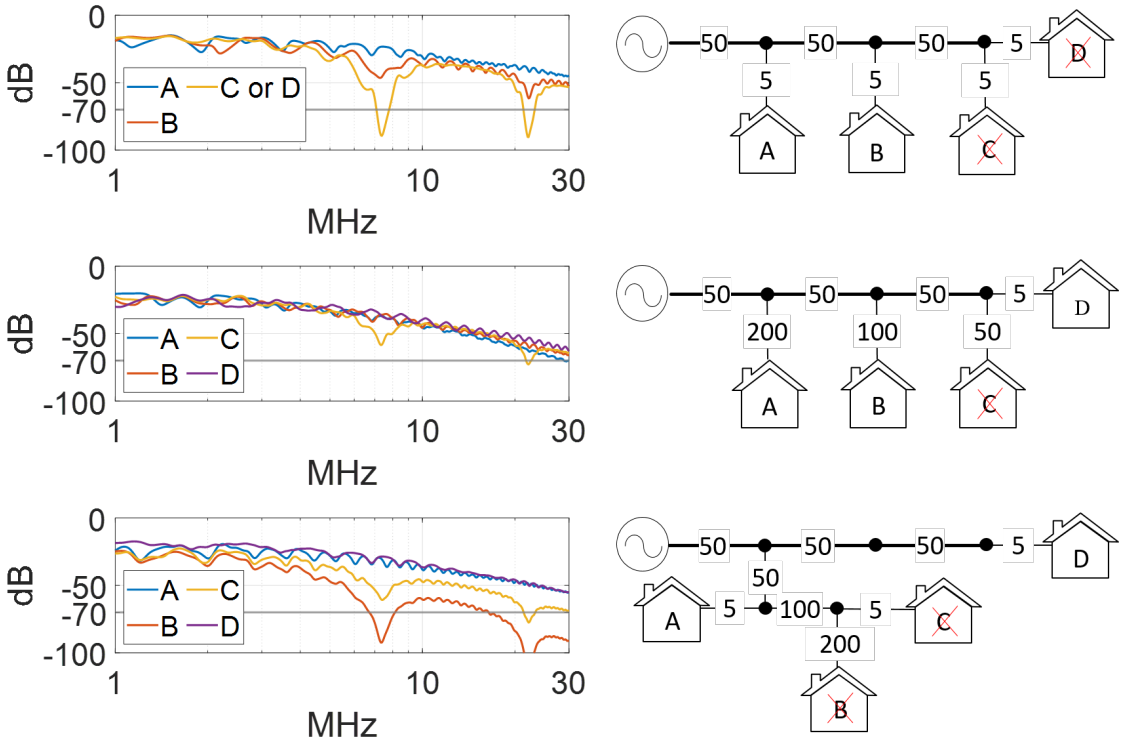

Figure 6.14: S_{21} model versus GP functionality of three experimental radial feeder networks with a) short 5 m branches b) long branches of mixed length and c) a complex network of branches extending from other branches of mixed lengths. Each branch is labelled with its respective length in meters. Cables represented by thick lines are SWA cables with 6 mm^2 cores while thin lines have 1.5 mm^2 cores. Microgrid power is on during the test. The red X indicates that the GP failed to connect. Such failures are due to notches that extend beyond −70 dB. In contrast, the AV established connectivity at every home in all three networks.

and Home A. The GP begins connecting after removing the three red branches. The GP sends and receives ping commands but is unable to transfer TCP or UDP data indicating the connection is not reliable. More branches would need to be removed for full functionality. The S_{21} measurements show two deep notches at 4 and 12 MHz descending to −85 dB which shallow to −54 dB and −66 dB respectively after removing the red branches. There are two other notches of similar severity at 6.2 and 7.4 MHz which do not improve after removing the three red branches. There are also many notches above 18 MHz, but since they are close to the VNA noise floor, it is difficult to conclude their characteristics and effect. From Fig. 6.13-Fig. 6.15 it is clear that the GP cannot make reliable connection in the presence of deep notches that extend below the microgrid power-on noise floor at −70 dB.

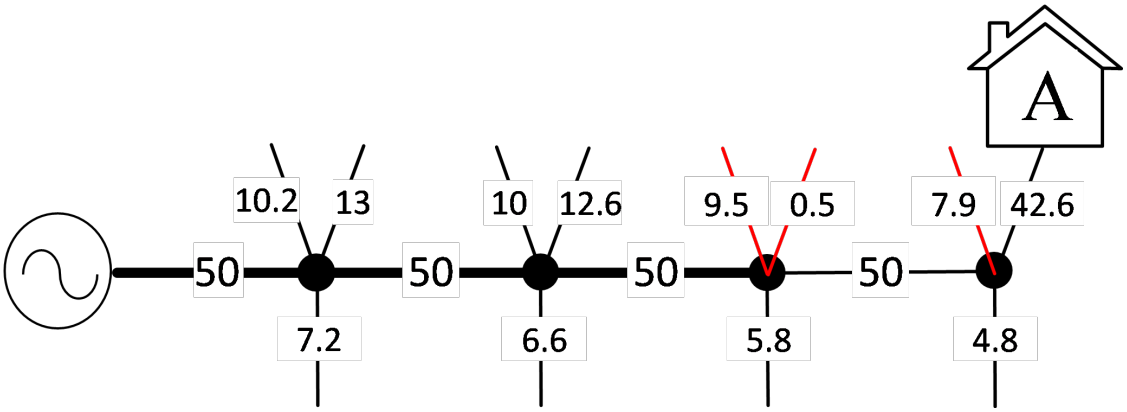

(a)

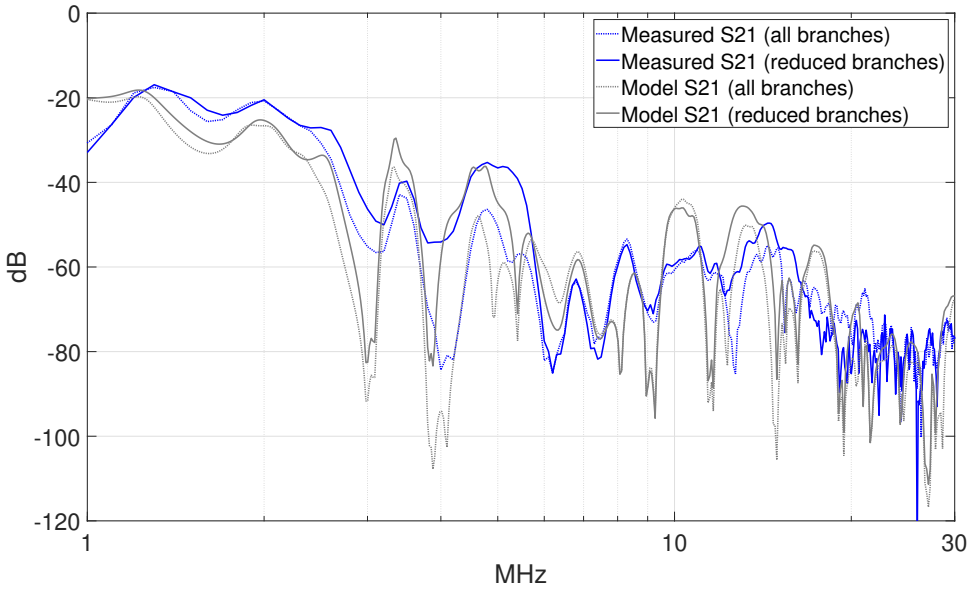

(b)

Figure 6.15: a) Complex experimental radial feeder network with several short branches each labelled with its respective length in meters. Cables represented by thick lines are SWA cables with 6 mm^2 cores while thin lines have 1.5 mm^2 cores. One measurement is taken with all the branches. Then red branches are removed one at a time until the GP begins to function. b) S_{21} measurements and model taken between the PLC source at the microgrid hub to Home A. All other branches are terminated with an open circuit. Dotted lines show the network with all branches connected while solid lines show the network without the red branches. The GP begins connecting after removing the three red branches due to the shallowing of the deep notches at 4 and 12.7 MHz.

6.5 Cross coupling

VNA measurements show an unexpected rise in S_{21} at frequencies towards the higher end of the band of interest. The VNA noise floor is apparent when S_{21}

attenuation reaches −80 dB as demonstrated in the differential measurement of a 500 m cable in Fig. 6.7. The single-ended measurement of the same cable in Fig. 6.10(b) shows steady gain after reaching the −80 dB minimum at 17 MHz. This rise is either due to a measurement error or some other phenomena. In any case, S_{21} measurements become unreliable after attenuation falls below −80 dB.

There are other complex phenomena occurring in this same range. First, the GP coupling AFE transformer, modeled in Section 6.3, has a leakage inductance that causes gain after 35 MHz as illustrated in Fig. 6.6. Yet, this leakage gain is built into the model; and therefore, it would also appear in the model S_{21} curves, but it does not. Furthermore, the rise in gain at higher frequencies also occurs when taking single-end measurements of only the cable, confirming it is at least not exclusively due to AFE leakage inductance.

FEXT for an uncoiled 50 m cable is shown in Fig. 5.11(d). Many of the VNA measurements in the RELCON test lab were conducted with the cables coiled on drums. The same uncoiled FEXT is compared to the FEXT of a coiled cable of the same length in Fig. 6.16. A distinct rise occurs in the coiled cable at the higher end of the band. This could be contributing to S_{21} rise in the single-ended VNA measurements.

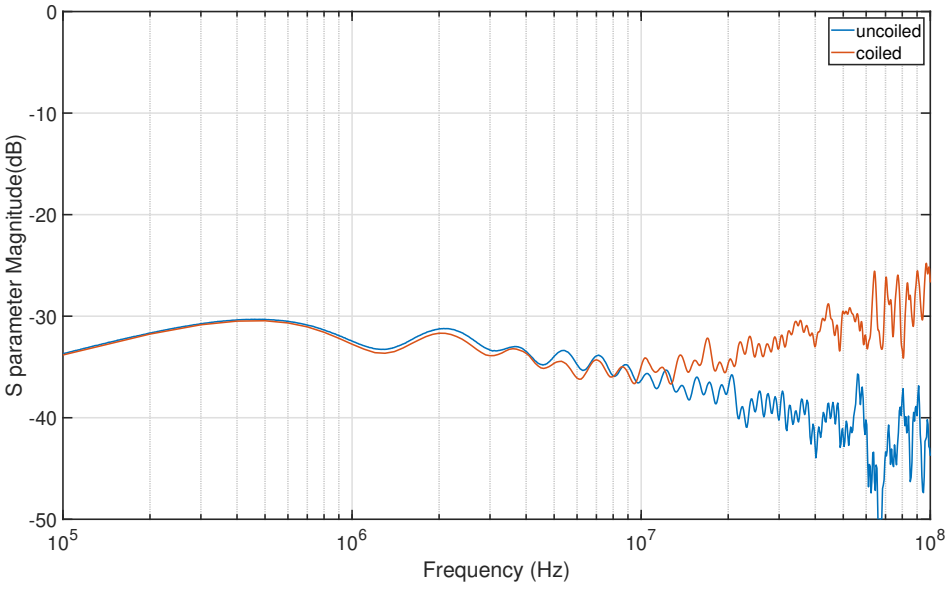

Figure 6.16: FEXT of uncoiled vs. coiled 50 m cable

Related to FEXT is the possibility of capacitive coupling between DUT Port 1 and 2 during measurements, possibly from the SMA connectors soldered to the core conductors seen in Fig. 5.5.

Multiple measurements were taken to explore the idea of cross coupling. Both the AV and GP can communicate over the air in certain situations. For example, connection can be made when a transmitting cable termination is within 10 cm of the receiver or when at least 3 m of transmitting cable lies in parallel and almost touching a receiving cable. In other words, despite the SWA, the cable acts as an antenna. As expected, cross coupling also occurs very reliably between conductor pairs within the same multiconductor cable.

Most of the S_{21} measurement errors occur above the GP utilization band of 1.8–30 MHz and are therefore irrelevant to the GP results. However, it is unclear whether the S_{21} rise at higher frequencies affect AV2 performance. To limit the influence of FEXT, all the measurements in this chapter are made on two-core cables and performance tests were accomplished twice, once inside with coiled cables, and again outside with uncoiled cables with over 50 m of spacing between nodes. Performance of the HomePlug devices were similar in both circumstances. If coupling was suspected, the results were not used.

6.6 Results

A bottom-up approach to network modelling yields a tool to predict PLC functionality on microgrids. Using the modified two-wire TLM as a building block, complex networks are built in AWR Microwave Office to rapidly produce S_{21} frequency response curves, validated by VNA measurements, that predict PLC functionality for a given microgrid network structure.

Experimentation reveals the HomePlug AV has a star feeder reach of 600 m in the presence of power converter noise and performs well on complex branched networks due to ABL. 600 m corresponds to a maximum cable attenuation of -122 dB at 68 MHz. Throughput bit rates exceed 10 Mbps even in the most extreme cases

which surpasses communication requirements for microgrids defined in Chapter 3. Average SNR reported by the AV QCA must exceed 1.0 for connectivity.

The GP also performs well on star feeders less than 450 m which equates to an attenuation of −60 dB at 30 MHz. It also performs well on radial feeders with longer branches (> 30 m) assuming the total signal path length is less than 400 m. However, the GP struggles to make reliable connection on radial feeders with short branches due to frequency selective notching. S_{21} curves must not contain notches in the PLC bandwidth (1.8-30 MHz) that dip below −70 dB.

Digital communication requirements for microgrids can be satisfied with HomePlug devices after considering these limitations. Due to the HomePlug plug-and-play design and IP-based protocol, the devices can be integrated easily into a microgrid control system. The AV appears to be the superior choice due to its increased range and adaptability on radial feeders with various branch lengths. Additionally, the AV is an affordable and common product available all over the world as compared to the relatively obscure and still expensive GP.

7 Conclusion

Low voltage islanded microgrids are an attractive solution for remote electrification due to their flexible and autonomous nature. Like all power systems, high capital costs must be amortised through customer subscriptions. The greatest challenge for microgrid deployment is making energy affordable whilst simultaneously recovering capital costs and achieving profit, especially in remote low-income communities. Although the addition of a communication system to a microgrid increases capital cost, it has the potential to reduce overall cost by improved metering and billing, reducing overall capacity, and enabling coordinated control of microgrid components.

7.1 Question #1

How does communication reduce microgrid costs?

The single most potent energy price reducing technology is prepayment. Fig. 4.2 shows a 17% reduction in LCOE from the installation of a pre-pay meter that eliminates both the need for utility visits for manual meter reading and unpaid bills. Although prepayment strategies can be implemented through the installation of a digital communication FAN to the microgrid, prepayment can also be achieved through much simpler UEC methods like a direct-WAN or a simple token-based prepay meter.

Similar cost reductions are possible through some form of AMR. Most macrogrid utility companies are pursuing AMR through direct-WAN smart meters using cellphone technology since these power grids already have pre-existing control systems. However, in the context of an islanded LV microgrid deployment, the addition of a FAN can enable AMR while also serving as the foundation for secondary and tertiary control. AMR can reduce LCOE by another 4% through the collection of consumption data that informs the sizing exercise of subsequent microgrid designs reducing load profile uncertainty and the oversize of DERs.

Cost reductions from secondary control are minimal, offset by hardware costs and increased technical losses. Still, secondary control increases power quality, increases system longevity, eliminates theft and is requisite to realise tertiary control measures.

An additional 10% reduction in LCOE is possible through tertiary control executing DSM strategies like demand shifting. This study recommends a DSM strategy for the electrification of a rural village consisting of a dual-pronged CRT to:

1. curtail peak power with a monthly power ceiling subscription and
2. incentivise daytime consumption during high production periods to minimize storage size and usage with a two-period TOU PAYG energy tariff.

This blended market DR strategy outlined in Table 3.4 aims to enable low-income customer participation while preventing night-time load curtailments.

7.2 Question #2

> *What are the costs and benefits of adding a digital communication system to the microgrid?*

There are two main capital expenses to install a digital communication FAN in a microgrid: the transceivers at each meter and the backhaul link to connect the FAN to the utility. For a remote islanded LV microgrid, the backhaul link will most likely use either cellular or satellite technology. Transceiver costs are cataloged in Table 4.1. Available products range in cost between \$12-\$33 per customer. Assuming the installation of a FAN that supports both secondary and tertiary control, additional CAPEX are the EMS, control sensors, and an IHD for each meter. Average CAPEX

for a FAN is approximately $96 per customer. OPEX include data and mobile banking fees that add another $5 per customer over 20 years. After amortising this expense over the microgrid lifetime, cost becomes only a minor design delineator.

The techno-economic analysis summarized in Fig. 4.2 demonstrate the economical benefit of adding a digital communication system and shows a potential reduction in LCOE of 32%. That is to say, using every realistic tertiary control technique from Table 4.3, the cost-reflective LCOE for a Tier-3 rural microgrid (like the RELCON system described in Section 3.4) would be $0.51/kWh as compared to $0.75/kWh for the communication-less baseline case. Not only does communication reduce the cost of energy, but it also reduces CML, increases grid efficiency, improves power quality, lengthens system lifetime, and eliminates theft and unpaid bills.

7.3 Question #3

What capability (bit rate & latency) is required for various services?

Microgrid FAN communication technologies fall into three medium categories: dedicated wire, PLC, and wireless. Range, bit rate, latency and cost for each is cataloged in Table 4.1. All the listed technologies meet the latency and bit rate requirements for microgrid control as defined in Table 3.1. Although wired solutions tend to boast the lowest latency and highest bit rates, they are not affordable beyond an average range of 100 m per customer connection. PLC technologies have superior range and can still offer reliability like dedicated wire solutions. Therefore, there is no single superior technology. Selection of a communication technology for a microgrid FAN depends on nuanced factors like geography, reliability, product availability in local markets, interoperability with control software, and integration complexity.

Secondary control fixes the upper limit on the latency requirement: < 100 ms. Tertiary control fixes the lower limit on the bit rate requirement: ≥ 1 kbps. Additional services are available with higher bit rates like RTP, remote firmware updates, or bundled telecommunications. However, as illustrated in Fig. 4.2, a point of diminishing return occurs after increasing the communication link capability beyond 10 kbps where system costs begin to outweigh the benefits to

LCOE. Furthermore, as discussed in Section 3.3 RTP is not realistic for rural electrification due to its complexity.

7.4 Question #4

Is PLC a competitive technology to meet the communication requirement?

Since all the technologies in Table 4.1 meet latency and bit rate microgrid communication requirements, this study selects BB PLC as a candidate technology to evaluate its suitability and limitations for microgrid control. BB PLC devices, like those that incorporate HomePlug AV standards, were designed initially to extend indoor internet service using pre-existing power cables. The HomePlug GP subsequently aimed to address the communication needs of smart grids, like EV charging networks and can be purchased from select vendors for $\sim$ \$33 per device. Later, AV2 devices integrated lessons learned from both previous standards and are now widely available around the world for approximately $\sim$ \$20 per device. This study defines the limitations of both the GP and AV2 devices through performance tests on real-world microgrid hardware from the RELCON electrification project described in Section 3.4. Tests are preceded by developing a model of the powerline. The distributed element two-wire TLM is modified to account for the frequency dependent dielectric behaviour and proximity effects of multi-conductor cables to provide an accurate prediction of channel attenuation at broadband PLC frequencies (1–100 MHz). The modified model is verified with scattering parameter measurements from a 2-port VNA and is then used as a building block for complex microgrid network modelling. Powerline communication performance tests are conducted using both the HomePlug GP and HomePlug AV2 and their limitations are summarized in Figures 6.9 and 6.14.

The AV2 performs up to 600 m on star feeders and on complex radial feeders in the presence of power converter noise. Functionality requires cable attenuation less than -122 dB at 68 MHz and signal-to-noise ratios above 1.0. The HomePlug GreenPHY performs up to 450 m on star feeders and on radial feeders with long branches (> 30 m). However, it cannot connect reliably on radial feeders with short branches (< 30 m) due to frequency selective notching. Multiple short branches of similar

length hanging from the same junction are especially problematic since they deepen notches. Functionality requires cable attenuation less than −60 dB at 30 MHz and the absence of notches that penetrate below −70 dB within the band 1.8–30 MHz.

Therefore, this study demonstrates BB PLC is a viable technology for a microgrid FAN. The AV2 is a sensible choice for digital communication in a remote islanded LV microgrid with node distances less than 600 m and most conceivable branching configurations.

7.5 Further study

Future work can be broken up by chapter. First, from Chapter 3, the next step in the study of DSM is a field trial of the proposed CRT in a rural village in SSA with the following objectives:

1. Validate assumptions made in cost inventory.
2. Confirm unsubsidised energy can reach low income customers.
3. Project the microgrid IRR.
4. Measure economic activity and energy growth of community.
5. Test dual-pronged TOU DSM strategy and whether it lowers the cost of LCOE and increases system lifetime.
6. Evaluate the efficacy and limitations of mobile money PAYG.
7. Experiment with the IHD and its efficacy in communicating grid information to the customer.
8. Conduct a sensitivity test of the influence of price changes on demand shift.

Second, from Chapter 4, Fig. 4.1 shows that all the digital communication technologies surveyed in this study meet the bit rate and latency requirements for a remote islanded LV microgrid FAN including Power Electronic PLC. This term refers to bespoke software techniques that take advantage of terminating converters that modulate a digital signal onto the powerline using the power electronic switches. The techniques in the literature are limited to bit rates on the order of 1 kbps with latency around 100 ms. Despite the lower capability of Power Electronic PLC compared to the other technologies, it is sufficient to deliver most of the services

of secondary and tertiary control while achieving much greater ranges. Since it operates at lower frequencies, reflections no longer cause problems and the cable can be modelled as a lumped sum circuit. The technology promises communication with little to no added hardware further reducing the LCOE. Additionally, the lower frequencies have a greater range and could serve larger grids. The bespoke PLC technique developed in [189] should be lab tested running the RELCON DSM strategy and compared to the BB HomePlug devices and the original LoRa network.

Finally, from Chapters 5 and 6, the modified two-wire TLM can be expanded to include a model of the coupling effects described in Section 6.5. Additionally, various cable types (*e.g.*, overhead lines, unshielded cables) and coupling configurations (*e.g.*, core to shield, multiple signals on one multi-core cable) can be compared to assess PLC performance differences similar to the research efforts in [136] and [137]. Ultimately, the HomePlug AV2 should be employed as a FAN in a remote islanded microgrid field test to validate its performance limitations.

References

[1] P. Conceição, "Human development report 2019," UNDP, Tech. Rep., 2019. [Online]. Available: http://hdr.undp.org/sites/default/files/hdr2019.pdf.

[2] IEA, *World Energy Outlook 2019*. Paris: OECD, 2019. DOI: 10.1787/caf32f3b-en.

[3] M. Bhatia and N. Angelou, "Beyond connections: Energy access redefined," World Bank, Tech. Rep., Jul. 2015. [Online]. Available: https://www.worldbank.org.

[4] IEA, "Africa energy outlook 2019," in Paris: IEA, 2019. DOI: 10.1787/caf32f3b-en.

[5] IRENA, "Solar PV in Africa: Costs and markets," International Renewable Energy Agency, Tech. Rep., 2016. [Online]. Available: https://www.irena.org/publications.

[6] S. Duby and T. Engelmeier, "Kenya: The world's microgrid lab," TFE, Tech. Rep., May 2017.

[7] US Department of Energy, "Doe microgrid workshop report," Office of Electricity Delivery and Energy Reliability Smart Grid RD Program, Tech. Rep., Aug. 2011.

[8] D. A. Schroth, "Green mini-grids in Sub-Saharan Africa: Analysis of barriers to growth and the potential role of the African development bank in supporting the sector," African Development Bank Group, Tech. Rep., 2016.

[9] P. Palensky and D. Dietrich, "Demand side management: Demand response, intelligent energy systems, and smart loads," *IEEE TII*, vol. 7, no. 3, pp. 381–388, Aug. 2011. DOI: 10.1109/TII.2011.2158841.

[10] J. M. Guerrero and R. Kandari, *Microgrids*. London, United Kingdom: Academic Press, Elsevier, 2022.

[11] P. Dambrauskas, M. H. Syed, S. M. Blair, *et al.*, "Impact of realistic communications for fast-acting demand side management," *CIRED - Open Access Proceedings Journal*, vol. 2017, no. 1, pp. 1813–1817, Oct. 2017. DOI: 10.1049/oap-cired.2017.1162.

[12] G. Lopez, J. Matanza, D. D. L. Vega, *et al.*, "The role of power line communications in the smart grid revisited: Applications, challenges, and research initiatives," *IEEE Access*, vol. 7, pp. 117 346–117 368, 2019. DOI: 10.1109/access.2019.2928391.

[13] V. C. Gungor, D. Sahin, T. Kocak, *et al.*, "A survey on smart grid potential applications and communication requirements," *IEEE TII*, vol. 9, no. 1, pp. 28–42, Feb. 2013. [Online]. Available: https://ieeexplore.ieee.org/abstract/document/6298960.

[14] devolo, "dLAN® Green PHY Module," Tech. Rep.

[15] L. Yonge, J. Abad, K. Afkhamie, *et al.*, "An overview of the HomePlug AV2 technology," *Journal of Electrical and Computer Engineering*, vol. 2013, pp. 1–20, Jan. 2013. DOI: 10.1155/2013/892628.

[16] D. C. Neal, D. J. Rogers, and M. McCulloch, "A techno-economic survey of communication in islanded microgrids," unpublished.

[17] T. Sauter and M. Lobashov, "End-to-end communication architecture for smart grids," *IEEE TII*, vol. 58, no. 4, pp. 1218–1228, Apr. 2011. DOI: 10.1109/TIE.2010.2070771.

[18] C. Cano, A. Pittolo, D. Malone, L. Lampe, A. M. Tonello, and A. G. Dabak, "State of the art in power line communications: From the applications to the medium," *IEEE Journal on Selected Areas in Communications*, vol. 34, no. 7, pp. 1935–1952, Jul. 2016. DOI: 10.1109/JSAC.2016.2566018.

[19] D. Neal, Y. Ding, I. Bello, *et al.*, "Demand side energy management and customer behavioral response in a rural islanded microgrid," in *PowerAfrica*, Nairobi, Kenya: IEEE, 2020. [Online]. Available: https://ieeexplore.ieee.org/abstract/document/9219818.

[20] Center for Global Development, *Electricity consumption and development indicators*, Mar. 2016. [Online]. Available: https://www.cgdev.org/media/electricity-consumption-and-development-indicators.

[21] "IEEE standard for broadband over power line networks: Medium access control and physical layer specifications," *IEEE Std 1901-2020 (Revision of IEEE Std 1901-2010)*, pp. 1–1622, 2021. DOI: 10.1109/IEEESTD.2021.9329263.

[22] D. C. Neal, D. J. Rogers, and M. McCulloch, "Broadband powerline communication for low-voltage microgrids," unpublished.

[23] K. Lee, E. Brewer, C. Christiano, *et al.*, "Electrification for "under grid" households in rural Kenya," *Development engineering*, vol. 1, no. C, pp. 26–35, 2016. DOI: 10.1016/j.deveng.2015.12.001.

[24] B. Tenenbaum, C. Greacen, T. Siyambalapitiya, and J. Knuckles, "From the bottom up: How small power producers and mini-grids can deliver electrification and and renewable energy in Africa," The World Bank, Tech. Rep., 2014.

[25] C. Blodgett, E. Moder, L. Kickham, and H. Leaf, "Powering productivity: Early insights into mini grid operations in rural Kenya," Vulcan Inc., Tech. Rep., 2016.

[26] T. J. Reber, S. S. Booth, D. S. Cutler, X. Li, and J. A. Salasovich, "Tariff considerations for micro-grids in sub-saharan Africa," Tech. Rep., Feb. 2018. DOI: 10.2172/1422366.

[27] Castalia and Ecoligo, "Mini grids in Kenya, a case study of a market at a turning point," The World Bank, Tech. Rep., 2017.

[28] R. Golumbeanu and D. Barnes, "Connection charges and electricity access in Sub-Saharan Africa," World Bank, Tech. Rep., 2013.

[29] S. K. Jha, P. Stoa, and K. Uhlen, "Socio-economic impact of a rural microgrid," in *ICDRET*, Dhaka, Bangladesh: IEEE, 2016, pp. 1–4. DOI: 10.1109/ICDRET.2016.7421518.

[30] C. Blodgett, E. Moder, L. Kickham, and H. Leaf, "Financing the future of rural electrification, achieving mini-grid scalability in Kenya," Vulcan Inc., Tech. Rep., Oct. 2017.

[31] L. Gollwitzer and J. Cloke, "Lessons from collective action for the local governance of mini-grids for pro-poor electricity access," LCEDN, Tech. Rep., May 2018. [Online]. Available: www.lcedn.com.

[32] S. Hirmer, "Improving the sustainability of rural electrification schemes: Capturing value for rural communities in uganda," Ph.D. dissertation, 2018. DOI: 10.17863/CAM.25024.

[33] S. Faris, *The solar company making a profit on poor Africans*, Dec. 2015. [Online]. Available: https://www.bloomberg.com/features/2015-mkopa-solar-in-Africa/.

[34] K. Lee, E. Miguel, and C. Wolfram, "Experimental evidence on the economics of rural electrification," *Journal of Political Economy*, Mar. 2020. DOI: 10.1086/705417.

[35] S. Mandelli, M. Merlo, and E. Colombo, "Novel procedure to formulate load profiles for off-grid rural areas," *Energy for Sustainable Development*, vol. 31, pp. 130–142, Apr. 2016. DOI: 10.1016/j.esd.2016.01.005.

[36] T. Labert, P. Gilman, and P. Lilienthal, "Micropower system modeling with homer," in (Integration of Alternative Sources of Energy), Integration of Alternative Sources of Energy. Hoboken, N.J: Wiley, 2006, pp. 393–395.

[37] B. Soltowski, D. Campos-Gaona, S. Strachan, and O. Anaya-Lara, "Bottom-up electrification introducing new smart grids architecture—concept based on feasibility studies conducted in Rwanda," *Energies*, vol. 12, p. 2439, Jun. 2019. DOI: 10.3390/en12122439.

[38] A. Werth, N. Kitamura, and K. Tanaka, "Conceptual study for open energy systems: Distributed energy network using interconnected DC nanogrids," *IEEE TSG*, vol. 6, no. 4, pp. 1621–1630, 2015. DOI: 10.1109/TSG.2015.2408603.

[39] Y. Shimizu, K. Arakaki, K. Kuwae, and H. Kitano, "Smart grids and stability a whole year evaluation of an inhabited DC microgrid with energy exchange," in *ICDRET*, IEEE, Dec. 2018, pp. 102–106. DOI: 10.1109/ISGWCP.2018.8634458.

[40] A. Graillot, M. Briganti, M. Solano-Peralta, and X. Vallvé, "15 years of field experience with the "daily energy allowance" concept as the basis for load control and guide for social behaviour in rural micro grids," in *6th European PV-Hybrid and Mini-Grid Conference*, Trama TecnoAmbiental, Apr. 2012.

[41] Powerhive, Inc., *A scalable, sustainable approach to energy access in emerging markets.* 2015.

[42] S. Abdullah and P. W. Jeanty, "Willingness to pay for renewable energy: Evidence from a contingent valuation survey in Kenya," *Renewable and Sustainable Energy Reviews*, vol. 15, no. 6, pp. 2974–2983, 2011. DOI: 10.1016/j.rser.2011.03.016.

[43] R. Anker and M. Anker, "Kenya living wage report: With a focus on rural mount Kenya area," Global Living Wage Coalition, Tech. Rep. 10, Jun. 2015, p. 30.

[44] M. Grimm, L. Lenz, J. Peters, and M. Sievert, "Demand for off-grid solar electricity: Experimental evidence from Rwanda," *Journal of the Association of Environmental and Resource Economists*, vol. 7, no. 3, pp. 417–454, May 2020. DOI: 10.1086/707384.

[45] S. Faris, *The solar company making a profit on poor Africans*, Dec. 2015. [Online]. Available: https://www.bloomberg.com/features/2015-mkopa-solar-in-Africa/.

[46] M. Obermaier, A. Szklo, E. L. L. Rovere, and L. P. Rosa, "An assessment of electricity and income distributional trends following rural electrification in poor northeast Brazil," *Energy Policy*, vol. 49, no. 1, pp. 531–540, Oct. 2012. DOI: 10.1016/j.enpol.2012.06.057.

[47] C. Dominguez, K. Orehounig, and J. Carmeliet, "Understanding the path towards a clean energy transition and post-electrification patterns of rural households," *Energy for Sustainable Development*, vol. 61, pp. 46–64, Apr. 2021. DOI: 10.1016/j.esd.2021.01.002.

[48] F. Riva, F. D. Sanvito, F. T. Tonini, E. Colombo, and F. Colombelli, "Modelling long-term electricity load demand for rural electrification planning," in *Power Tech*, IEEE, Jun. 2019, pp. 1–6. DOI: 10.1109/PTC.2019.8810727.

[49] G. Prinsloo, R. Dobson, and A. Brent, "Scoping exercise to determine load profile archetype reference shapes for solar co-generation models in isolated off-grid rural African villages," *Journal of Energy in Southern Africa*, vol. 27, no. 3, pp. 11–27, Aug. 2016. DOI: 10.17159/2413-3051/2016/v27i3a1375.

[50] B. Shakya, A. Bruce, and I. MacGill, "Survey based characterisation of energy services for improved design and operation of standalone microgrids," *Renewable and Sustainable Energy Reviews*, vol. 101, pp. 493–503, 2019. DOI: 10.1016/j.rser.2018.11.016.

[51] N. J. Williams, P. Jaramillo, B. Cornell, I. Lyons-Galante, and E. Wynn, "Load characteristics of east African microgrids," in *PowerAfrica*, IEEE, Jun. 2017, pp. 236–241. DOI: 10.1109/PowerAfrica.2017.7991230.

[52] A. Clements, "Data-driven approaches enabling the design of community energy systems in the global south," Ph.D. dissertation, 2018. [Online]. Available: http://ethos.bl.uk/OrderDetails.do?uin=uk.bl.ethos.780620.

[53] T. B. Smith, "Electricity theft: A comparative analysis," *Energy Policy*, vol. 32, no. 18, 2004. DOI: 10.1016/s0301-4215(03)00182-4.

[54] P. Antmann, "Reducing technical and non-technical losses in the power sector," World Bank, Washington, DC, Tech. Rep., Jul. 2009. [Online]. Available: http://hdl.handle.net/10986/20786.

[55] T. Winther, "Electricity theft as a relational issue: A comparative look at Zanzibar, Tanzania, and the Sunderban Islands, India," *Energy for Sustainable Development*, vol. 16, no. 1, pp. 111–119, Mar. 2012. DOI: 10.1016/j.esd.2011.11.002.

[56] F. B. Lewis, "Costly 'throw-ups': Electricity theft and power disruptions," *The Electricity Journal*, vol. 28, no. 7, pp. 118–135, Aug. 2015. DOI: 10.1016/j.tej.2015.07.009.

[57] M. Buevich, X. Zhang, O. Shih, *et al.*, "Microgrid losses: When the whole is greater than the sum of its parts," in *ICCPS*, IEEE, Apr. 2016, pp. 1–10. DOI: 10.1109/ICCPS.2016.7479107.

[58] D. Carr and M. Thomson, "Non-technical electricity losses," *Energies*, vol. 15, no. 6, p. 2218, Mar. 2022. DOI: 10.3390/en15062218.

[59] J. Taneja, "Measuring electricity reliability in Kenya," *SSRN Electronic Journal*, 2018. DOI: 10.2139/ssrn.3310479.

[60] E. Dialynas and N. D. Hatziargyriou, "Impact of microgrids on service quality," in *Power Engineering Society General Meeting*, IEEE, Jun. 2007. DOI: 10.1109/pes.2007.385972.

[61] J. T. Lee and D. S. Callaway, "The cost of reliability in decentralized solar power systems in sub-Saharan Africa," *Nature Energy*, vol. 3, no. 11, pp. 960–968, Nov. 2018. DOI: 10.1038/s41560-018-0240-y.

[62] P. A. Madduri, J. Poon, J. Rosa, M. Podolsky, E. A. Brewer, and S. R. Sanders, "Scalable DC microgrids for rural electrification in emerging regions," *IEEE Journal of Emerging and Selected Topics in Power Electronics*, vol. 4, no. 4, pp. 1195–1205, Dec. 2016. DOI: 10.1109/JESTPE.2016.2570229.

[63] P. Loka, S. Moola, K. Polsani, S. Reddy, S. Fulton, and A. Skumanich, "A case study for micro-grid PV: Lessons learned from a rural electrification project in India," *Progress in Photovoltaics*, vol. 22, no. 7, pp. 733–743, Jul. 2014. DOI: 10.1002/pip.2429.

[64] N. G. Paterakis, O. Erdinç, and J. P. S. Catalão, "An overview of demand response: Key-elements and international experience," *Renewable and Sustainable Energy Reviews*, vol. 69, pp. 871–891, 2017. DOI: 10.1016/j.rser.2016.11.167.

[65] W. Abrahamse, L. Steg, C. Vlek, and T. Rothengatter, "The effect of tailored information, goal setting, and tailored feedback on household energy use, energy-related behaviors, and behavioral antecedents," *Journal of Environmental Psychology*, vol. 27, no. 4, pp. 265–276, 2007. DOI: 10.1016/j.jenvp.2007.08.002.

[66] B. J. Kirby, "Energy use in buildings enabling technologies title spinning reserves from responsive loads," Oak Ridge National Laboratory, Tech. Rep., 2003.

[67] V. Mehra, R. Amatya, and R. J. Ram, "Estimating the value of demand-side management in low-cost, solar micro-grids," *Energy*, vol. 163, pp. 74–87, Nov. 2018. DOI: 10.1016/j.energy.2018.07.204.

[68] R. J. Campbell, "The smart grid: Status and outlook," Congressional Research Service, Tech. Rep., Apr. 2018.

[69] B. Davito, H. Tai, and R. Uhlaner, "The smart grid and the promise of demand-side management," *McKinsey on Smart Grid*, vol. 3, pp. 8–44, 2010.

[70] A. Faruqui, S. Sergici, and A. Sharif, "The impact of informational feedback on energy consumption—a survey of the experimental evidence," *Energy*, vol. 35, no. 4, pp. 1598–1608, Apr. 2010. DOI: 10.1016/j.energy.2009.07.042.

[71] D. S. Parker, D. Hoak, and J. Cummings, "Pilot evaluation of energy savings from residential energy demand feedback devices," Tech. Rep., Jan. 2008. DOI: 10.2172/1219080.

[72] J. Pierce, C. Fan, D. Lomas, G. Marcu, and E. Paulos, "Some consideration on the (in)effectiveness of residential energy feedback systems," in *DIS*, ACM, Aug. 2010, pp. 244–247. DOI: 10.1145/1858171.1858215.

[73] T. Hargreaves, "Beyond energy feedback," *Building Research and Information: Feedback on energy demand reduction*, vol. 46, no. 3, pp. 332–342, Apr. 2018. DOI: 10.1080/09613218.2017.1356140.

[74] A. Nilsson, M. Wester, D. Lazarevic, and N. Brandt, "Smart homes, home energy management systems and real-time feedback: Lessons for influencing household energy consumption from a Swedish field study," *Energy and Buildings*, vol. 179, pp. 15–25, 2018. DOI: 10.1016/j.enbuild.2018.08.026.

[75] C. Valor, C. Escudero, V. Labajo, and R. Cossent, "Effective design of domestic energy efficiency displays: A proposed architecture based on empirical evidence," *Renewable and Sustainable Energy Reviews*, vol. 114, p. 109 301, Oct. 2019. DOI: 10.1016/j.rser.2019.109301.

[76] A. R. Jordehi, "Optimisation of demand response in electric power systems, a review," *Renewable and Sustainable Energy Reviews*, vol. 103, pp. 308–319, Apr. 2019. DOI: 10.1016/j.rser.2018.12.054.

[77] A. Lavrik, Y. Zhukovskiy, and P. Tcvetkov, "Optimizing the size of autonomous hybrid microgrids with regard to load shifting," *Energies*, vol. 14, no. 16, p. 5059, Aug. 2021. DOI: 10.3390/en14165059.

[78] M. F. Zia, E. Elbouchikhi, and M. Benbouzid, "Optimal operational planning of scalable DC microgrid with demand response, islanding, and battery degradation cost considerations," *Applied Energy*, vol. 237, pp. 695–707, Mar. 2019. DOI: 10.1016/j.apenergy.2019.01.040.

[79] A. A. Abdelsalam, H. A. Zedan, and A. A. ElDesouky, "Energy management of microgrids using load shifting and multi-agent system," *Journal of Control, Automation and Electrical Systems*, vol. 31, no. 4, pp. 1015–1036, Aug. 2020. DOI: 10.1007/s40313-020-00593-w.

[80] T. Logenthiran, D. Srinivasan, and T. Z. Shun, "Demand side management in smart grid using heuristic optimization," *IEEE TSG*, vol. 3, no. 3, pp. 1244–1252, Sep. 2012. DOI: 10.1109/TSG.2012.2195686.

[81] K. Wang, H. Li, S. Maharjan, Y. Zhang, and S. Guo, "Green energy scheduling for demand side management in the smart grid," *IEEE TGCN*, vol. 2, no. 2, pp. 596–611, 2018. DOI: 10.1109/tgcn.2018.2797533.

[82] B. Dey, F. P. G. Márquez, and A. Bhattacharya, "Demand side management as a mandatory inclusion for economic operation of rural and residential microgrid systems," *Sustainable Energy Technologies and Assessments*, vol. 54, p. 102 903, Dec. 2022. DOI: 10.1016/j.seta.2022.102903.

[83] B. Dey, S. Dutta, and F. P. G. Marquez, "Intelligent demand side management for exhaustive techno-economic analysis of microgrid system," *Sustainability*, vol. 15, no. 3, p. 1795, Jan. 2023. DOI: 10.3390/su15031795.

[84] F. M. Mwaura, "Adopting electricity prepayment billing system to reduce non-technical energy losses in Uganda: Lesson from Rwanda," *Utilities Policy*, vol. 23, no. 1, pp. 72–79, Dec. 2012. DOI: 10.1016/j.jup.2012.05.004.

[85] F. de Souza Savian, J. C. M. Siluk, T. B. Garlet, F. M. do Nascimento, J. R. Pinheiro, and Z. Vale, "Non-technical losses: A systematic contemporary article review," *Renewable and Sustainable Energy Reviews*, vol. 147, p. 111 205, Sep. 2021. DOI: 10.1016/j.rser.2021.111205.

[86] G. Otchere-Appiah, S. Takahashi, M. S. Yeboah, and Y. Yoshida, "The impact of smart prepaid metering on non-technical losses in Ghana," *Energies*, vol. 14, no. 7, p. 1852, Apr. 2021. DOI: 10.3390/en14071852.

[87] K. Sridharan and N. N. Schulz, "Outage management through amr systems using an intelligent data filter," *IEEE TPD*, vol. 16, no. 4, pp. 669–675, Oct. 2001. DOI: 10.1109/61.956755.

[88] Department for Business, Energy and Industrial Strategy, "Smart meter roll-out cost benefit analysis," Open Government Licence, Tech. Rep., Sep. 2019. [Online]. Available: https://www.gov.uk/government/publications/smart-meter-roll-out-cost-benefit-analysis-2019.

[89] M. Harper, "Review of strategies and technologies for demand-side management on isolated mini-grids," Tech. Rep., Mar. 2013. DOI: 10.2172/1171615.

[90] J. M. Guerrero, J. C. Vasquez, J. Matas, L. G. de Vicuna, and M. Castilla, "Hierarchical control of droop-controlled AC and DC microgrids—a general approach toward standardization," *IEEE TIE*, vol. 58, no. 1, pp. 158–172, 2011. DOI: 10.1109/tie.2010.2066534.

[91] T. Dragicevic, X. Lu, J. C. Vasquez, and J. M. Guerrero, "DC microgrids-Part I: A review of control strategies and stabilization techniques," *IEEE TPEL*, vol. 31, no. 7, pp. 4876–4891, Jul. 2016. DOI: 10.1109/TPEL.2015.2478859.

[92] I. Serban, S. Cespedes, C. Marinescu, C. Azurdia-Meza, J. S. Gomez, and D. Saez, "Communication requirements in microgrids: A practical survey," *IEEE Access*, vol. 8, Mar. 2020. DOI: 10.1109/ACCESS.2020.2977928. [Online]. Available: https://ieeexplore.ieee.org/abstract/document/9023471.

[93] W. Du, R. H. Lasseter, and A. S. Khalsa, "Survivability of autonomous microgrid during overload events," *IEEE TSG*, vol. 10, no. 4, pp. 3515–3524, Jul. 2019. DOI: 10.1109/TSG.2018.2829438.

[94] M. Ahmed, L. Meegahapola, A. Vahidnia, and M. Datta, "Stability and control aspects of microgrid architectures-a comprehensive review," *IEEE Access*, vol. 8, pp. 144 730–144 766, 2020. [Online]. Available: https://ieeexplore.ieee.org/abstract/document/9162105.

[95] A. K. Sahoo, K. Mahmud, M. Crittenden, J. Ravishankar, S. Padmanaban, and F. Blaabjerg, "Communication-less primary and secondary control in inverter-interfaced AC microgrid: An overview," *IEEE Journal of Emerging and Selected Topics in Power Electronics*, vol. 9, no. 5, pp. 5164–5182, Oct. 2021. [Online]. Available: https://ieeexplore.ieee.org/abstract/document/8999492.

[96] Kirakosyan, El-Saadany, Moursi, Yazdavar, and Al-Durra, "Communication-free current sharing control strategy for DC microgrids and its application for AC/DC hybrid microgrids," *IEEE TPWRS*, vol. 35, no. 1, pp. 140–151, Jan. 2020. DOI: 10.1109/TPWRS.2019.2925779.

[97] N. L. Diaz, J. C. Vasquez, and J. M. Guerrero, "A communication-less distributed control architecture for islanded microgrids with renewable generation and storage," *IEEE TPEL*, vol. 33, no. 3, pp. 1922–1939, Mar. 2018. [Online]. Available: https://ieeexplore.ieee.org/abstract/document/7911341.

[98] A. Bidram, A. Davoudi, F. L. Lewis, and Z. Qu, "Secondary control of microgrids based on distributed cooperative control of multi-agent systems," *IET Generation, Transmission and Distribution*, vol. 7, no. 8, pp. 822–831, Aug. 2013. DOI: 10.1049/iet-gtd.2012.0576.

[99] Q. Shafiee, J. M. Guerrero, and J. C. Vasquez, "Distributed secondary control for islanded microgrids-a novel approach," *IEEE TPEL*, vol. 29, no. 2, pp. 1018–1031, Feb. 2014. DOI: 10.1109/TPEL.2013.2259506.

[100] M. Saleh, Y. Esa, and A. Mohamed, "Impact of communication latency on the bus voltage of centrally controlled DC microgrids during islanding," *IEEE TSTE*, vol. 10, no. 4, pp. 1844–1856, Oct. 2019. DOI: 10.1109/TSTE.2018.2873699.

[101] F. Katiraei, R. Iravani, N. Hatziargyriou, and A. Dimeas, *Microgrids management*, May 2008. DOI: 10.1109/MPE.2008.918702.

[102] M. Lexuan, T. Dragicevic, J. C. Vasquez, and J. M. Guerrero, "Tertiary and secondary control levels for efficiency optimization and system damping in droop controlled DC-DC converters," *IEEE TSG*, vol. 6, no. 6, pp. 2615–2626, Nov. 2015. DOI: 10.1109/TSG.2015.2435055.

[103] J. M. Guerrero, P. C. Loh, T.-L. Lee, and M. Chandorkar, "Advanced control architectures for intelligent microgrids-Part II: Power quality, energy storage, and AC/DC microgrids," *IEEE TIE*, vol. 60, no. 4, pp. 1263–1270, Apr. 2013. DOI: 10.1109/TIE.2012.2196889.

[104] J. M. Guerrero, M. Chandorkar, T. Lee, and P. C. Loh, "Advanced control architectures for intelligent microgrids-Part I: Decentralized and hierarchical control," *IEEE TIE*, vol. 60, no. 4, pp. 1254–1262, Apr. 2013. DOI: 10.1109/TIE.2012.2194969.

[105] E.-K. Lee, W. Shi, R. Gadh, and W. Kim, "Design and implementation of a microgrid energy management system," *Sustainability*, vol. 8, no. 11, p. 1143, Nov. 2016. DOI: 10.3390/su8111143.

[106] A. M. Annaswamy and M. Amin, *Ieee vision for smart grid controls: 2030 and beyond*, Jun. 2013. DOI: 10.1109/IEEESTD.2013.6577608.

[107] Department of Energy, *Communications requirements of smart grid technologies*, Oct. 2010. [Online]. Available: https://search.proquest.com/docview/757319116.

[108] H. Wilms, D. Mildt, M. Cupelli, *et al.*, *Microgrid field trials in Sweden: Expanding the electric infrastructure in the village of Simris*, Dec. 2018. DOI: 10.1109/MELE.2018.2871295.

[109] S. Marzal, R. Salas, R. González-Medina, G. Garcerá, and E. Figueres, "Current challenges and future trends in the field of communication architectures for microgrids," *Renewable and Sustainable Energy Reviews*, vol. 82: pp. 3610–3622, Feb. 2018. [Online]. Available: https://www.sciencedirect.com/science/article/pii/S1364032117314703.

[110] M. Kuzlu and M. Pipattanasomporn, "Assessment of communication technologies and network requirements for different smart grid applications," in *ISGT*, Washington, D.C.: IEEE, Feb. 2013. DOI: 10.1109/ISGT.2013.6497873.

[111] S. Ghosh, C. K. Chanda, and J. K. Das, "A comprehensive survey on communication technologies for a grid connected microgrid system," in *ICAIS*, IEEE, Mar. 2021, pp. 1525–1528. DOI: 10.1109/ICAIS50930.2021.9395820.

[112] N. Andreadou, M. Guardiola, and G. Fulli, "Telecommunication technologies for smart grid projects with focus on smart metering applications," *Energies*, vol. 9, May 2016. [Online]. Available: https://www.mdpi.com/1996-1073/9/5/375.

[113] A. B. Shyam, S. R. Sahoo, S. Anand, and J. M. Guerrero, "Comparative study of various communication technologies for secondary controllers in DC microgrid," in *ICPS*, Piscataway: IEEE, Dec. 2021, pp. 1–6. DOI: 10.1109/ICPS52420.2021.9670303.

[114] S. Safdar, B. Hamdaoui, E. Cotilla-Sanchez, and M. Guizani, "A survey on communication infrastructure for micro-grids," in *IWCMC*, IEEE, Jul. 2013, pp. 545–550. DOI: 10.1109/IWCMC.2013.6583616.

[115] S. Güzelgöz, H. Arslan, A. Islam, and A. Domijan, "A review of wireless and PLC propagation channel characteristics for smart grid environments," *Journal of Electrical and Computer Engineering*, vol. 2011, pp. 1–12, Dec. 2011. DOI: 10.1155/2011/154040.

[116] G. van de Kaa, T. Fens, J. Rezaei, D. Kaynak, Z. Hatun, and A. Tsilimeni-Archangelidi, "Realizing smart meter connectivity: Analyzing the competing technologies power line communication, mobile telephony, and radio frequency using the best worst method," *Renewable and Sustainable Energy Reviews*, vol. 103, pp. 320–327, 2019. DOI: 10.1016/j.rser.2018.12.035.

[117] S. Erlinghagen, B. Lichtensteiger, and J. Markard, "Smart meter communication standards in Europe – a comparison," *Renewable and Sustainable Energy Reviews*, vol. 43, pp. 1249–1262, 2015. DOI: 10.1016/j.rser.2014.11.065.

[118] H. P. Alliance, "HomePlug Green PHY: The standard for in-home smart grid powerline communications," HomePlug Powerline Alliance, Inc., Tech. Rep., Jun. 2010.

[119] H. P. Alliance, "HomePlug AV White Paper," HomePlug Powerline Alliance, Inc., Tech. Rep., 2005.

[120] H. Latchman, S. Katar, L. Yonge, and A. Amarsingh, "High speed multimedia and smart energy PLC applications based on adaptations of homeplug AV," in *ISPLC*, IEEE, 2013, pp. 143–148. DOI: 10.1109/ISPLC.2013.6525840.

[121] M. Yigit, V. C. Gungor, G. Tuna, M. Rangoussi, and E. Fadel, "Power line communication technologies for smart grid applications: A review of advances and challenges," *Computer Networks*, vol. 70, pp. 366–383, 2014. DOI: 10.1016/j.comnet.2014.06.005.

[122] M. Zimmermann and K. Dostert, "A multipath model for the powerline channel," *IEEE TCom*, vol. 50, no. 4, pp. 553–559, Apr. 2002. DOI: 10.1109/26.996069.

[123] R. Aquilue, M. Ribo, J. R. Regue, J. L. Pijoan, and G. Sanchez, "Scattering parameters-based channel characterization and modeling for underground medium-voltage power-line communications," *IEEE TPD*, vol. 24, no. 3, pp. 1122–1131, Jul. 2009. DOI: 10.1109/TPWRD.2008.2002963.

[124] H. C. Ferreira, L. Lampe, J. Newbury, and T. G. Swart, *Power Line Communications*. Hoboken: Wiley, 2010, ISBN: 0470740302. DOI: 10.1002/9780470661291.

[125] A. M. Tonello, F. Versolatto, B. Bejar, and S. Zazo, "A fitting algorithm for random modeling the PLC channel," *IEEE TPD*, vol. 27, no. 3, pp. 1477–1484, Jul. 2012. DOI: 10.1109/TPWRD.2012.2196714.

[126] S. Galli and T. Banwell, "A novel approach to the modeling of the indoor power line channel-Part II: Transfer function and its properties," *IEEE TPD*, vol. 20, no. 3, pp. 1869–1878, Jul. 2005. DOI: 10.1109/TPWRD.2005.848732.

[127] B. Masood and S. Baig, "Standardization and deployment scenario of next generation NB-PLC technologies," *Renewable and Sustainable Energy Reviews*, vol. 65, pp. 1033–1047, Nov. 2016. DOI: 10.1016/j.rser.2016.07.060.

[128] A. M. Tonello and F. Versolatto, "Bottom-up statistical PLC channel modeling-Part I: Random topology model and efficient transfer function computation," *IEEE TPD*, vol. 26, no. 2, pp. 891–898, Apr. 2011. DOI: 10.1109/TPWRD.2010.2096518.

[129] F. J. Canete, J. A. Cortes, L. Diez, and J. T. Entrambasaguas, *A channel model proposal for indoor power line communications*, Dec. 2011. DOI: 10.1109/MCOM.2011.6094022.

[130] S. Galli and T. C. Banwell, "A deterministic frequency-domain model for the indoor power line transfer function," *IEEE Journal on Selected Areas in Communications*, vol. 24, no. 7, pp. 1304–1316, Jul. 2006. DOI: 10.1109/JSAC.2006.874428.

[131] M. Gotz, M. Rapp, and K. Dostert, *Power line channel characteristics and their effect on communication system design*, Apr. 2004. DOI: 10.1109/MCOM.2004.1284933.

[132] F. Grassi and S. A. Pignari, "Immunity to conducted noise of data transmission along DC power lines involving twisted-wire pairs above ground," *IEEE Transactions on Electromagnetic Compatibility*, vol. 55, no. 1, pp. 195–207, Feb. 2013. DOI: 10.1109/TEMC.2012.2208117.

[133] H. Meng, S. Chen, Y. L. Guan, *et al.*, "Modeling of transfer characteristics for the broadband power line communication channel," *IEEE TPD*, vol. 19, no. 3, pp. 1057–1064, Jul. 2004. DOI: 10.1109/TPWRD.2004.824430.

[134] J. Liu, B. Zhao, J. Wang, Y. Zhu, and J. Hu, "Application of power line communication in smart power consumption," in *ISPLC*, IEEE, 2010, pp. 303–307. DOI: 10.1109/ISPLC.2010.5479945.

[135] T. K. Tran, H. Yahoui, D. Genon-Catalot, N. Siauve, and N. Forty, "G3 power line communication for controlling an autonomous DC microgrid system," in *ECTI-CON*, IEEE, 2019, pp. 250–253. DOI: 10.1109/ECTI-CON47248.2019.8955256.

[136] A. Pinomaa, J. Ahola, and A. Kosonen, "PLC concept for LVDC distribution systems," *IEEE Communications Magazine*, vol. 49, no. 12, pp. 55–63, Dec. 2011. DOI: 10.1109/MCOM.2011.6094006.

[137] A. G. Lazaropoulos and P. G. Cottis, "Broadband transmission via underground medium-voltage power lines-Part II: Capacity," *IEEE TPD*, vol. 25, no. 4, pp. 2425–2434, Oct. 2010. DOI: 10.1109/TPWRD.2010.2052113.

[138] F. Aalamifar, A. Schlögl, D. Harris, and L. Lampe, "Modelling power line communication using network simulator-3," in *GLOBECOM*, IEEE, Dec. 2013, pp. 2969–2974. DOI: 10.1109/GLOCOM.2013.6831526.

[139] S. Robson, A. Haddad, and H. Griffiths, "A new methodology for network scale simulation of emerging power line communication standards," *IEEE TPD*, vol. 33, no. 3, pp. 1025–1034, Jul. 2018. DOI: 10.1109/TPWRD.2016.2595639.

[140] F. Hao, S. Zhao, and H. Zhao, "Medium voltage buried cable carrier communication channel model considering partial conductor grounding," in *ICITEE*, Association for Computing Machinery, Dec. 2019.

[141] T. Dragicevic, X. Lu, J. C. Vasquez, and J. M. Guerrero, "DC microgrids-Part II: A review of power architectures, applications, and standardization issues," *IEEE TPEL*, vol. 31, no. 5, pp. 3528–3549, May 2016. DOI: 10.1109/TPEL.2015.2464277.

[142] V. Krishnamurthy and A. Kwasinski, "Effects of power electronics, energy storage, power distribution architecture, and lifeline dependencies on microgrid resiliency during extreme events," *IEEE Journal of Emerging and Selected Topics in Power Electronics*, vol. 4, no. 4, pp. 1310–1323, Dec. 2016. DOI: 10.1109/JESTPE.2016.2598648.

[143] A. M. Bouzid, J. M. Guerrero, A. Cheriti, M. Bouhamida, P. Sicard, and M. Benghanem, "A survey on control of electric power distributed generation systems for microgrid applications," *Renewable and Sustainable Energy Reviews*, vol. 44, pp. 751–766, Apr. 2015. DOI: 10.1016/j.rser.2015.01.016.

[144] M. S. Mahmoud, *Microgrid*. San Diego, CA, USA: Elsevier Science, 2016, ISBN: 9780081017531. [Online]. Available: https://international.scholarvox.com/book/88836489.

[145] M. Saleh, Y. Esa, and A. A. Mohamed, "Communication-based control for DC microgrids," *IEEE TSG*, vol. 10, no. 2, pp. 2180–2195, Mar. 2019. DOI: 10.1109/TSG.2018.2791361.

[146] X. Lu, J. M. Guerrero, K. Sun, and J. C. Vasquez, "An improved droop control method for DC microgrids based on low bandwidth communication with DC bus voltage restoration and enhanced current sharing accuracy," *IEEE TPEL*, vol. 29, no. 4, pp. 1800–1812, Apr. 2014. DOI: 10.1109/TPEL.2013.2266419.

[147] X. C. Shangguan, C.-K. Zhang, Y. He, *et al.*, "Robust load frequency control for power system considering transmission delay and sampling period," *IEEE TII*, vol. 17, no. 8, pp. 5292–5303, 2021. DOI: 10.1109/TII.2020.3026336.

[148] B. Cotton, "VRLA battery lifetime fingerprints - Part 1," in *INTELEC*, Scottsdale, AZ, USA: IEEE, Sep. 2012, pp. 1–8. DOI: 10.1109/INTLEC.2012.6374495.

[149] J. Garche and A. Jossen, "Battery management systems (BMS) for increasing battery life time," in *TELESCON*, IEEE, 2000, pp. 81–88. DOI: 10.1109/TELESC.2000.918409.

[150] G. Barbose, C. Goldman, and B. Neenan, "A survey of utility experience with real time pricing," Lawrence Berkeley National Laboratory, Tech. Rep., Dec. 2004. DOI: 10.2172/836966.

[151] G. Association, *Network coverage maps*. [Online]. Available: https://www.gsma.com/coverage/.

[152] D. Semiconductor, *Tech brief 16: Accuracy: What do you really need?* [Online]. Available: https://pdfserv.maximintegrated.com/en/an/AppNote569.pdf.

[153] T. Flaim, B. Neenan, and J. Robinson, "Pilot paralysis: Why dynamic pricing remains over-hyped and underachieved," *The Electricity Journal*, no. 4, May 2013. [Online]. Available: https://www.sciencedirect.com/science/article/pii/S1040619013000808.

[154] K. Steriotis, G. Tsaousoglou, N. Efthymiopoulos, P. Makris, and E. Varvarigos, "A novel behavioral real time pricing scheme for the active energy consumers' participation in emerging flexibility markets," *Sustainable Energy, Grids and Networks*, vol. 16: pp. 14–27, Dec. 2018. [Online]. Available: https://www.sciencedirect.com/science/article/pii/S2352467718300201.

[155] R. Han, M. Tucci, A. Martinelli, J. M. Guerrero, and G. Ferrari-Trecate, "Stability analysis of primary plug-and-play and secondary leader-based controllers for DC microgrid clusters," *IEEE TPWRS*, vol. 34, no. 3, pp. 1780–1800, May 2019. DOI: 10.1109/TPWRS.2018.2884876.

[156] Y. Ding, T. Morstyn, and M. D. McCulloch, "Distributionally robust joint chance-constrained optimization for networked microgrids considering contingencies and renewable uncertainty," *IEEE TSG*, vol. 13, no. 3, pp. 2467–2478, May 2022. DOI: 10.1109/TSG.2022.3150397.

[157] M. S. Saeed, M. W. Mustafa, N. N. Hamadneh, *et al.*, "Detection of non-technical losses in power utilities—a comprehensive systematic review," *Energies*, vol. 13, no. 18, p. 4727, Sep. 2020. DOI: 10.3390/en13184727.

[158] J. L. Viegas, P. R. Esteves, R. Melício, V. M. F. Mendes, and S. M. Vieira, "Solutions for detection of non-technical losses in the electricity grid: A review," *Renewable and Sustainable Energy Reviews*, vol. 80: pp. 1256–1268, Dec. 2017. DOI: 10.1016/j.rser.2017.05.193.

[159] S. Phenninger and I. Staffell, *Renewables.ninja*. [Online]. Available: https://www.renewables.ninja/.

[160] M. A. Abdulgalil, M. N. Khater, M. Khalid, and F. Alisamail, "Sizing of energy storage systems to enhance microgrid reliability," in *ICIT*, IEEE, 2018, pp. 1302–1307. DOI: 10.1109/ICIT.2018.8352366.

[161] Mirdiansyah, A. Taqwa, and Y. Bow, "Monitoring depth of discharge of a valve regulated lead acid battery in a standalone PV system," in *FIRST*, Atlantis Press, 2021, pp. 233–237. DOI: 10.2991/ahe.k.210205.042.

[162] D. Vutetakis and H. Wu, "The effect of charge rate and depth of discharge on the cycle life of sealed lead-acid aircraft batteries," in *International Power Sources Symposium*, IEEE, 1992, pp. 103–105. DOI: 10.1109/IPSS.1992.282019.

[163] M. I. Hlal, V. K. Ramachandaramurthy, A. Sarhan, A. Pouryekta, and U. Subramaniam, "Optimum battery depth of discharge for off-grid solar PV/battery system," *Journal of Energy Storage*, vol. 26, p. 100 999, 2019. DOI: https://doi.org/10.1016/j.est.2019.100999.

[164] I. Alsaidan, A. Khodaei, and W. Gao, "Determination of optimal size and depth of discharge for battery energy storage in standalone microgrids," in *NAPS*, IEEE, 2016, pp. 1–6. DOI: 10.1109/NAPS.2016.7747845.

[165] R. E. Ciez and J. Whitacre, "Comparative techno-economic analysis of hybrid micro-grid systems utilizing different battery types," *Energy Conversion and Management*, vol. 112, pp. 435–444, 2016. DOI: https://doi.org/10.1016/j.enconman.2016.01.014.

[166] *Alibaba*. [Online]. Available: https://www.alibaba.com/.

[167] *Mouser*. [Online]. Available: https://www.mouser.com/.

[168] *Microchip*. [Online]. Available: https://www.microchip.com/.

[169] *Digikey*. [Online]. Available: https://www.digikey.com/.

[170] *Cable monkey*. [Online]. Available: https://www.cablemonkey.co.uk/.

[171] S. Kumar, S. Islam, and A. Jolfaei, "Microgrid communications: Protocols and standards," English, in *Variability, Scalability and Stability of Microgrids*, S. Muyeen, S. Islam, and F. Blaabjerg, Eds. IET, 2019, pp. 291–326, ISBN: 9781785616938. DOI: 10.1049/PBPO139E_ch9.

[172] I. Corporation, "Low latency - how low can you go? background and drivers," Infinera Corporation, Tech. Rep., 2020.

[173] G3-PLC Alliance, "G3-PLC user guidelines," G3-PLC Alliance, Tech. Rep., May 2020.

[174] A. G. devolo, *G3-PLC modem 500k downloads*. [Online]. Available: https://www.devolo.global/support/download/download/g3-plc-modem-500k.

[175] N. Maskey, S. Horsmanheimo, and L. Tuomimäki, "Analysis of latency for cellular networks for smart grid in suburban area," in *ISGT*, IEEE, 2014, pp. 1–4. DOI: 10.1109/ISGTEurope.2014.7028750.

[176] H. Axelsson, A. Bergstrom, P. Bjorken, P. de Bruin, and M. Sundberg, "Improved latency performance with gsm/edge continued evolution," in *VTC*, IEEE, 2006, pp. 1–5. DOI: 10.1109/VTCF.2006.272.

[177] K. Mekki, E. Bajic, F. Chaxel, and F. Meyer, "A comparative study of lpwan technologies for large-scale iot deployment," *ICT Express*, vol. 5, no. 1, Mar. 2019. [Online]. Available: https://www.sciencedirect.com/science/article/pii/S2405959517302953.

[178] N. Saqib, K. F. Haque, K. Yelamarthi, P. Yanambaka, and A. Abdelgawad, "D2D-LoRa latency analysis: An indoor application perspective," in *WF-IoT)*, IEEE, 2021, pp. 29–34. DOI: 10.1109/WF-IoT51360.2021.9595324.

[179] J. Zhang, A. Huynh, Q. Ye, and S. Gong, "Reliability and latency enhancements in a zigbee remote sensing system," in *SensorComm*, IEEE, 2010, pp. 196–202. DOI: 10.1109/SENSORCOMM.2010.38.

[180] H. H. R. Sherazi, R. Iqbal, S. U. Hassan, M. H. Chaudary, and S. A. Gilani, "Zigbee's received signal strength and latency evaluation under varying environments," *Journal of Computer Networks and Communications*, vol. 2016, pp. 1–8, Jan. 2016. DOI: 10.1155/2016/9409402.

[181] C. Pei, Y. Zhao, G. Chen, *et al.*, "Wifi can be the weakest link of round trip network latency in the wild," in *IEEE INFOCOM 2016 - The 35th Annual IEEE International Conference on Computer Communications*, 2016, pp. 1–9. DOI: 10.1109/INFOCOM.2016.7524396.

[182] K. Sui, M. Zhou, D. Liu, *et al.*, "Characterizing and improving wifi latency in large-scale operational networks," in *MOBISYS*, Singapore, Singapore: ACM, 2016, pp. 347–360, ISBN: 9781450342698. DOI: 10.1145/2906388.2906393.

[183] *Jumia Kenya*. [Online]. Available: https://www.jumia.co.ke/.

[184] *Hubtech*. [Online]. Available: https://www.techyshop.co.ke/.

[185] G. Association, *Network coverage maps*. [Online]. Available: https://www.gsma.com/coverage/.

[186] *Worldwide mobile data pricing 2021*. [Online]. Available: https://www.cable.co.uk/mobiles/worldwide-data-pricing/.

[187] T.-S. Choi, K.-R. Ko, S.-C. Park, Y.-S. Jang, Y.-T. Yoon, and S.-K. Im, "Analysis of energy savings using smart metering system and ihd (in-home display)," in *Transmission and Distribution*, IEEE, Oct. 2009, pp. 1–4. DOI: 10.1109/TD-ASIA.2009.5356956.

[188] W. Stefanutti, S. Saggini, P. Mattavelli, and M. Ghioni, "Power line communication in digitally controlled DC-DC converters using switching frequency modulation," *IEEE TIE*, vol. 55, no. 4, pp. 1509–1518, Apr. 2008. [Online]. Available: https://ieeexplore.ieee.org/abstract/document/4441353.

[189] R. Han and D. J. Rogers, "Zero-additional-hardware power line communication for DC-DC converters," *IEEE TPEL*, May 2022. [Online]. Available: https://ieeexplore.ieee.org/abstract/document/9782545.

[190] M. Buevich, D. Schnitzer, T. Escalada, A. Jacquiau-Chamski, and A. Rowe, "Fine-grained remote monitoring, control and pre-paid electrical service in rural microgrids," in *IPSN*, IEEE, Apr. 2014, pp. 1–12. DOI: 10.1109/IPSN.2014.6846736.

[191] *Glassdoor*. [Online]. Available: glassdoor.co.uk.

[192] T. D. Tamarkin, "Automatic meter reading," *Public Power*, vol. 50, no. 5, Oct. 1992.

[193] J. Taneja, "If you build it, will they consume? key challenges for universal, reliable, and low-cost electricity delivery in Kenya," *SSRN Electronic Journal*, 2018. DOI: 10.2139/ssrn.3310479.

[194] Safaricom, *Paybill*. [Online]. Available: https://www.safaricom.co.ke/personal/m-pesa/lipa-na-m-pesa/paybill.

[195] N. O. Shokoya and A. K. Raji, "Electricity theft: A reason to deploy smart grid in South Africa," in *DUE*, Wellington, South Africa: IEEE, Mar. 2019, pp. 96–101. [Online]. Available: https://ieeexplore.ieee.org/document/8734431.

[196] Y. Wang, P. Liu, D. Liu, F. Deng, and Z. Chen, "Enhanced hierarchical control framework of microgrids with efficiency improvement and thermal management," *IEEE Transactions on Energy Conversion*, vol. 36, no. 1, pp. 11–22, Mar. 2021. DOI: 10.1109/TEC.2020.3002670.

[197] A. A. A. Al-karakchi, G. Lacey, and G. Putrus, "A method of electric vehicle charging to improve battery life," in *UPEC*, Stoke on Trent, UK: IEEE, Sep. 2015, pp. 1–3. DOI: 10.1109/UPEC.2015.7339846.

[198] G. Angenendt, S. Zurmühlen, R. Mir-Montazeri, D. Magnor, and D. U. Sauer, "Enhancing battery lifetime in PV battery home storage system using forecast based operating strategies," *Energy Procedia*, vol. 99: pp. 80–88, Nov. 2016. DOI: 10.1016/j.egypro.2016.10.100.

[199] F. D. Garcia, F. P. Marafao, W. A. de Souza, and L. C. P. da Silva, "Power metering: History and future trends," in *Green*, IEEE, Mar. 2017, pp. 26–33. DOI: 10.1109/GreenTech.2017.10.

[200] M. S. Javed, J. Jurasz, M. McPherson, Y. Dai, and T. Ma, "Quantitative evaluation of renewable-energy-based remote microgrids: Curtailment, load shifting, and reliability," *Renewable and Sustainable Energy Reviews*, vol. 164: p. 112 516, Aug. 2022. DOI: 10.1016/j.rser.2022.112516.

[201] H. S. K. Nunna and S. Doolla, "Energy management in microgrids using demand response and distributed storage-a multiagent approach," *IEEE TPD*, vol. 28, no. 2, pp. 939–947, Apr. 2013. DOI: 10.1109/TPWRD.2013.2239665.

[202] A. Dimeas, S. Drenkard, N. Hatziargyriou, *et al.*, *Smart houses in the smart grid: Developing an interactive network*, Mar. 2014. DOI: 10.1109/MELE.2013.2297032.

[203] S. Chen and C.-C. Liu, "From demand response to transactive energy: State of the art," *Journal of Modern Power Systems and Clean Energy*, vol. 5, no. 1, pp. 10–19, Jan. 2017. DOI: 10.1007/s40565-016-0256-x.

[204] G. Babatunde, *Nigerians consume over 80 million gigabytes of data per month despite paying more*, Mar. 2021. [Online]. Available: https://technext.ng/2021/03/02/nigerians-consume-over-80-million-gigabytes-of-data-per-month-despite-paying-more/.

[205] C. R. Paul, *Analysis of multiconductor transmission lines*, 2nd ed. Hoboken, NJ: Wiley, 2008, ISBN: 0470131543. [Online]. Available: http://catdir.loc.gov/catdir/toc/ecip0714/2007013722.html.

[206] Rohde and Schwarz, *Measuring balanced components with vector network analyzer zvb*, Sep. 2004.

[207] V. Degardin, P. Laly, M. Lienard, and P. Degauque, "Compromising radiated emission from a power line communication cable," *Journal of Communications Software and Systems*, vol. 7, no. 1, pp. 16–21, 2011. DOI: 10.24138/jcomss.v7i1.183.

[208] A. M. Baker, C. K. Ng, N. K. Noordin, and S. Khatun, "Phy and mac, cross-layer optimization and design," in *NCTT-MCP*, IEEE, Aug. 2008, pp. 192–197. DOI: 10.1109/NCTT.2008.4814269.

[209] D. M. Pozar, *Microwave engineering*, Fourth edition, international adaptation. Hoboken, NJ: Wiley, 2021, ISBN: 1119770610.

[210] B. Sareni, L. Krahenbuhl, A. Beroual, and C. Brosseau, "Effective dielectric constant of periodic composite materials," *Journal of Applied Physics*, vol. 80, no. 3, pp. 1688–1696, Aug. 1996. DOI: 10.1063/1.362969.

[211] D. W. Knight, *Components and materials: Part 6*, Sep. 2021. [Online]. Available: http://g3ynh.info/zdocs/comps/part_6.html.

[212] S. Morsalin, T. B. Phung, M. Danikas, and D. Mawad, "Diagnostic challenges in dielectric loss assessment and interpretation: A review," *IET Science, Measurement and Technology*, vol. 13, no. 6, pp. 767–782, Aug. 2019. DOI: 10.1049/iet-smt.2018.5597.

[213] B. Gustavsen, J. A. Martinez, and D. Durbak, "Parameter determination for modeling system transients-Part II: Insulated cables," *IEEE TPD*, vol. 20, no. 3, pp. 2045–2050, Jul. 2005. DOI: 10.1109/TPWRD.2005.848774.

[214] M. Kane, A. Ahmad, and P. Auriol, "Multiwire shielded cable parameter computation," *IEEE TransMag*, vol. 31, no. 3, pp. 1646–1649, May 1995. DOI: 10.1109/20.376350.

[215] J. Ortmann and H. Bessai, "A ghz-mimo perspective of shielded multi-wire transmission lines using proximity effect analysis," in *ICTRS*, ACM, Oct. 2018, pp. 10–14. DOI: 10.1145/3278161.3278163.

[216] S. Ramo, J. R. Whinnery, and T. V. Duzer, *Fields and waves in communication electronics*, 3rd ed. New York: Wiley, 1994, ISBN: 9780471585510.

[217] J. van der Merwe, H. C. Reader, and J. H. Cloete, "S-parameter measurements yielding the characteristic matrices of multiconductor transmission lines," *IEEE Transactions on Electromagnetic Compatibility*, vol. 40, no. 3, pp. 249–256, Aug. 1998. DOI: 10.1109/15.709423.

[218] L. Franek and P. Fiedler, "A multiconductor model of power line communication in medium-voltage lines," *Energies*, vol. 10, no. 6, p. 816, Jun. 2017. DOI: 10.3390/en10060816.

[219] W. Fan, A. Lu, L. L. Wai, and B. K. Lok, "Mixed-mode s-parameter characterization of differential structures," in *EPTC*, IEEE, 2003, pp. 533–537. DOI: 10.1109/EPTC.2003.1271579.

[220] J. C. Tippet and R. A. Speciale, "A rigorous technique for measuring the scattering matrix of a multiport device with a 2-port network analyzer," *IEEE TMTT*, vol. 30, no. 5, pp. 661–666, May 1982. DOI: 10.1109/TMTT.1982.1131118.

[221] B. Simonovich, *A guide for single-ended to mixed-mode s-parameter conversions*, Jul. 2020. [Online]. Available: https://www.signalintegrityjournal.com/articles/1832-a-guide-for-singleended-to-mixedmode-s-parameter-conversions.

[222] L. Yonge, J. Abad, K. Afkhamie, *et al.*, "An overview of the HomePlug AV2 technology," *Journal of Electrical and Computer Engineering*, vol. 2013, pp. 1–20, Jan. 2013. DOI: 10.1155/2013/892628.

[223] A. K. Agrawal, K.-m. Lee, L. D. Scott, and H. M. Fowles, "Experimental characterization of multiconductor transmission lines in the frequency domain," *IEEE Transactions on Electromagnetic Compatibility*, vol. EMC-21, no. 1, pp. 20–27, Feb. 1979. DOI: 10.1109/TEMC.1979.303792.

[224] T. M. Inc., *Rf toolbox version: 4.3 (r2022a)*, Natick, Massachusetts, United States, 2022. [Online]. Available: https://www.mathworks.com.

[225] I. Cadence Design Systems, *Awr microwave office*, San Jose, California, United States, 2023. [Online]. Available: https://www.cadence.com.

[226] T. M. Inc., *Communications toolbox version: 7.7 (r2022a)*, Natick, Massachusetts, United States, 2022. [Online]. Available: https://www.mathworks.com.

[227] Qualcomm, *Qualcomm atheros open powerline toolkit.* qca/open-plc-utils, Apr. 2023. [Online]. Available: https://github.com/qca/open-plc-utils.

[228] H. P. Alliance, "HomePlug AV Specification Version 1.1," HomePlug Powerline Alliance, Inc., Tech. Rep., May 2005.

[229] M. Kerrisk, *Linux man pages online*, 2023. [Online]. Available: https://man7.org/linux/man-pages/index.html.

[230] C. Ltd., *Ubuntu manpage repository*, 2019. [Online]. Available: https://manpages.ubuntu.com/.

[231] ESnet, *Iperf version: 3.9 - deb package*, 2016. [Online]. Available: https://iperf.fr/.

[232] devolo, "dLAN® Green PHY eval board II," devolo, Tech. Rep.

[233] devolo, "Broadband PLC transformers," Tech. Rep. [Online]. Available: https://www.codico.com/en/coupler-82977-ut11359.

[234] F. Caspers, "Rf engineering basic concepts: S-parameters," Cornell University Library, arXiv.org, Tech. Rep., Jan. 2012. [Online]. Available: https://search.proquest.com/docview/2086208243.

[235] K. Technologies, "E5061b data sheet," Keysight Technologies, Tech. Rep., Oct. 2020. [Online]. Available: http://www.keysight.com.